MOLECULAR PHYSIOLOGICAL STUDIES ON THE PEPTIDE TRANSPORTER-1, PepT1

A PhD thesis submitted to

UNIVERSITÀ DEGLI STUDI DELL'INSUBRIA

FACOLTÀ DI SCIENZE MM.FF.NN

"Dottorato di ricerca XXIV ciclo in Biologia Cellulare e Molecolare"

Scuola di dottorato in Science Mediche e Biologiche

Laboratory of Cellular and Molecular Physiology

Docente guida Professor Antonio Peres

Coordinatore Prof.ssa Magda de Eguileor

Dottorando Dottore Ayodele Stephen Oyadeyi

July, 2012

To Fisayo, Fimidara, Feyisola, & Moyosore;

for their belief and patience.

Acknowledgements

I gratefully acknowledge the Government of Italy, the Universita of Insubria and the Laboratory of Cellular and Molecular Physiology; for the doctoral fellowship awarded to me for this work.

My sincere thanks go to Professor Antonio Peres for thorough academic mentorship and to Dr Elena Bossi for her all-round support. I cannot thank you enough.

I appreciate all laboratory colleagues, past and present, with whom I have worked. Thanks for providing a beautiful atmosphere.

I am deeply indebted to my family who cheered me on while patiently enduring the absence of an itinerant son, husband and father, now we can all say this is it!

Table of Contents

Summary

The peptide transporter-1, PepT1, is responsible for the uptake of peptides in the mammalian intestine after protein digestion. It has also been shown to transport a wide range of pharmacological agents; thus making it important in drug design and delivery. Many studies have addressed structure-function relationships in the transporter, using biochemical and uptake assays; however PepT1 is an electrogenic transporter whose activities could be more clearly studied using electrophysiological methods.

In this work therefore, the transporter has been studied using the two electrode voltage clamp technique on the transporter expressed in *Xenopus laevis* oocytes.

Temperature effects on the kinetics of the three isoforms studied (rabbit, zebrafish, seabass) is reported here with a suggestion of a possible structural adaptation in the transporter. Since the transporter is also of interest in animal feed formulation, transport characteristics of a range of dipeptide combinations are also presented; with a recommendation on the possible optimal lysine supplementation in feeds that require essential amino acids supplementation.

Reverse operation in transporters may be the result of or lead to pathophysiological states. Experimental data here show that mutants in Arginine 282 and aspartate 341 exhibit properties that make them suitable as models to study possible reverse operation in PepT1. To understand the physiological significance of reverse

operation, the structural and functional basis of this phenomenon was also explored.

CHAPTER 1 INTRODUCTION

1.1 Transport and transporters

The human body is a complex organization of inter-connected cells, tissues and organs that perform different, yet inter-dependent functions; with the ultimate goal of preserving life. Of necessity therefore is the need to exchange and move substances and molecules from one part of the system to another. This has given rise to diverse transport systems within the organism. The movement of molecules in and out of the cell is an integral part of cellular homeostasis, this movement is usually facilitated by membrane proteins which, based on operational mechanisms, are classified as transporters or ion channels or pumps (Braun, 2009).

Transporters typically move an ion down its electrochemical gradient and then harness the free energy associated with this process to facilitate the trans-membrane movement of another ion or organic molecule (e.g. glucose, bicarbonate, neurotransmitter, amino acid, peptides etc.) in either the same or opposite direction.

Sometimes, the movement of the co-transported substance may be against its cellular concentration gradient; thereby allowing a cell to either accumulate or export a given ion or compound. Mechanistically, transporters typically undergo a cycle of conformational changes or states, in which access to the substrate-

binding sites on each site of the membrane is controlled by gates that sequentially open and close(Braun, 2009).

Transporters are ubiquitous proteins and as such subserve different cellular organizations and systems. Among the different types of transporters is the peptide transporter -1 (PepT1), a transporter which functions primarily in the movement of the products of protein digestion, i.e. peptides.

1.2 Protein digestion and absorption

1.2.1 Gastric phase

The digestion of dietary protein begins in the stomach where proteolysis is initiated by two types of pepsins (Freeman & Kim Y.S., 1978;Van, 1989b). These are the major gastric proteases that are autocatalytically activated from zymogen precursors at acidic pH. The action of these enzymes results in a mixture of large polypeptides, smaller polypeptides and some free amino acids. These hydrolytic products may influence a number of gastric functions that are under hormonal control such as secretion of acid and pepsinogen, rate of gastric emptying, and control of the pyloric sphincter (Freeman & Kim Y.S., 1978) The gastric phase may however not play a critical role in protein digestion since patients with total gastrectomy can digest and assimilate dietary protein with little apparent difficulty (Freeman & Kim Y.S., 1978;Van, 1989a).

1.2.2 Pancreatic phase

In normal individuals, the pancreatic phase of protein digestion is important in converting the ingested protein to a mixture of small oligopeptides and free amino acids. This is accomplished by several proteolytic enzymes synthesized and released by pancreatic acinar cells as inactive zymogens. These enzymes are activated in the duodenum, where the rise in pH to neutral or slightly alkaline conditions inactivates the gastric pepsins.

Activation of the pancreatic proenzymes is initiated by enteropeptidase, an enzyme associated with the brush border membrane and localized to the duodenal enterocytes. Its only known function is to activate trypsin thereby initiating a cascade of proteolytic events that results in fully activated trypsin, chymotrypsin, elastase and carboxypeptidases A and B (Rinderknecht, 1986).

These three enzymes have a serine amino acid residue at their active site and thus are collectively classified as serine proteases. Trypsin cleaves peptide bonds on the carboxyl side of basic amino acids (Arginine, Lysine), while chymotrypsin favors bonds where the carbonyl group is aromatic (Tyrosine, Trptophan). Elastase hydrolyzes elastin and cleaves bonds in polypeptides where the amino acid residue contributing the carboxyl group is aliphatic (Alanine, Leucine, Glycine, Valine, Isoleucine). Carboxypeptidases A and B are the major exopeptidases found in pancreatic secretions. Both are zinc-containing metallopeptidases of defined specificity in removing single amino acids from the carboxyl terminal ends of proteins and oligopeptides.

The specificities of the five pancreatic proteases are complementary to one another (Van, 1989a); as a result the majority of proteins are reduced to a mixture of free amino acids and oligopeptides (Alpers, 2012) that account for approximately 40% and 60% of the total luminal α-amino nitrogen respectively (Chung *et al.*, 1979;Freeman & Kim Y.S., 1978)). Thus the pancreatic phase of digestion is more critical than the gastric phase for effective protein assimilation in humans.

1.2.3 Small Intestine Phase

Previously it was believed that dietary proteins were rapidly and completely digested by the actions of gastric and pancreatic proteases. Thus the primary function of the small intestine epithelium was thought to be solely involved with amino acid absorption and transport to the portal blood. However, it is now known that the final steps in the digestion of peptides take place in the intestinal lumen and are associated with small intestine mucosal cells.

These cells are highly polarized and present to the intestinal lumen a brush border membrane containing a number of peptidases that participate in the final phases of protein digestion. These peptidases are usually dimeric, integral membrane proteins attached by either a hydrophobic membrane-spanning segment or, in at least one instance, by covalent attachment to glycosyl-phosphatidyl-inositol (Matsumoto *et al.*, 1989). The active site is associated with a large hydrophilic portion of the peptide chain that projects into the lumen of the intestine.

These enzymes are translated and synthesized in the rough endoplasmic reticulum, glycosylated in the Golgi membranes, and specifically inserted into the brush border membrane (Semenza, 1986). Probably the most abundant peptidase is aminopeptidase N, which sequentially removes the N-terminal amino acids from short oligopeptides. Interestingly, the intestinal brush border membrane contains at least four peptidases that have high hydrolytic rates with peptides containing a proline residue at the site of cleavage. Dipeptidyl aminopeptidase IV and aminopeptidase P cleave prolyl peptides from the amino terminus, while angiotensin-converting enzyme and carboxypeptidase P work in a concerted fashion to hydrolyze prolyl peptides from the carboxy terminal end (Yoshioka *et al.*, 1988).

The specificities of these enzymes are believed to be complementary to those of pancreatic proteases, which have little or no ability to hydrolyze peptide bonds involving proline. The brush border membrane also contains several neutral metallopeptidases (Guan *et al.*, 1988) that cleave the interior peptide bonds of relatively large proteins and polypeptides but are different from the pancreatic endopeptidases discussed above. These enzymes can initiate the hydrolysis of relatively large proteins such as α-casein, fibrinogen and histone, this reduces them to small peptides and amino acids even without the action of pancreatic proteases (Guan *et al.*, 1988).

The collective result of the action of the gastric, pancreatic, and brush border membrane proteases is to reduce the majority of dietary protein to a mixture of free amino acids, dipeptides, and

tripeptides, which thereby makes it available to the various carrier-transporters of the brush border membrane.

1.2.4 Transport and absorption phase: amino acid transporters

Transfer of amino acids across the hydrophobic domain of the plasma membrane is mediated by proteins that recognize, bind, and transport these amino acids from the extracellular medium into the cell, or vice versa (Palacín *et al.*, 1998). These proteins are known as amino acid transporters, and they vary in nomenclature based on the specific amino acid types they transport. Current analysis (Hediger *et al.*, 2004) of the SLC families identifies, in mammals, 59 functional amino acid transport proteins that are grouped into 12 separate SLC families. Orphan transporters are present in many of these families, suggesting that the total number of mammalian amino acid transport proteins is actually much greater than the 59 identified to date (Thwaites & Anderson, 2011)

1.2.5 Transport and absorption phase: peptide transporters

While the body of knowledge detailing absorption of amino acids is relatively recent in terms of full scientific acceptance, the absorption of peptides as an established biological concept on the other end is quite old. The first evidence for peptide transport was provided in the 1950s (Newey & Smyth, 1957;Newey & Smyth, 1959).Today, it is universally accepted that the primary route of intestinal absorption of peptides is via the Peptide transporter-1

(PepT1). In addition to transport through PepT1, peptides may also be absorbed through alternate routes including paracellular movement and by cell-penetrating peptides (CPP) that are capable of moving cargo across the plasma membrane(Gilbert *et al.*, 2008).

1.3 The Peptide transporter-1 (PepT1)

1.3.1 Journey of discovery

Multiple research groups had independently identified a peptide transporter expressed in the basolateral membrane of enterocytes that was responsible for movement of peptides from inside the cell to the portal circulation. This kind of transporter is different from other peptide transporters, expressed on the apical, luminal surface and which is responsible for moving dipeptides from the lumen into the enterocytes. It had even been suggested, though not proven, that the enterocyte contained high concentrations of intra-cellular peptidases that hydrolyzed peptides into their constituent amino acids (AA) resulting in only free AA transport out of the cell.

Then, in 1974, Kim and co-workers (Kim *et al.*, 1974) detected peptidase activity in the brush border and soluble fractions of rat intestinal mucosa for 13 dipeptides and 5 tripeptides with the soluble fractions constituting 80 to 90% and brush border constituting 10 to 15% of total activity. The authors acknowledged that significant cross-contamination of each fraction occurred and lability of the peptide hydrolases prevented further purification and functional characterization of specific enzymes. Although these data demonstrated the presence of intracellular peptidases, they in no way

demonstrated complete hydrolysis of all dietary protein-derived peptides. Inside the cell, peptides may be hydrolyzed into free AA by peptidases and transported across the basolateral membrane by free AA transporters, or intact peptides may be transported out of the cell by a peptide transporter.

The discovery of a peptide transporter in the basolateral membrane of enterocytes (Terada *et al.*, 1999) and the knowledge that some peptides are relatively resistant to hydrolysis provides at least presumptive evidence that a carrier-mediated mechanism exists for transport of intact peptides to the bloodstream. In recent years, peptide transport from inside the cell to the basolateral compartment has been studied to evaluate transport characteristics of the basolateral peptide transporter.

Although results from many studies demonstrated uptake of peptides into intestinal cells, the transporter responsible for peptide uptake was not identified until the 1990s. In 1994, the first PepT1 mRNA was cloned from the rabbit (Fei *et al.*, 1994).The PepT1 (SLC15) was cloned by microinjecting mRNA isolated from rabbit intestine into *Xenopus* oocytes resulting in functional expression of the protein, predicted to consist of 12 transmembrane domains (Boll *et al.*, 1994;Fei *et al.*, 1994)

1.3.2 Characterization

The first characterization of the peptide transporter in a livestock animal was reported by Matthews and co-workers; in which sheep omasal RNA encoding for the peptide transporter was expressed

in *Xenopus* oocytes and dipeptide transport was demonstrated (Matthews *et al.*, 1996). They observed that Gly-Sar uptake was saturatable (Kt = 0.4 mM) and inhibited 44% by carnosine, 94% by methionylglycine, and 91% by glycylleucine, but not by free glycine. The presence of mRNA that encodes for a peptide transporter in sheep omasal epithelia was confirmed by (Pan *et al.*, 1997) when they demonstrated transport for di- and tripeptides in oocytes injected with poly(A)+ RNA.

1.3.3 Classification and species isoforms

The mammalian peptide transporter proteins are part of the Proton-coupled Oligopeptide Transporter (POT) superfamily (SLC15) which is also called Peptide Transporter (PTR) family (Steiner *et al.*, 1995). The characteristics of each family member are summarized in Table 1.1.

The peptide transporter, PepT1, has been cloned in multiple vertebrate species including the rabbit, rat, mouse, sheep, chicken, turkey, dog, human, pig, cattle, monkey, Atlantic cod, zebra fish and seabass. The size of PepT1 ranges from 707 to 729 AA. Expression or activity, or both, of PepT1 has been detected in other species including the guinea pig (Himukai *et al.*, 1983), hamster (Burston & Matthews, 1990), and the black bear (Gilbert *et al.*, 2007). Peptide transporters have also been found in bacteria, yeast, plants, and invertebrates (Daniel, 2004). Recently, a prokaryotic H^+-dependent peptide transporter, *YdgR*, was characterized and found to have features very similar to mammalian PepT1 (Weitz *et al.*, 2007).

Human Gene Name	Protein Name	Aliases	Predominant Substrates	Transport type/Coupling ions	Tissue distribution and cellular/ subcellular expression
SLC15A1	PTR1	Oligopeptide transporter-1, H^+/peptide transporter-1	Di-,and tripeptides, protons	C / H^+	Intestine, kidney apical, lysosomal membrane
SLC15A2	PTR2	Oligopeptide transporter-2, H^+/peptide transporter-2	Di-,and tripeptides, protons	C / H^+	Kidney, lung, brain, mammary gland, bronchial epithelium
SLC15A3	PHT2 PTR3	Peptide/histidine transporter 2, human peptide transporter 3	Histidine, di- and tripeptides protons	C / H^+	Lung, spleen, thymus (faintly in brain, liver, adrenal gland, heart)
SLC15A4	PTR1 PTR4	Peptide/histidine transporter-1, human peptide transporter-4	Histidine, di- and tripeptides protons	C / H^+	Brain, retina, placenta

Table 1.1: The SLC15 family (Adapted from (Daniel & Kottra, 2003))

1.4 PepT1: structure-function relationships

1.4.1 Membrane topology

An in-depth analysis of the structure of the PEPT protein has not been performed. However, an epitope insertion study suggests that the membrane topology model predicted by the hydropathicity analysis of the amino acidic sequence may be correct (Covitz *et al.*, 1998). The membrane topology is shown in figure 1.1.

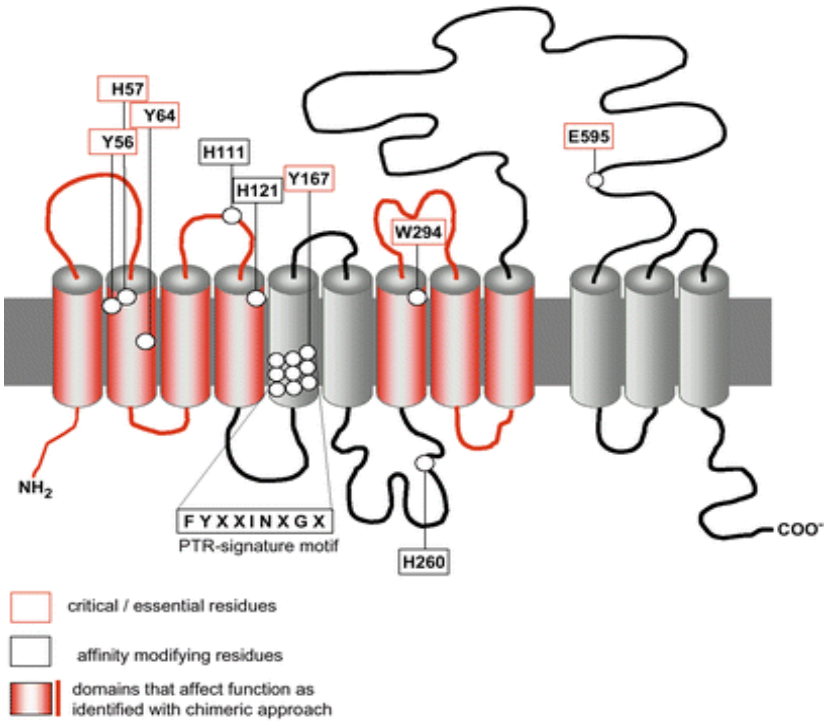

Fig. 1.1 Membrane topology model of PEPT1. Protein domains and individual amino acid residues that have been identified as relevant in determining the functional characteristics of the protein are marked in colours. Predicted protein kinase recognition domains and glycosylation sites have not been included, since their relevance has not been proven experimentally. (Source: (Daniel & Kottra, 2003)

1.4.2 Stoichiometry and kinetics

To study the proton-to-peptide stoichiometry and the dependence of the kinetic parameters on extracellular pH, Steel and co (1997) employed uptake studies of radiolabelled neutral and charged dipeptides and reported that PepT1 did not display the substrate-gated anion conductances that have been found to be characteristic of members of the Na^+- and H^+-coupled high-affinity glutamate transporter family, and that peptide-evoked charge fluxes of PepT1 are

entirely due to H^+ movement (Steel *et al.*, 1997). In addition, they concluded that the rate of acidification, the initial rates of the uptake of radiolabelled peptides and the associated charge fluxes gave proton-substrate coupling ratios of 1:1, 2:1 and 1:1 for neutral, acidic and basic dipeptides, respectively. They also showed that at physiological pH (pH 5.5-6.0) PepT1 prefers neutral and acidic peptides(Steel *et al.*, 1997).

1.4.3 Critical amino acid residues

A variety of single point mutations has been introduced into PEPT1 and PEPT2 and have led to the identification of some essential and critical residues. Of central importance for PEPT1 activity is the extracellular histidine residue (H57) on the interface of the second transmembrane domain and the extracellular side (Figure 1.1) (Chen *et al.*, 2000;Fei *et al.*, 1997;Terada *et al.*, 1996). PEPT1 was shown to be inactivated efficiently by diethlypyrocarbonate as a histidine-modifying agent (Terada *et al.*, 1996) and mutation of H57 led to a completely inactive transporter (Fei *et al.*, 1997). The adjacent tyrosine residue (Y56) was also shown to be involved in substrate interaction by a reduction in the affinity for differently charged dipeptides when mutated to a phenylalanine (Chen *et al.*, 2000).

Another tyrosine residue predicted to lie in the second transmembrane domain (Y64) also appears to be involved in substrate translocation since the subtle change to a phenylalanine residue almost abolished transport (Chen *et al.*, 2000). Moreover, Y167 in the fifth transmembrane domain and part of the PTR-family signature motif also seems to be essential for PEPT1 activity (Yeung *et al.*, 1998). In

view of the pH dependence of the transporters, additional histidine residues such as H111 and H121 and H260 have also been mutated, but did not yield convincing evidence for an essential role in the transport process (Chen *et al.*, 2000;Fei *et al.*, 1997).

1.5 Insights from a prokaryote homologue

1.5.1 Crystal structure

In 2010, Newstead and coworkers reported the crystal structure of a peptide transporter (*PeptSo*) from the bacterium *Shewanella oneidensis* (Newstead *et al.*, 2011). It shows a high degree of sequence conservation within the TM region (~30% identity) to the mammalian PepT1 and PepT2 proteins. All previously identified residues proposed to be functionally important in the mammalian transporters are conserved, including a critical histidine residue.

PepTSo contains 14 TM helices (Figure 1.2A), the N- and C-terminal six-helix bundles, formed by helices H1–H6 and H7–H12, come together to form a 'V'-shaped transporter, related by a pseudo two-fold symmetry axis running perpendicular to the membrane plane. *PepTSo* has two additional TM helices, HA and HB, which are inserted into the cytoplasmic loop connecting the N- and C-terminal bundles. These form a hairpin-like structure in the membrane that packs against the periphery of the protein (Figure 1.2C).

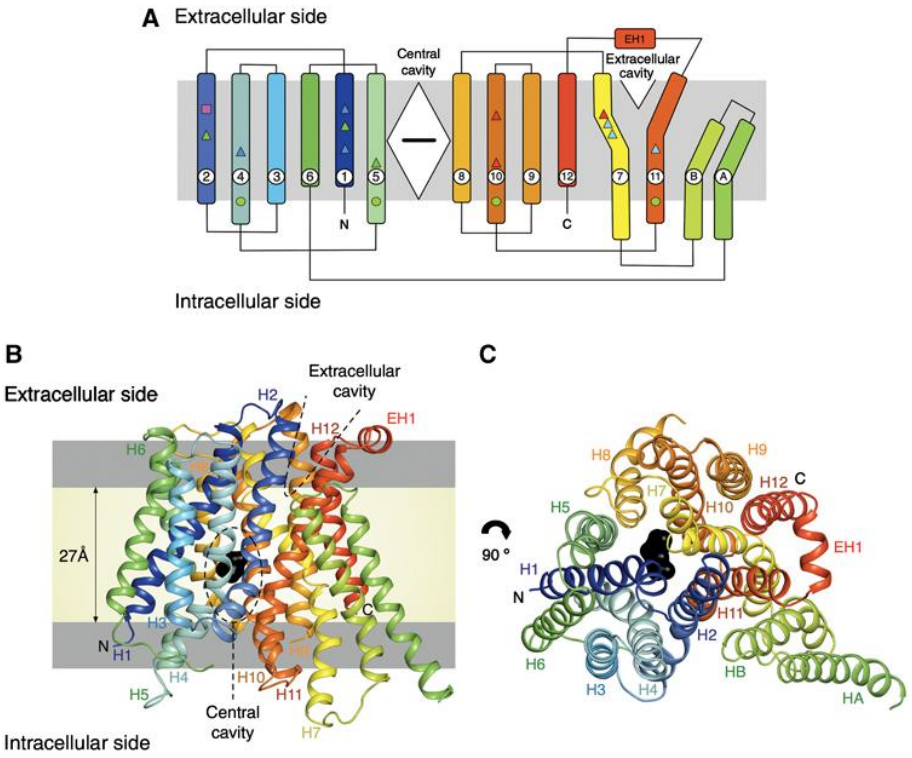

Figure 1.2: Structure of PepTSo. (A) PepTSo topology. The central and extracellular cavities are shown as a closed diamond and open triangle, respectively. A bound ligand in the central cavity is represented as a black horizontal bar. (B) PepTSo structure viewed in the plane of the membrane. The two hydrophilic cavities present in the structure are outlined in dashed lines. The hydrophobic core of the membrane (pale yellow) is distinguished from the interfacial region (light grey). N and C represent the N- and C-termini, respectively. Bound ligand is shown in black. Helices are labeled. (C) View from the extracellular side of the membrane. (Source: (Newstead *et al.*, 2011)

The apparent KM for transport of the hydrolysis resistant di-peptide glycylsarcosine is 1.5±0.15 mM, similar to the value reported for human PepT1 of 1.1±0.1 mM (Brandsch *et al.*, 1994) (Figure 1.3A). Uptake of a fluorescent di-peptide, β-Ala-Lys-Ne-7-amino-4-methylcoumarin-3-acetic acid (β-Ala-Lys-(AMCA)) in cells

overexpressing the PepTSo gene was reduced upon addition of either di- or tri-alanine peptides to the media. Addition of L-alanine or the larger tetra-alanine peptide, however, had little effect, suggesting a similar preference for di- and tri-peptides as reported for the mammalian transporters (Fei et al, 1994).

Uptake was also abolished by the proton ionophore carbonyl cyanide p-chlorophenylhydrazone, consistent with a dependence on the proton electrochemical gradient ($\Delta\mu H+$) to drive transport.

1.5.2 Transport mechanism

The mode of transport is depicted in figure 1.3

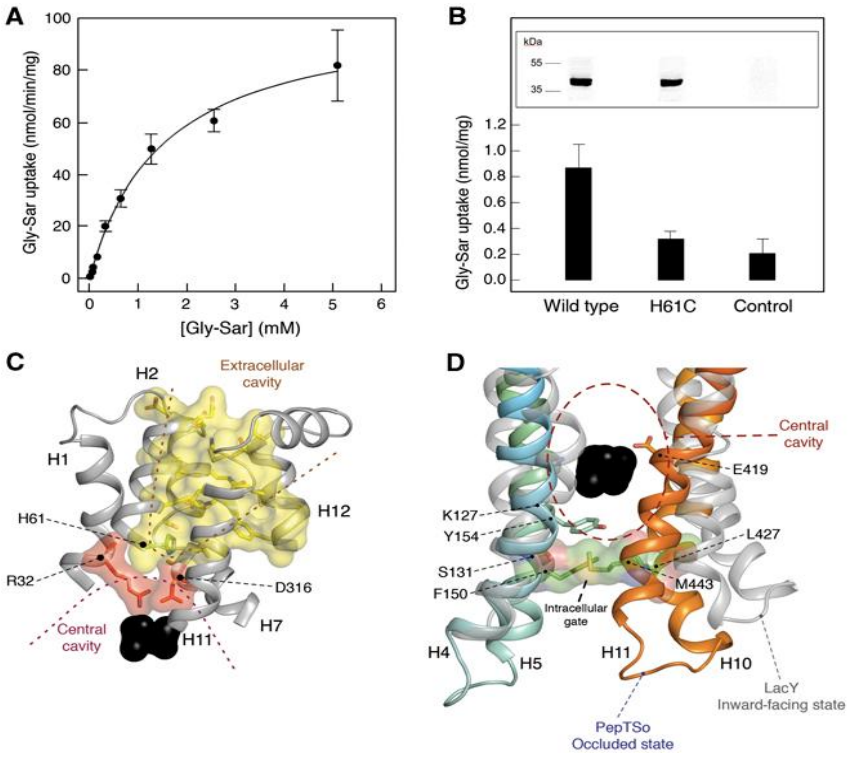

Figure 1.3: Transport of peptides by PepTSo. (A). Concentration dependence of PepTSo-mediated glycylsarcosine (Gly-Sar) uptake in E. coli. Results shown, expressed per milligram of His-tagged PepTSo protein, are mean values ± s.d. (n=4). (B) Effect on transport activity of mutating His61 to cysteine. Uptake of [3H]-glycylsarcosine (Gly-Sar) over a period of 10 min was measured in E. coli cells expressing the indicated forms of His-tagged PepTSo or in control cells lacking the transporter. Results shown are mean values ± s.d. (n=3) and are expressed per milligram dry weight of bacteria. The inset shows western blots of equivalent samples from each culture, stained with a monoclonal antibody against oligohistidine. (C) Extracellular cavity viewed in the membrane plane. The central and extracellular cavities are isolated from each other by a putative extracellular gate. Residues in the central and extracellular cavities are highlighted in red and yellow, respectively. His61, part of the proposed proton–substrate coupling machinery is shown in green. Bound ligand is shown as a black CPK model of a di-alanine peptide. (D) Intracellular gate viewed in the membrane plane. Residues forming the gate are shown as stick models with transparent CPK surfaces. LacY helices (grey) are superposed onto PepTSo. Bound ligand is shown as a black CPK model as in C. Source:(Newstead et al., 2011)

1.5.3 The peptide-binding site

As previously noted, many of the residues conserved between PepTSo and the mammalian peptide transporters cluster around the central hydrophilic cavity, with approximate dimensions of 13 × 12 × 11 Å (Figure 1.4). These dimensions are sufficient to accommodate both di- and tri-peptides, although would be sterically restrictive for larger tetra-peptide ligands. According to (Newstead *et al.*, 2011) the dimensions of the cavity could explain the lack of affinity for single amino acids, as these would presumably be incapable of interacting sufficiently with both the N- and C-terminal domains of the transporter.

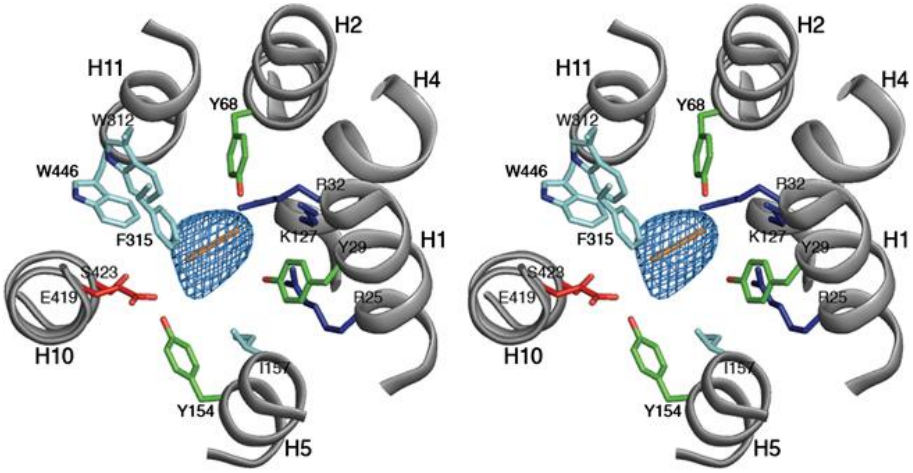

Figure 1.4: The peptide-binding site. Stereo view of the central cavity as viewed from above on the extracellular side of the membrane. Conserved residues between PepTSo and the mammalian peptide transporters are labelled and coloured according to side-chain type, Arg and Lys (blue), Glu and Ser (red), Tyr (green) and Trp, Phe and Leu (cyan). A di-peptide sized Cα baton (orange) is fitted as a size reference into the mFo-DFc electron density observed in the central cavity (blue mesh). (Source: (Newstead et al., 2011)

The binding site is formed by residues from helices H1, H2, H4 and H5 from the N-terminal six-helix bundle and from helices H7, H8, H10 and H11 from the C-terminal bundle. On the N-terminal side of the binding site, three conserved positively charged residues, Arg25(27), Arg32(34) and Lys127(140) extend into the cavity. The numbers in brackets represent the location of the same residues in the human isoform. It has been reported that mutation of Arg25(27) in human PepT2 to a histidine completely inactivates transport (Terada et al, 2004). Two conserved tyrosine residues, Tyr29(31) and Tyr68(64), are positioned close to this positively charged cluster. On the C-terminal side of the binding site, at a distance of ~13 Å from Lys127(140), are two further strictly conserved residues, Glu419(595) and Ser423(599), located in close proximity to Tyr154(167).

Various mutants of Glu419(595) in PepT1 have been reported to drastically reduce transport activity, except where mutation was to an aspartic acid (Xu *et al.*, 2009), indicating the importance of a negatively charged residue at this position. The arrangement of opposite charges within the binding site may have an important role in the recognition and orientation of peptides through the creation of a dipole moment. The presence of several possible hydrogen-bond donors and acceptors could be advantageous in adapting to peptides of various lengths, sequences and charges.

Most of the other residues in the binding site are conserved hydrophobic residues, including Ile157(170), Trp312(294), Phe315(297) and Trp446(622). These residues are likely to provide a suitable environment for peptide side chains that in general are more

hydrophobic than the peptide backbone. This idea is supported by the fact that mutation of Trp312(294) of PepT1 to alanine reduces substrate uptake in HEK293 cells (Bolger *et al.*, 1998)(Bolger et al, 1998).

Interestingly, some conserved residues are not located within the central cavity. The PTR2_1 motif, also conserved throughout the POT family (Daniel et al, 2006), spans the cytoplasmic linker connecting helices H2 and H3 (Newstead *et al.*, 2011). Residues within this motif do not make any contribution to the interior of the protein and most likely sit in the interfacial region of the lipid bilayer, a location also suggested by the coarse-grained MD simulations. Glu21(23) and Glu24(26) on helix H1 are also well conserved among the POTs. These residues are not located in the peptide-binding site but are in close proximity to Arg25(27) and Lys127(140), and may have an important role in positioning these residues.

1.5.4 Transport model

Figure 1.5 summarizes a possible model for transport.

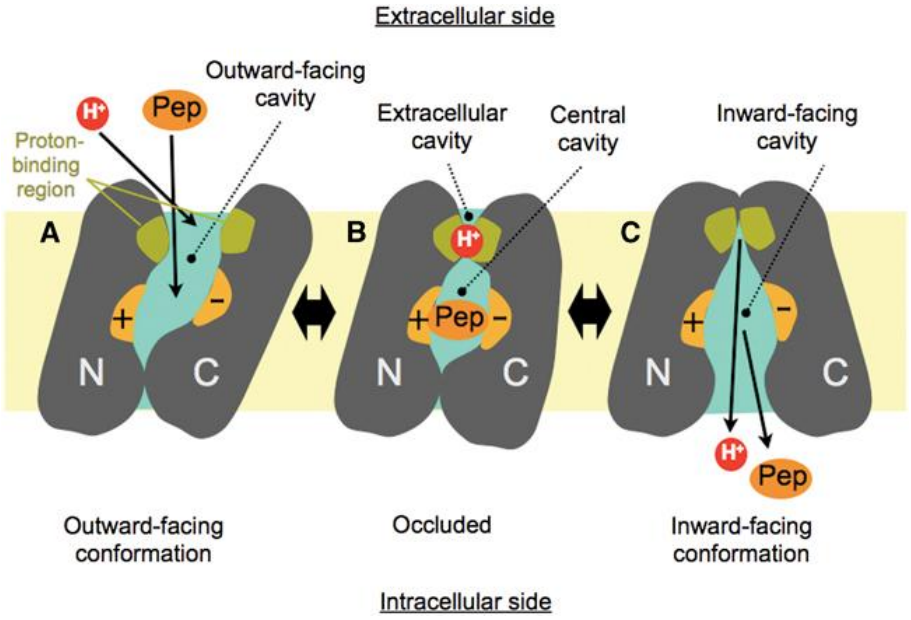

Figure 1.5: A possible mechanism for peptide–proton symport. (A) Outward-facing state: peptide (Pep) and proton (H^+) can access respective binding sites through the outward-facing cavity that is open towards the extracellular side of the membrane. The peptide-binding site is made from the surfaces of both the N- and C-terminal helix bundles (indicated by + and − signs), whereas the proton-binding site is located in the area close to the extracellular gate. (B) Occluded state: both ends of the central cavity are closed with peptide occluded into the central cavity. The proton-binding site is still exposed to the extracellular side through the extracellular cavity. (C) Inward-facing state: peptide and proton are released on the intracellular side of the membrane through the inward-facing cavity. Note that the proton-binding site is exposed to the intracellular side in this conformation.

1.5.5 Regulation of transport activity

The transport activity of PEPT1 can be modulated to meet physiological needs by regulation at either the transcriptional level or by the translocation of preformed transporter proteins to the cell surface. The latter has been shown to occur in response to acute insulin or leptin treatment or prolonged exposure to dipeptides in Caco-2 cells that express hPEPT1. A brief fast or starvation (in rats) can upregulate PEPT1 expression with increased mRNA and protein levels (Ihara *et al.*, 2000). Rats made diabetic by streptozotocin showed increased PEPT1 activity and increased protein levels most likely by enhanced stabilization of its mRNA(Gangopadhyay *et al.*, 2002). Furthermore, PEPT1 undergoes diurnal regulation in its activity and at the mRNA and protein expression level (Pan *et al.*, 2002).

As PEPT1 transport activity also depends on the transmembrane proton gradient, which is mainly generated by the apical Na/H exchanger, any manoeuvres that alter pH gradients and membrane potential secondarily affect PEPT1 activity (Thwaites *et al.*, 2002). In Caco-2 cells, PEPT1 expression is reduced by treatment with thyroid hormone (Ashida *et al.*, 2002) whereas $Ca2^{+}$ channel blockers, by decreasing intracellular calcium, increase PEPT1 activity acutely whereas elevating intracellular free calcium decreases the maximal transport activity (Wenzel *et al.*, 2002).

A very interesting adaptation is observed in patients with short bowel syndrome whose colonic epithelial cells express substantial quantities of PEPT1 protein, which is normally not found in the

human colon or present in only very low levels (Ziegler *et al.*, 2002). An equally interesting adaptation is the existence of a Ca^{2+} and taste receptor-coordinated network that modulates the expression of peptide, glucose and excitatory amino acid transporters (Mace *et al.*, 2009).

1.5.6 PepT1 in human pathophysiology

An involvement of PEPT1 in inflammatory processes has been shown based on the finding that it is expressed in inflamed colonic tissues (Crohn's disease, chronic ulcerative colitis) and its capability to transport formyl-Met-Leu-Phe (fMLP), a known neutrophile attractant peptide derived from certain bacterial species (Dalmasso *et al.*, 2010;Ingersoll *et al.*, 2012;Zucchelli *et al.*, 2009). The functional coupling of PEPT1-mediated uptake of fMLP and increased neutrophile activation and migration suggests that PEPT1 – when it is expressed in colon – could amplify inflammatory processes. In addition, genetic polymorphisms in the Pept1 gene have been linked to inflammatory bowel disease (Zucchelli *et al.*, 2009).

1.5.7 PepT1 as a pharmacological target

The capability of PEPT1 to transport a huge variety of compounds enables the rational design of pharmacological compounds that, in addition to their activity, possess good oral availability by delivery via PEPT1. This concept has yielded nucleoside-based antiviral drugs for various indications that, by coupling of the active core drug to an amino acid (mostly Val), improves the intestinal absorption of the compounds by uptake via

PepT1. DOPA derivatives (DOPA-Phe) and Pro-Phe-esters of bisphosphonates have also been developed and shown to be transported by the peptide transporter (Ezra *et al.*, 2000;Tamai *et al.*, 1998).

Classic and well-characterized drug substrates of PEPT1 and PEPT2 are the numerous amino beta-lactam antibiotics of the cephalosporin and penicillin classes (Ganapathy *et al.*, 1995), as well as selected angiotensin-converting enzyme inhibitors such as captopril and the ester prodrugs enalapril and fosinopril (Zhu *et al.*, 2000). Their interaction with PEPT1 in the gut epithelium provides very good oral availability (generally between 40% and 90% of a dose) of these drugs.

Other interesting drugs shown to be PEPT1-substrates include sulpiride, a selective dopamine D2 receptor antagonist (Watanabe *et al.*, 2002), and the dipeptide-mimetic bestatin that, as a peptidase inhibitor also acts as an antitumor agent (Terada *et al.*, 1997). The capability of peptide transporters for the uptake of delta-aminolevulinic acid (ALA) can be also used for tumor therapy. ALA is a precursor of cellular porphyrin synthesis and was shown to be a good peptide transporter substrate (Doring *et al.*, 1998;Neumann & Brandsch, 2003). When delivered to cells, efficient ALA uptake bypasses the normal tight control of endogenous ALA synthesis, leading to high level accumulation of porphyrins. Photodynamic therapy of tumors based on ALA administration uses laser-induced photoactivation of the accumulated porphyrins to submit tumor cells to necrosis (Kelty *et al.*, 2002).

1.6 Electrophysiological characteristics of ion-coupled transporters

1.6.1 Electrical activities

Overexpression of ion-coupled cotransporters in heterologous systems, especially *Xenopus laevis* oocytes, allows precise electrophysiological measurements which reveal detailed features in the kinetic mechanism. PepT1 as well as most cotransporters display two main kinds of electrical activity: in the absence of organic substrate, transient presteady-state currents (I_{pre}) are generated by charge relocation during voltage steps; in the presence of substrate, transport-associated currents (I_{tr}) are recorded.

1.6.2 Presteady-state currents and transport-associated currents

I_{pre} has the characteristics of an intramembrane charge movement, as it is transient, saturable and symmetric (Bossi et al., 1999b;Forlani et al., 2001;Mager et al., 1993b). Conversely, I_{tr} is true transmembrane current, as the actual charge carriers physically move from the extracellular to the cytosolic compartment or vice versa. I_{pre} and I_{tr} are reminiscent of two distinct currents in voltage-dependent ionic channels: the gating current and ionic current through the channel itself, respectively (Armstrong & Bezanilla, 1974;Hille, 2001).

In ionic channels, clearly distinct functions have been assigned to the two currents. The gating currents are believed to signal the conformational changes that accompany opening (or closing) of the

permeation pathway (Catterall, 1993). The current through the channel can only occur when the gates are open, and therefore a simple relation, based on Ohm's law, exists between the probability of the channel being open and the current flux. Whereas the ionic current obviously depends on the presence of an electrochemical gradient for the permeating ion and this parameter does not affect the gating currents (Fesce et al., 2002b).

In cotransporters the situation is certainly less clear; in fact, the charges responsible for I_{pre} cannot be clearly distinguished from those giving rise to the transmembrane current flux. I_{pre} of cotransporter may also be explained as due to rearrangement of a charged portion of the protein in the membrane field (Loo *et al.*, 1998;Mager *et al.*, 1996b); however, the charge relocation might be due to the motion of ions that move back and forth between the external solution and an open vestibule in the transporter facing the extracellular side (Lester *et al.*, 1996;Mager *et al.*, 1996a).

Whatever the actual mechanism, it is generally agreed that presteady-state currents represent a partial step in the transport cycle. The time integral of this kind of current represents the amount of charges that moves in the membrane electrical field in response to the voltage change. It is possible to note that the same amount of charges moves during the "on" (from the holding potential, V_h, to a given potential) and the "off" (when the voltage is returned to V_h) of the voltage pulse (Fig.6 B). Such behavior is reproduced by a simple electrical circuit constituted by a resistor and a capacitor in series (Figure 1.6 A)

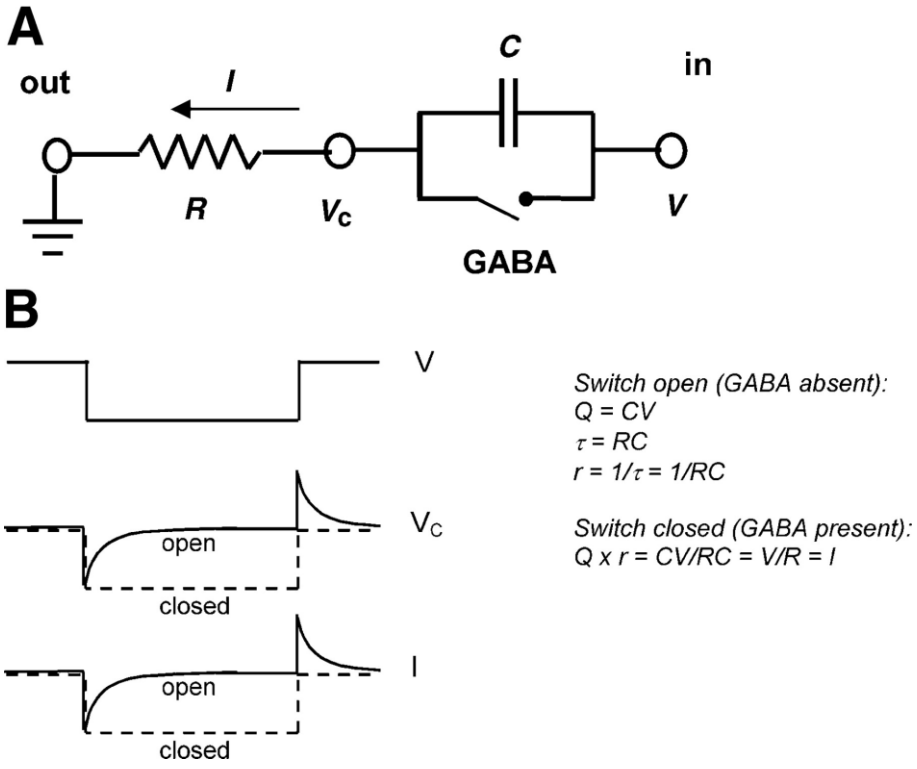

Figure 1.6: A: electrical analog of rGAT1. The switch "GABA" is open in absence of GABA; therefore voltage jumps will displace a charge Q = CV on the capacitor plates, with rate r = 1/τ = 1/RC. Hence the product Q•r is equal to V/R, i.e., to the current flowing in the circuit when the switch is closed by the presence of GABA. B: time course of the relevant electrical quantities in response to a step voltage change across the membrane. Source: (Peres et al., 2004)

1.6.3 Intramembrane charge movement

The electrophysiological observations represent the starting point for the development of kinetic schemes of heterologously expressed transporters. In the simplest formalization, a two-state

system is assumed: in state A the electrical charge associated with the transporter is located near the internal limit of the membrane electrical field, while in state B the charge is displaced toward the outer membrane margin (Fig.1.7). Clearly, the relative occupation of the two states will depend on the membrane potential: assuming a positive mobile charge, state A in Fig.1.7 will be populated at negative internal potentials, while at positive potentials the most populated state will be B. This description may be translated in terms of reaction kinetics described in figure 1.7:

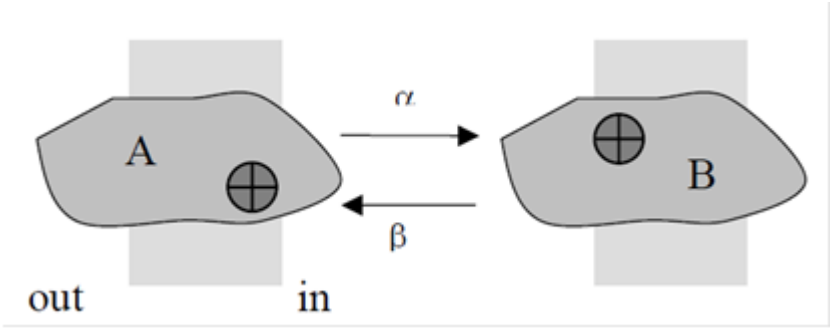

Figure 1.7: Elementary representation of a two-state system explaining intramembrane charge movement. Source:(Peres et al., 2004)

in which α and β are the voltage-dependent unidirectional rate constants (dimensions s^{-1}) for the outward and inward charge movement, respectively.

Consistent with the laws of electrodiffusion, α and β will depend on the membrane voltage according to the following general kind of expressions:

$$\alpha = k_{\alpha} \exp(q\delta V / 2kT)$$

[eqs 1.2]

$\beta = k_\beta \exp(- q\delta V / 2kT)$

Where q is the elementary charge, δ is the fraction of electrical field over which the charge movement occurs, k is Boltzmann's constant, T the absolute temperature and k_α and k_β are the zero-voltage rate constants. Clearly, α will increase as the membrane potential is made more positive and β will increase as the membrane potential is made more negative.

Considering a given population of molecules that can undergo reaction in Fig.1.7, $A + B =$constant, and defining the relative amounts of A and B as:

$A^* = \frac{A}{A+B}$ and $B^* = \frac{B}{A+B}$ [eqs 1.3]

we have:

$$\frac{dA^*}{dt} = -\alpha A^* + \beta B^*$$

[eqs 1.4]

$$\frac{dB}{dt} = \alpha A^* - \beta B^*$$

it is easy to verify that at equilibrium, B* is given by:

$B^* = \alpha \ (\alpha + \beta)$ [eq.1.5]

and therefore, replacing eqs 1.2 in eq.1.5:

$B^* = \frac{1}{1+\frac{k_\beta}{k_\alpha}\exp(-1'q\delta/kT)}$ [eq.1.6]

which is a Boltzmann relation with slope $s = q\delta/kT$, and in which the molecules are equidistributed in the two states at voltage

$V_{1\ 2} = \ln(k_\beta / k_\alpha)$/s.

From eqs 1.4 it is also easy to derive the differential equation that describes the approach to equilibrium following a voltage jump:

$$\frac{dB^*}{dt} = \alpha - (\alpha + \beta)B^* \qquad \text{[eq.1.7]}$$

which may be solved to give:

$$B^* = B_0^* + (B_\infty^* - B_0^*)(1\text{-}exp[-t/\tau]) \qquad \text{[eq.1.8]}$$

where the subscript 0 and ∞ respectively refer to the value before and after the voltage jump, so that B_0^* and B_∞^* are the fractions of molecules in state B before and after the voltage change respectively; they may be obtained from eq.1.5 by using the corresponding values of α and β:

$$B_0^* = \frac{\alpha_0}{\alpha_0 + \beta_0} \qquad \text{[eq 1.9]}$$

$$B_\infty^* = \frac{\alpha_\infty}{\alpha_\infty + \beta_\infty}$$

The time constant of the exponential (τ) is:

$$\tau = 1/(\alpha_\infty + \beta_\infty) \qquad \text{[eq.1.10]}$$

And therefore depends only on the final voltage but not on the starting voltage.

Calling Q_{max} the total amount of electrical charge involved in the process, the time course of the transient current elicited by voltage changes can be obtained by differentiating eq.1.8 and multiplying the result by Q_{max}, which gives:

$$I = \frac{Q_{max}(B_\infty^* - B_0^*)}{\tau}\exp(-t/\tau) \qquad \text{[eq.1.11]}$$

This expression constitutes the basis for the analysis of the presteady-state currents observed in transporters. Fitting eq.1.11 to the experimental traces of transient current yields the time constant of decay, τ, while the time integral gives:

$$\int_0^\infty I = Q_{max}(B_\infty^* - B_0^*) \qquad \text{[eq.1.12]}$$

which represents the amount of charge moved by the voltage jump. In particular, at any membrane voltage the quantity of charge displaced towards the inner side is given by $Q_{in}\ V\ = Q_{max} A^* = Q_{max}\frac{\beta}{\alpha+\beta}$. If, in agreement with standard notation, a minus sign is assigned to inward charge movement, this may be rewritten as: $Q\ V\ = -Q_{max}\frac{\beta}{\alpha+\beta}$.

The analysis of presteady-state currents is performed by first of all isolating these currents from the endogenous components of the oocytes membrane and from other contributions to the total current; this may be achieved by subtracting the traces recorded in conditions in which the presteady-state currents have been eliminated, by the use, for instance, of saturant concentration of substrate (Fig.1.8B), from the corresponding traces recorded in control conditions (Fig.1.8A) (Bossi *et al.*, 1999). A correction of the baseline may consequently be necessary before performing the integration of the transients (Fig.1.8C). The graph of the integrated charge against voltage shows the typical sigmoidal shape (Fig.1.8E) expected from eq.1.6. For each voltage step the "on" and "off" integrals coincide, as expected in a process in which the fraction of charge in the two positions at equilibrium conditions is determined only by voltage.

The relaxation time constant τ may be obtained by fitting single exponentials to the isolated current records at each potential; a representative τ vs. V plot is shown in Fig.1.11D. The τ vs. V plot is bell-shaped, confirming the expectations of equations 1.2 and 1.10. Furthermore, the theory outlined above predicts that the maximum value of τ should occur at the voltage where 50% of the charge is in

one position and 50% in the other and τ should depend only on the voltage after the jump.

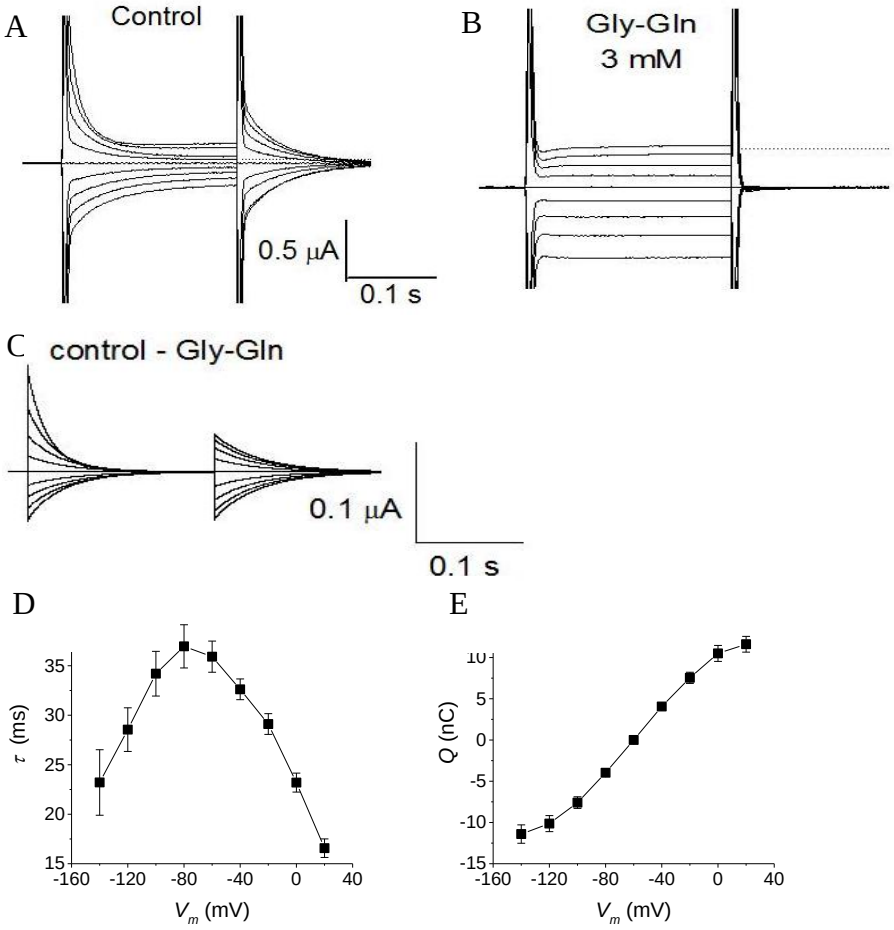

Figure 1.8: Analysis of presteady-state currents for the oligopeptide transporter rbPepT1. A: traces recorded in physiological solution, containing 98 mM Na^+ among other ions; B: traces from the same oocyte after adding 3 mM Gly-Gln; C: isolated presteady-state currents resulting by the subtraction of the traces in B from those in A. D: relaxation time constant of the transient currents in C as function of voltage; E: charge vs. V plot from the integration of the transient currents. Source: (Peres *et al.*, 2004).

CHAPTER 2 MATERIALS AND METHODS

2.1 Molecular Biology

2.1.1 PepT1 cDNAs

Complementary deoxyribonucleic acids (cDNAs) encoding PepT1 were cloned in pSPORT1 vector between *Sal*I and *Not*I sites (for rbPepT1-FLAG cDNA) (Mertl *et al.*, 2008) and between *Sal*I and *Hind*III sites (for sb and zf PepT1 cDNAs). pSPORT1 (Figure 2.1) is an expression vector that presents ampicillin resistance (AP^r) and the reported multi cloning site (MCS). At both ends of the MCS there are promoter sites for T7, T3 and M13 RNA polymerases.

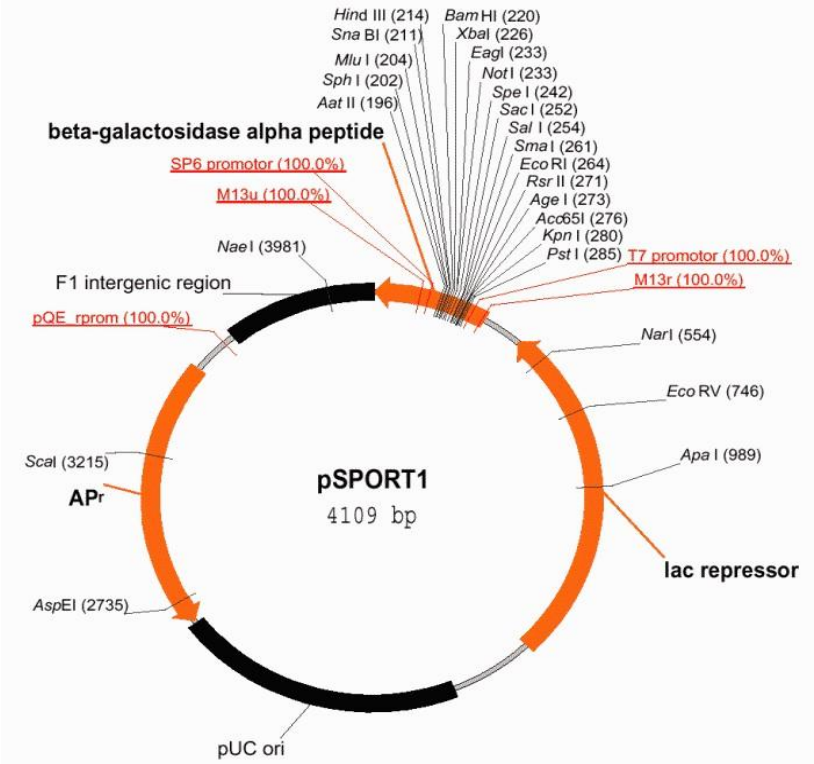

Figure 2.1: pSPORT1 vector

2.1.2 Construction of point mutations

Mutations in rabbit PepT1 were obtained by site-directed mutagenesis (Quickchange Site-Directed Mutagenesis Kit, Stratagene Inc., Milano, Italy). Briefly, 20 ng of the plasmid containing the FLAG-wild-type PepT1 cDNA (Mertl *et al.*, 2008) were amplified with 2.5 units of *Pfu* DNA polymerase in the presence of overlapping primers containing in their sequence the mutated codons:

*rbPepT1 D341R: 5'-cctggtccccatcatg**cgc**gccgtggtgtatcc-3'*

*rbPepT1 H57R: 5'-ggacgacaacctgtccacggt**cgt**ctaccacacgttcgtc-3'*

*rbPepT1 R282X:5'-cgcgcagatcaagatggttacg**xxx**gtgctgttcctgtacatccc-3'* where the original sequence *agg* was transformed to *xxx* that corresponds to the following triplet: for R282D ***gat***, for R282A ***gcg***, for R282E ***gag***, for R282K ***aag***, for R282Q ***gac*** and for R282C ***tgt***.

Polymerase chain reaction (PCR) amplification was performed with 25 thermal cycles of 95°C for 30 s, 55°C for 1 min, and 68°C for 14 min. Then, 10 units of *Dpn*I were added directly to the amplification reaction, and the sample was incubated for 1 h at 37 °C to digest the parental, methylated DNA. JM109 super-competent cells were finally transformed with 1 µl of the reaction mixture and plated onto LB-ampicillin plates (see below for details). After plasmid purification, plasmid cDNAs were fully sequenced (Eurofin MWG Operon Biotech).

2.1.3 Plasmid amplification, extraction and purification

The vectors containing PepT1 cDNAs were introduced into JM109 strain of E. Coli by the means of the heat-shock procedure following the instructions of the bacteria supplier (Promega). Transformed bacteria were then left to grow for about 1 h in SOC medium. The medium contained : [(tryptone 2% (w/v), yeast extract 0.5% (w/v), NaCl 10 mM, KCl 2.5 mM, glucose 20 mM)]. After, the cells were centrifuged, plated on plates containing medium (LB-Agar + 50 µg/ml ampicillin) and incubated over night at 37°C.

The day after, colonies were picked up and inoculated in liquid selective medium (LB added + 50 µg/ml ampicillin). Bacteria were left to grow over night at 37°C after which the plasmid DNA was extracted using Wizard® Plus SV Miniprep (Promega); following

supplier's instruction. The extracted DNA was loaded on a 1% agarose gel in TAE 1X buffer to check the quality and to estimate the concentration.

2.1.4 In vitro transcription

In order to achieve an efficient *in vitro* transcription, the clone containing the cDNA of interest has to be linearized in the 3' direction with respect to the coding region. The cDNA encoding rabbit PepT1-FLAG transporters was linearized with *Not*I and the cDNA encoding seabass and zebrafish transporters with *Hind* III. 8-10 μg of plasmid DNA were digested, then purified using the Wizard® SV Gel and PCR Clean-Up System (Promega) and eluted in 35 μl of nuclease free water. 3 μl were loaded on a 1% agarose gel in TAE 1X buffer to check the linearization. The remaining DNA was used for the *in vitro* transcription as detailed previously (Bossi *et al.*, 2007).

Briefly, the linearized DNA was incubated at 37°C for 3h in the presence of 200 units of T7 RNA polymerase, 18 μl of 5X Trascription Buffer, 8 μl of 100 mM DTT, 2.5 μl of RNasin 30 U/μl, 13 μL NTPs mix (ATP, CTP, UTP 10 mM and GTP 0.5 mM), 6.5 μL of 10 mM Cap Analog (Promega), 10 μl RNA polymerase 20 U/μl (final volume 90 μL). After 10, 20, and 40 min from the beginning of the incubation, 1 μL of 25 mM GTP was added to the reaction. After 1 h from the start of the transcription, a mix of 4 μl of 5X TB, 1 μl of 100 mM DTT, 1 μl of RNasin 30 U/μl, 5 μl of NTPs mix, 1 μl of T7 RNA polymerase 20 U/μl, 1 μl of 25 mM GTP, 4 μl of nuclease-free water was added to each sample. At the end of 3 h, the reaction was

stopped by adding nuclease-free water to a volume of 200 µl. All enzymes were supplied by Promega Italia, Milan, Italy.

The transcribed cRNA was extracted with phenol:chloroform:isoamyl alcohol, 25:24:1, pH 6.6, precipitated with LiCl 8M and washed with 70% EtOH. The dried cRNA was then resuspended in a small volume of nuclease-free water and the concentration estimated using a spectrophotometer (1 A_{260nm} unit = 40 µg/ml).Transcribed cRNAs had a modification which mimics an *in vivo* condition: the process of 5' capping. The so called "Cap Analog" is a modified guanine ($m^7G(5')ppp(5')G$) which, although is not necessary for the protein expression, increases the translation efficiency and also protects the mRNA from degradation.

2.1.5 Heterologous expression in oocytes

Xenopus laevis oocytes are a powerful expression system (Fig.2.2) with numerous advantages: i) high expression rate of exogenous proteins (even after only 18 hours); ii) an efficient biosynthetic apparatus which allows all post-translational modifications necessary for the functionality and the correct targeting of the protein; iii) high density of proteins produced upon cytoplasmic mRNA injection; iv) dimensions well adapted for microinjection and voltage clamp; v) ease of maintaining in culture for quite a long period (ten or more days) with no particular sterile conditions; vi) co-expression of different proteins in various combinations by simply co-injecting the respective cRNAs; vii) low expression levels of endogenous membrane proteins (the endogenous channels have been

well characterized, thus it is easy to distinguish them from the injected proteins).

Xenopus oocytes however have some disadvantages: i) the expression of exogenous protein is transient; ii) the ideal temperature for their survival (about 18°C) is usually lower than the temperature appropriate for exogenous proteins (37°C for mammalian proteins) and this can affect the folding process; iii) although quiescent cells, oocytes possess their own genetic ensemble which might interfere with the exogenous proteins.

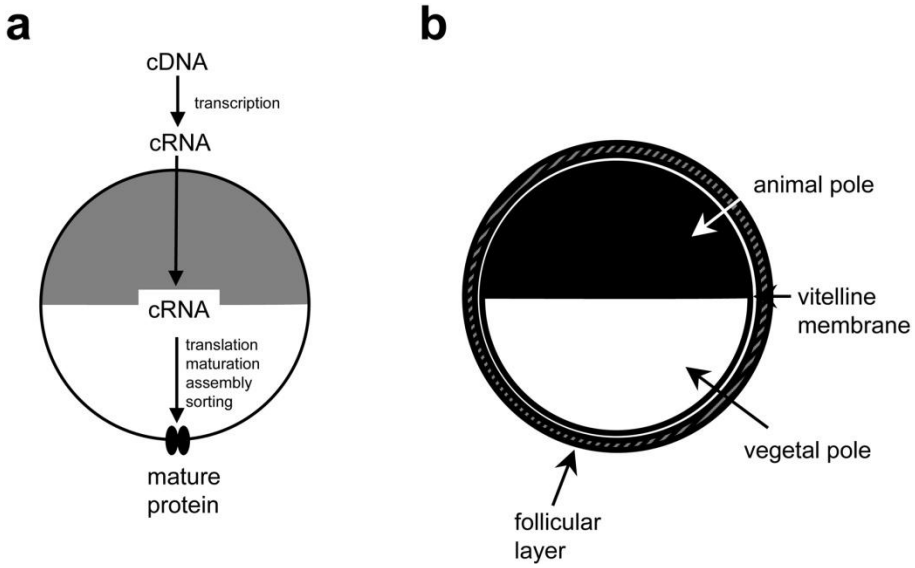

Figure 2.2: Exogenous protein expression in Xenopus laevis oocytes

Oocytes were prepared as described previously (Bossi *et al.*, 2007). They were obtained from adult female *Xenopus laevis,* the frogs were anaesthetised in MS222 (tricaine methansulfonate) 0.10%(w/v) solution in tap water and portions of the ovary were removed through an incision on the abdomen. The oocytes were

treated with collagenase (Sigma Type IA), 1 mg/ml in ND96 Ca^{+} free, for at least 1 h at 18°C. After 24 hours at 18°C in modified Barth's saline solution (MBS), the healthy looking oocytes, were injected with 12.5 ng of cRNA in 50 nl of water, using a manual microinjection system (Drummond). The oocytes were then incubated at 18°C for 3-4 days in MBS before electrophysiological studies.

The experiments were carried out according to the institutional and national ethical guidelines.

2.2 Protein localization

2.2.1 Single-oocyte chemiluminescence

The expression of PepT1-FLAG isoforms at the oocyte plasma membrane was determined by the single oocyte chemiluminescence (SOC) technique (Zerangue *et al.*, 1999),(McAlear *et al.*, 2006;Rauh *et al.*, 2010), that employs enzyme amplification with a chemiluminescent substrate and sensitive linear detection with a luminometer.

Oocytes expressing different FLAG-PepT1 isoforms, as well as non-transfected oocytes, were washed twice for 5 min in ice-cold ND96 pH 7.6 and then fixed with 4% paraformaldehyde in ND96 for 15 min at 4 ° C, rinsed 3x5 min with equal volumes of ND96, and then incubated for 1 hour in a 1% BSA-ND96 blocking solution (used in subsequent antibody incubation steps).

Fixed and blocked oocytes were incubated for 1 h in primary mouse anti-FLAG M2 (Sigma, Milan Italy) monoclonal antibody (1 µg/ml in 1% BSA-ND96), washed 6x3min in 1% BSA-ND96, incubated for 1 hour in secondary peroxidase-conjugated goat anti-

mouse IgG 1 µg/ml, IgG-HRP (Jackson ImmunoResearch Laboratories), washed 6x3min in 1% BSA-ND96 and then 6x3min in ND96 alone.

For chemiluminescence reading, each oocyte was transferred into a well of a 96 wells plate (Assay Plate White not treated flat bottom-Corning Costar) filled with 50 µl SuperSignal Femto (Pierce); the washing solution was eliminated as much as possible. Chemiluminescence was quantified with a Tecan Infinity 200 microplate reader. The plates were read not later than 5 minutes after the transfer of the first oocyte. The data were then acquired at least three times in 10 minutes and for each oocyte the mean of three readings was calculated. Results were normalized to the mean value of wild-type FLAG-PepT1 for each batch and are given in relative light units (RLU).

2.2.2 Immunohistochemistry

Oocytes in which transport activity had been confirmed electrophysiologically were fixed in 100% methanol at −20°C for 2 h, then rehydrated at room temperature (RT) for 15 minutes in 50:50 (v/v) methanol/phosphate-buffered saline (PBS), followed by 2x15 minutes washes in PBS. The fixed oocytes were then embedded in Polyfreeze tissue freezing medium (Polysciences, Eppelheim, Germany) and immediately frozen in liquid nitrogen. Cryosections (7 µm) were obtained with a Leica CM 1850 cryostat. The sections were incubated in the blocking buffer [2% bovine serum albumin, BSA (w/v), 0.1% Tween in PBS] at RT for 30 min, then the primary

antibody, mouse anti-FLAG M2 (SIGMA, Milan Italy, 3.8 mg/mL) 1:1000 in blocking buffer was added and incubated at RT for 1 h.

Samples were washed 3x5 min in blocking buffer at RT. The oocyte sections were then incubated in the secondary antibody [Cy™ 3-conjugated AffiniPure Donkey Anti-Mouse (Jackson ImmunoResearch), 1.4 mg/mL, diluted to 1:1000 in blocking buffer] at RT for 45 min and again washed 3x5 min with blocking buffer. Images were observed with a fluorescence microscope Olympus BH2 through a rhodamine filter set (excitation/emission filters 550/580nm). Images were acquired with a DS-5M-L1 Nikon digital camera system.

2.3 Electrophysiology and data analysis

Membrane electrophysiology has several advantages over other techniques used in transport studies: i) the membrane voltage of the cell is under control, ii) the temporal resolution is high, iii) the results may be obtained immediately as data can be analyzed and interpreted in real-time, and consequently the protocols can be changed or adjusted during the same experimental session.

These benefits may be exploited in the study of transporters; thereby adding valuable information and significantly increasing efficiency. The activity of electrogenic transporters, that translocate electrical charge, by definition, during their working cycle, is strongly influenced by the trans-membrane potential. Thus, tracer flux experiments suffer from some uncertainty, because the membrane voltage is not under control, and not only the value of the electrical gradient is unknown, but also bound to change as a consequence of the electrogenic activity of the transporter itself. A more reliable

evaluation of the activity of the transporter is obtained instead when the membrane potential is "clamped".

2.3.1 Two-Electrode Voltage-Clamp (TEVC)

The "voltage-clamp" technique was introduced by Marmont and Cole (Cole & Curtis, 1941), and by Hodgkin, Huxley and Katz (Hodgkin *et al.*, 1952) to study the ionic currents underlying the action potential in nerve axons, and it has been extended to the study of transporters soon after the cloning and expression of the first transporters in *Xenopus laevis* oocytes (Hediger *et al.*, 1987;Ikeda *et al.*, 1989;Mager *et al.*, 1993;Parent *et al.*, 1992).

The TEVC technique is based on the use of two microelectrodes, one for recording the transmembrane voltage and one for passing current (Figure.2.3). The recorded membrane voltage is compared to the desired (command) voltage and a compensating current is automatically injected into the cell by the appropriate electronic apparatus. In this technique the independent (controlled) variable is the membrane voltage, controlled by the experimenter, while the dependent (measured) variable is the membrane current.

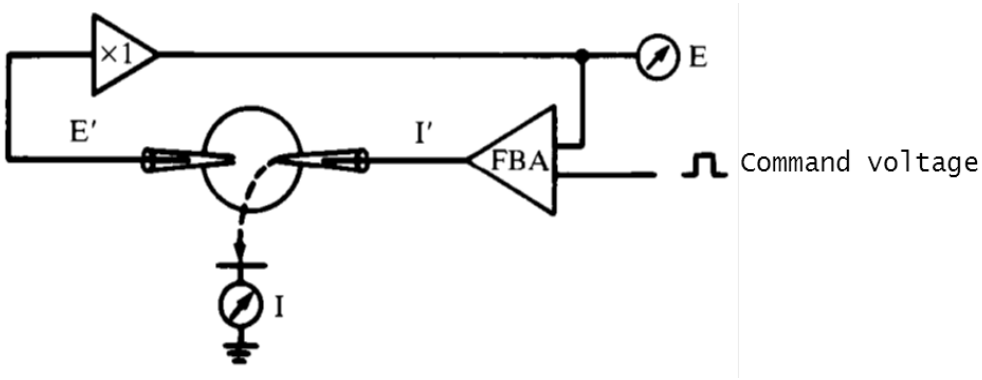

Figure.2.3 Two-Electrode Voltage-Clamp.FBA is the feedback amplifier, E' is the voltage electrode and I' is the current electrode.

When a current is generated due to the activity of the transport systems located in the membrane, a negative feedback in the circuitry injects into the oocyte a current that exactly compensates the charge flow through the cell membrane, in order to maintain trans-membrane voltage under control. In addition to keeping the membrane potential constant, membrane voltage changes of any desired form can be applied to the cell by the TEVC technique. In the case of ion-coupled transporters, the trans-membrane current is an indication of the transport activity, and the possibility of accurately controlling the membrane potential is particularly crucial in voltage-dependent processes.

The ideal voltage clamp simply consists of a battery, a switch, a wire, the cell and an ammeter (Figure.2.4). Since the wire has zero resistance when the switch is closed, the membrane potential steps instantly to the battery voltage. This generates an impulse of current that charges the membrane capacitance ($Q = C_m V_{cmd}$), followed by a

steady-state current ($I_m = V_{cmd}/R_m$) to sustain the voltage across the membrane resistance.

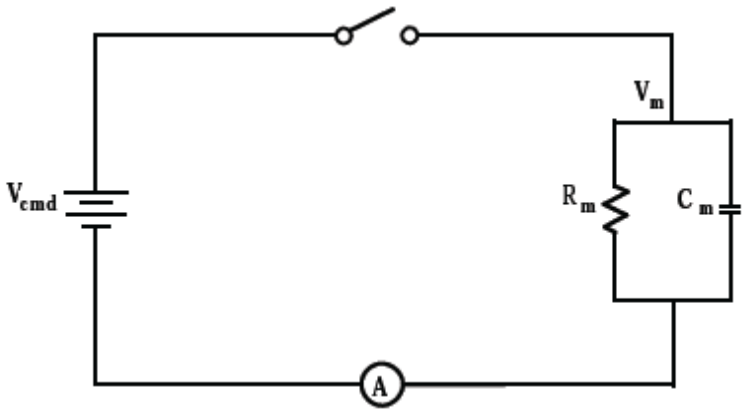

Figure 2.4 The ideal Voltage Clamp

In this work most of the experiments were conducted in voltage-clamp conditions, but some were also performed in current-clamp conditions, i.e. without voltage control, but with the possibility of constant current injections.

2.3.2 TEVC experimental setup

A schematic view of the TEVC experimental setup used in this work is shown in figure 2.5.

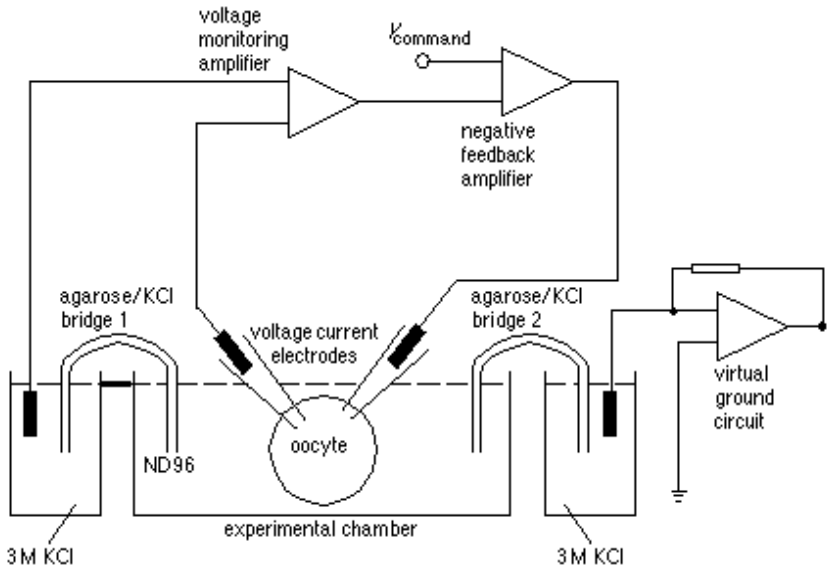

Figure 2.5 Schematic representation of the experimental setup

The voltage-clamp amplifier (GeneClamp, Axon Instruments Foster City, CA, USA or Oocyte Clamp OC-725B, Warner Instruments, Hamden, CT, USA) was connected to a computer through an AD/DA (analog-digital, digital-analog) converter (DigiData 1200, Axon Instr.). This device converts the analog signal from the amplifier to a digital signal intelligible for the computer, and vice versa. Usually, signals derived from the amplifier were also displayed on an oscilloscope (TDS 420, TekTronix Inc., Beaverton, OR, USA).

A dissection microscope (Wild M3B, Leica Microsystems AG, Wetzlar, Germany) was used to visualize the oocyte, and micromanipulators (MM-33, Märtzhäuser Wetzlar GmbH & Co. KG, Wetzlar-Steindorf, Germany) were used to move the electrodes. A perfusion system consisting of a set (16) of syringes delivered the

various solutions to the unique solution inlet of the chamber (a modified version of RC-1Z, Warner Instr.). All the syringes were connected to the inlet by the use of two manifolds (MP-8, Warner Instr.) and were all positioned at the same height in order to have the same flow rate for each solution. Selection of the desired solution was performed by pinch solenoid valves (Sirai, Milan, Italy).

The recording chamber has a small volume (about 200 µl, 85 *m*l/mm height) which allows a rapid solution exchange (about 8-10 seconds in our system). The solution is aspirated by a modified aquarium pump through a suction reservoir connected to the oocyte well. The oocyte was placed in the chamber and impaled with the two microelectrodes. These intracellular glass microelectrodes were filled with KCl (3M) and had tip resistances between 0.5 – 4 MΩ. These resistance values were usually obtained by gently breaking the tips on the bottom of the chamber. Agar bridges (3% agar in 3M KCl) connected the bath electrodes to the experimental chamber.

All the equipment needed for the recording (the dissection microscope, the perfusion system, the oocyte chamber, micromanipulators and reference electrode) are placed inside a Faraday cage, in order to reduce the noise derived from electromagnetic fields, and on an anti-vibration table. The cage and all the instrument inside it were electrically grounded.

2.3.3 Protocols and data analysis

In voltage-clamp mode the holding potential (V_h) was generally -60 mV, unless otherwise indicated. The standard protocol consisted of 200 milliseconds (ms) long pulses to test potentials from -

140 to +40 mV; in 20 mV increments. Other protocols including prepulses are described in the text. The current signal was filtered at 1 kHz before sampling at 2 kHz.

Two methods were used to isolate the presteady-state currents elicited by voltage jumps (Mertl *et al.*, 2008;Sangaletti *et al.*, 2009): in the first, the slow component of a double-exponential fitting of the transient was taken to represent the presteady-state currents, while in the second, the currents remaining after subtraction of the traces in the presence from those in the absence of substrate were assumed to represent the intramembrane charge movement.

The isolated traces were fitted with single exponentials to obtain the time constant of decline, and integrated to calculate the amount of displaced charge, after zeroing any residual steady-state transport current. The presence of gently decaying currents during the voltage pulse was sometimes observed in some mutants at alkaline pH. In these cases, a sloping baseline was subtracted before fitting and integration. The two methods gave generally equivalent results; the subtraction method was preferred when the presteady state currents were fast, with time constants approaching that of the endogenous capacitive transients.

The general procedures to analyse the electrophysiological data are summarized in figure 2.6. The voltage dependences of the decay time constant τ and the intramembrane charge movement Q are obtained from the isolated presteady-state currents.

As expected, the equilibrium distribution of the charge moved during the presteady-state currents shown in figure 2.6 is sigmoidal and can be described with the Boltzmann equation:

$$Q = \frac{Q_{\max}}{1 + \exp\left[\frac{-(V - V_{0.5})}{\sigma}\right]}, \qquad \text{[eq.2.1]}$$

where Q_{max} is the maximal moveable charge; $V_{0.5}$ is the voltage at which half of the charge is moved (that is, the midpoint of the sigmoidal Q/V curve); and $\sigma = kT/q\delta$ represents a slope factor, in which q is the elementary electronic charge, k is the Boltzmann constant, T is the absolute temperature, and δ is the fraction of electrical field over which the charge movement occurs.

The sigmoidal *Q/V* curve may represent the steady-state distribution of the transporter molecules between two conformations with the center of charge in two different locations of the membrane electrical field. The charge movement process may be described with the simple reaction:

$$Q_{in} \underset{inrate}{\overset{outrate}{\rightleftharpoons}} Q_{out},$$

where *outrate* and *inrate* are the unidirectional rate constants, and Q_{in} and Q_{out} are the amount of charge at an inner and outer position, respectively, in the membrane electrical field. It is easy to derive *outrate* and *inrate* from the experimental *Q/V* and *τ/V* curves, because:

$$\tau = \frac{1}{outrate + inrate} \text{ and } \frac{Q_{in}}{Q_{in} + Q_{out}} = \frac{Q_{in}}{Q_{\max}} = \frac{inrate}{outrate + inrate} \text{ [eqs 2.2]}$$

where Q_{max} is the maximal moveable charge, obtained from the saturating values of the *Q/V* sigmoidal curve. From eq 2.2, it is possible to derive (Fesce *et al.*, 2002) the unidirectional rate constants of the charge movement and their voltage dependency, according to the relations:

$$inrate = \frac{1}{\tau}\frac{Q_{in}}{Q_{\max}}$$

$$outrate = \frac{1}{\tau}\left(1 - \frac{Q_{in}}{Q_{\max}}\right)$$

[eq 2.3]

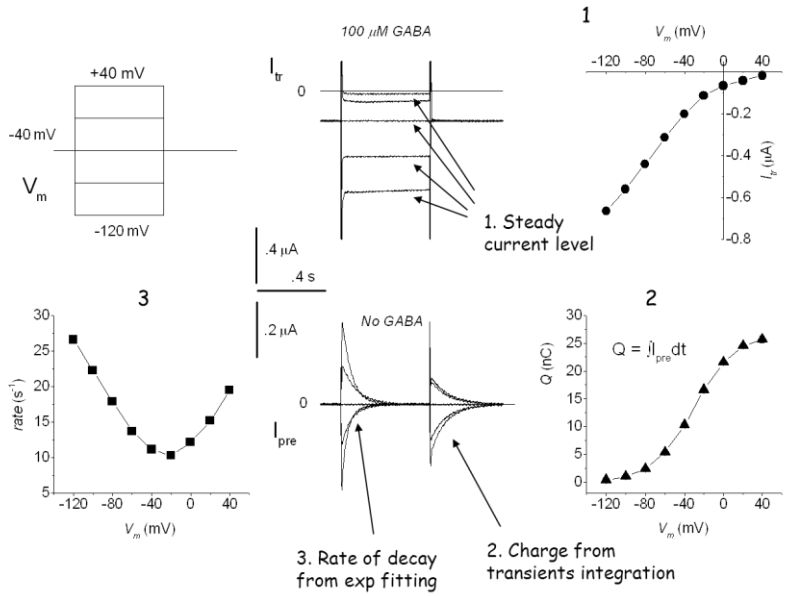

Figure 2.6.General procedures used to determine the electrophysiological characteristics of ion-coupled cotransporters (the GABA transporter GAT1, in this case): in the upper row, the voltage dependence of the transport current (rightmost panel) is derived from the steady current levels elicited at various voltages by a saturating amount of substrate; in the bottom row, exponential fitting of the isolated presteady-state currents gives the the voltage dependence of the rate of decay (1/□, left panel), while the charge-voltage relationship is obtained from the integration of the transients (Q, right panel).

Data were analyzed using Clampfit 8.2 (Axon Instruments), and figures were prepared with Origin 5.0 (Microcal Software Inc., Northampton, MA, USA).

2.4 Extracellular Solutions

The oocyte culture and washing solutions had the following composition (in mM),

1) ND96: NaCl 96, KCl 2, $MgCl_2$ 1, $CaCl_2$ 1.8, Hepes 5, pH 7.6;

2)MBS: NaCl 88, KCl 1, $NaHCO_3$ 2.4, Hepes 15, $Ca(NO_3)_2$ 0.30, $CaCl_2$ 0.41, $MgSO_4$ 0.82, sodium penicillin 10 µg/ml, streptomycin sulphate 10 µg/ml, gentamycin sulphate 100 µg/ml, nystatin 10 U/ml, pH 7.6

3) PBS: NaCl 138, KCl 2.7, Na_2HPO_4 8.1, KH_2PO_4 1.9, pH 7.6.

4) The external control solution had the following composition (mM): NaCl, 98; $MgCl_2$, 1; $CaCl_2$, 1.8.

Different pH buffers were used for the various pH values: for pH 6.5, Mes 5 mM was used; Hepes 5 mM was employed for pH 7.0 and 7.5, while for pH 8.0 the buffer was Taps 5 mM. The final pH values were adjusted with HCl and NaOH. Substrates were added at the indicated concentrations to the appropriate solutions.

The non-hydrolyzable substrate Gly-Sar was used for confirmatory intracellular injection experiments. A volume of 50 nl of a concentrated solution (200 mM Gly-Sar in pH 7.5 buffer) was injected; leading to an approximate final concentration of 20 mM (assuming an oocyte volume of about 500 nl).

All substrates for electrophysiology experiments were procured from Sigma, Milan, Italy. Irbesartan was a gift from Sanofi-Aventis.

Experiments were performed at room temperature (20–25 °C) except during the studies on the effects of temperature; where a range of temperature (20-30^{o}C) was used.

CHAPTER 3 RESULTS

3.1 PRESTEADY-STATE CURRENTS

The PepT1s of rabbit (rbPepT1), seabass (sbPepT1), and zebrafish (zfPepT1) exhibit presteady-state currents in the absence of organic substrate. Figure.3.1 compares the currents induced in each isoform by voltage pulses in the absence and presence of saturating Gly-Gln at pH 6.5. Although experiments have been performed in a more extended range (6.0–8.0), pH 6.5 seems to be close to the real physiological conditions, at least in rabbit PepT1 (based on the pH of the luminal surface of the mammalian small intestine) (Thwaites & Anderson, 2007).

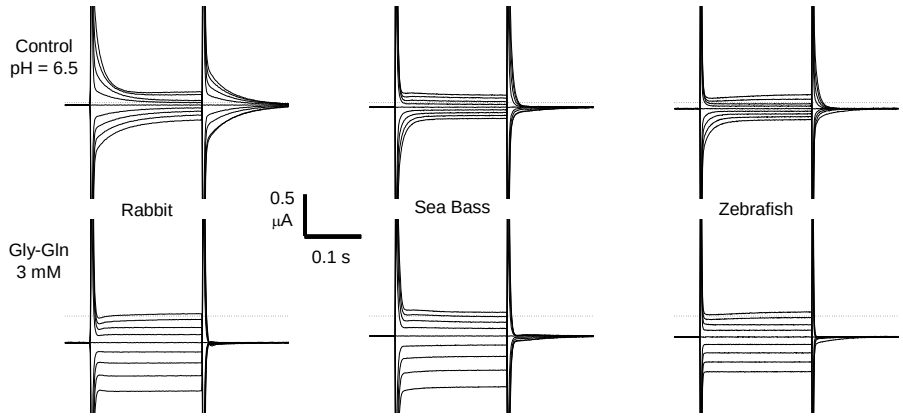

Figure 3.1 Comparison of PepT1 presteady-state currents from three species. In the absence of organic substrate (top row), all three transporters display slowly decaying transients in response to "on" and "off" voltage steps. The bottom row shows the steady currents induced in the same oocytes by the addition of 3 mM Gly-Gln and the simultaneous disappearance of the presteady-state currents.

Although the presteady-state currents of rbPepT1 and sbPepT1

have already been described and analyzed (Nussberger *et al.*, 1997;Sangaletti *et al.*, 2009), information on zfPepT1 is lacking. As shown in Fig.3.1 (top row), the two fish species, exhibited larger currents for hyperpolarizations than for depolarizations, while the transients from rbPepT1 are approximately symmetrical around the -60 mV holding potential. Adding saturating amounts of organic substrate (3 mM Gly-Gln) elicited steady transport currents (Fig.3.1, bottom row) and, as commonly observed in most electrogenic transporters, abolished the presteady-state currents.

The presteady-state currents were separated from the fast peaks due to the endogenous oocyte capacity, using two different procedures (see Materials and Methods for details). In the first, a double exponential function has been fitted to currents recorded in the absence of substrate. In the second, the current traces in the presence of saturating substrate have been subtracted from those in its absence and a single exponential fitted to the difference. In both cases, steady transport currents were subtracted before fitting the exponentials.

As previously observed (Mertl *et al.*, 2008;Sangaletti *et al.*, 2009), the two methods give virtually identical results. This is relevant not only to better understand the transporter mechanism, but is also important because of the intrinsic limitations of the two-exponential method. Namely, the separation of two exponentials by fitting is impossible when the two time constants are close in value. Because the time constants for charging the oocyte membrane capacity are generally around 1 ms, the two-exponential method becomes unreliable when the decay time constant of the presteady-state currents approaches this value (i.e., 2–3 ms). This is indeed the case

for both fish species at the most positive potentials explored (see below). In addition, both rabbit and seabass PepT1 exhibit an acceleration of the presteady-state current decay at alkaline pH (Nussberger *et al.*, 1997;Sangaletti *et al.*, 2009). For these reasons, the subtraction method has been used to isolate these currents.

3.2 TRANSPORT CURRENTS

The transport currents generated by rabbit, zebrafish, and seabass PepT1 have been previously studied (Kottra & Daniel, 2001;Sangaletti *et al.*, 2009;Steel *et al.*, 1997;Verri *et al.*, 2003). These three isoforms show a similar trend: in all cases, acidic external pH increases substrate affinity, but it either decreases (Kottra & Daniel, 2001;Verri *et al.*, 2003) or does not affect (Sangaletti *et al.*, 2009;Steel *et al.*, 1997) the maximal current. These features are illustrated in Fig.3.5 for the rabbit transporter; very similar curves can be observed for the zebrafish (Verri *et al.*, 2003) and seabass isoforms (Sangaletti *et al.*, 2009). In human PepT1, on the other hand, high acidity increases both substrate affinity and I_{max} (Fei *et al.*, 1994; Mackenzie *et al.*, 1996).

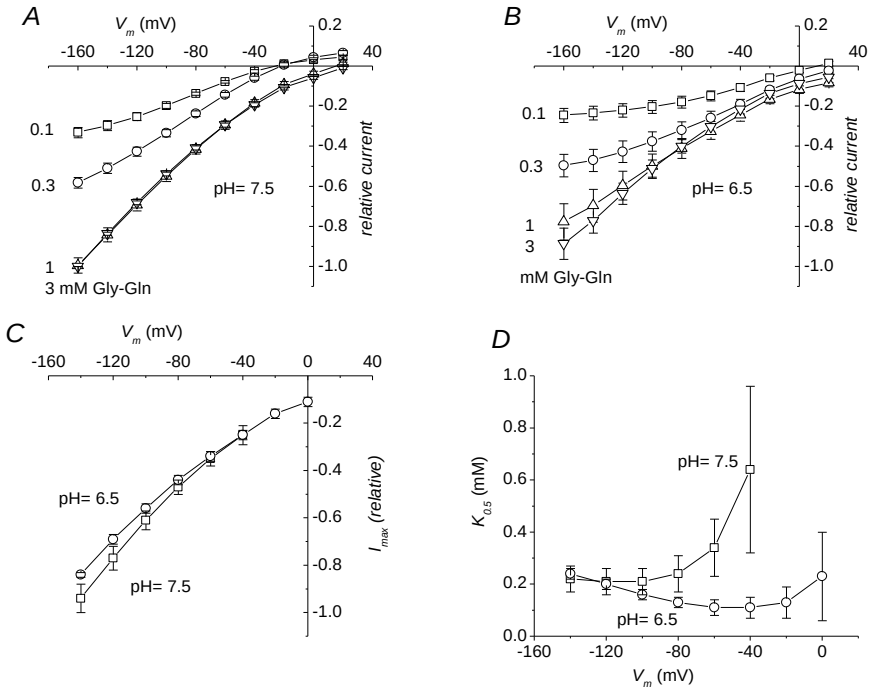

Figure.3.2 Transport-associated current from rabbit PepT1. Top row: I/V relationships of the transport-associated currents (substrate present minus substrate absent) at pH 7.5 (A) and 6.5 (B). Bottom row: values of I_{max} (C) and K_{05} (D) obtained by fitting the concentration-current relationships from (A and B) with the Michaelis-Menten equation.

The decrease in I_{max} at acidic pH in rabbit and fish transporters is unexpected given that the inwardly directed proton electrochemical gradient increases. This effect, however, might be explained by a decreased cycling rate related to the slowing of the charge movement caused by protonation (see (Renna *et al.*, 2011).

A useful index of the overall transport efficiency (Figure 3.3) is given by the ratio I_{max}/K_{05}, which is the slope of the Michaelis-Menten relationship at zero substrate concentration. The largest difference in efficiency, in favor of the more acidic solution in the physiological range of membrane potential, was observed in the rabbit transporter;

there was no significant difference in the zebrafish. This is in line with the acidic pH of the small intestine of rabbit but alkaline pH in zebrafish (Nalbant *et al.*, 1999).

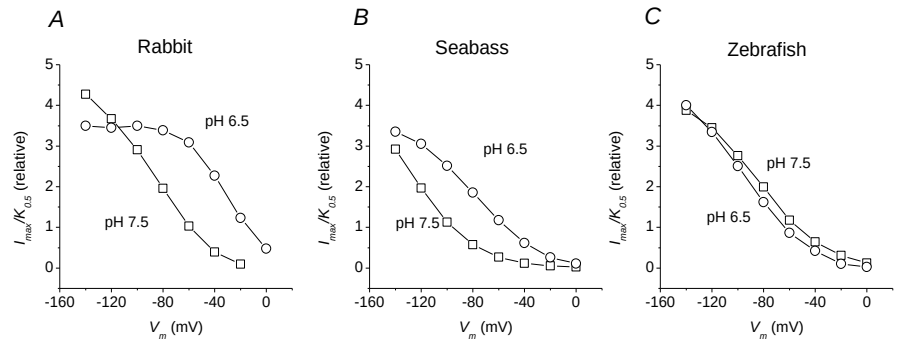

Figur.3.3 Transport efficiency. Plots of the ratio of relative I_{max}/K_{05} for rabbit (A) seabass (B) and zebrafish (C).

3.3 TEMPERATURE AND TRANSPORT KINETICS OF PepT1

A close look at Figure 3.2 shows marked differences in the kinetic behaviour of the proteins. In particular, at the same temperature the two fish isoforms show similar rates of decline of the presteady-state currents, while in rabbit PepT1 they are much slower. Furthermore, the voltage dependence of the intramembrane charge movement and of the rate of decline in the fish isoforms are significantly shifted toward more negative potentials compared to the rabbit isoform.

On the basis of these considerations, it may be hypothesized that the rabbit isoform of PepT1 exhibits slower kinetics at 22 – 24 °C compared to the fish isoforms because it is adapted to work at

temperatures around 37 °C, while the fish PepT1s may work optimally at this temperature. If the effect of increasing temperature on PepT1 is similar to those observed in GAT1 and SGLT1, i.e. an acceleration of the decay rate, accompanied by a shift towards more negative potentials of the presteady-state currents, then we may expect that the characteristics of rbPepT1 at its physiological temperature will approach those of sbPepT1 and zfPepT1 at lower temperature. Therefore, we examined the effects of temperature on PepT1 functions.

3.3.1 Temperature effects on rbPepT1 transport current

Raising the temperature of the bathing solution from 20 to 30 °C produces a strong increase in the transmembrane current generated by the activity of PepT1 exposed to 3 mM Gly-Gln. Sample records from the same oocyte are shown in Figure 3.4A. The traces are the recordings of the membrane current in response to a staircase voltage-clamp protocol from -120 to +40 mV from V_h = -40 mV. Black color denotes the currents in the absence of substrate, while the red traces are the currents in the presence of 3 mM Gly-Gln. The presteady-state currents in response to each voltage jumps are visible in the black traces but not in the red ones (arrows).

The average current-voltage relationships for the steady-state transport current from several oocytes tested at the three temperatures are plotted in Figure 3.4B, showing a large increase with higher temperatures. Figure 3.4C is an Arrhenius plot of the transport current amplitude at the various voltages, from which the activation energy of

the overall process can be estimated. According to the Arhenius equation:

$$\ln K = A - \frac{E_{act}}{RT}$$

the slope of these lines corresponds to E_{act}/R where R is the gas constant, and E_{act} is the activation energy of the transition.

Energies amounting to about 93 kJ/mol at -120 mV and to 72 kJ/mol at -40 mV were found from this analysis. These values are close to those reported from other transporters (Hazama *et al.*, 1997;Hilgemann & Lu, 1999;Wadiche & Kavanaugh, 1998;Zeuthen & MacAulay, 2012)

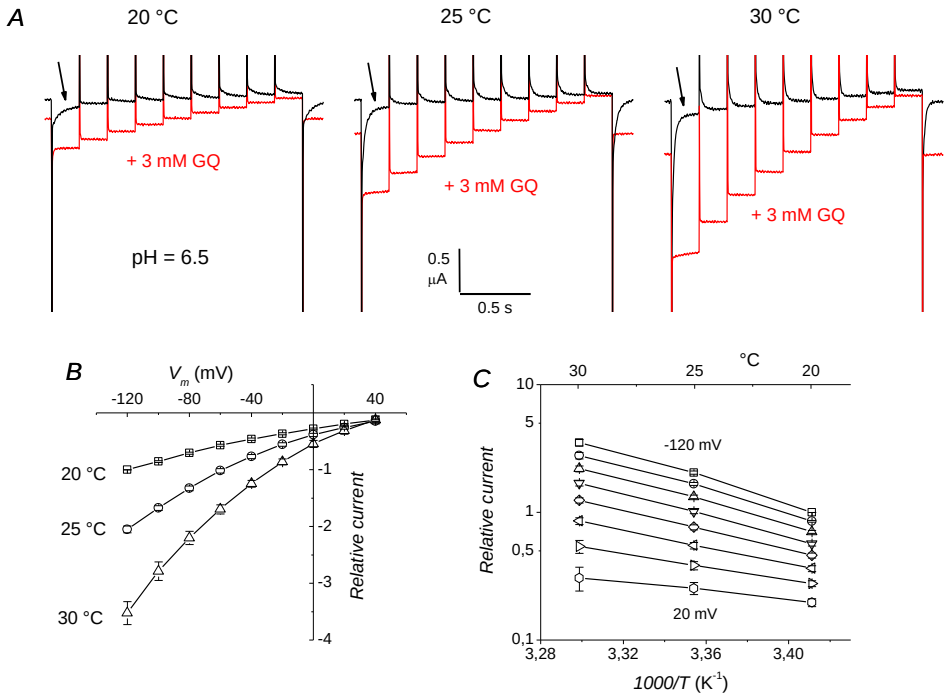

Figure 3.4. Temperature effect on the transport current at pH 6.5. A: representative recordings of the current before (black) and during (red) application of 3 mM Gly-Gln (GQ) in the same oocyte at the three indicated temperatures, and pH = 6.5. The voltage protocol consisted in a staircase of voltage steps from -120 to +40 mV in 20 mV increments, lasting each 200 ms from a -40 mV holding potential. The arrows point to the presteady-state currents visible in the absence of substrate. B: Voltage-dependence of the transport current (substrate present minus substrate absent) at the indicated temperatures. Values are mean ± SE from 9 oocytes (2 batches). Data have been normalized to the current value at -120 mV and 20 °C for each oocyte before averaging). C: Arrhenius plot of the current as a function of temperature at the different voltages.

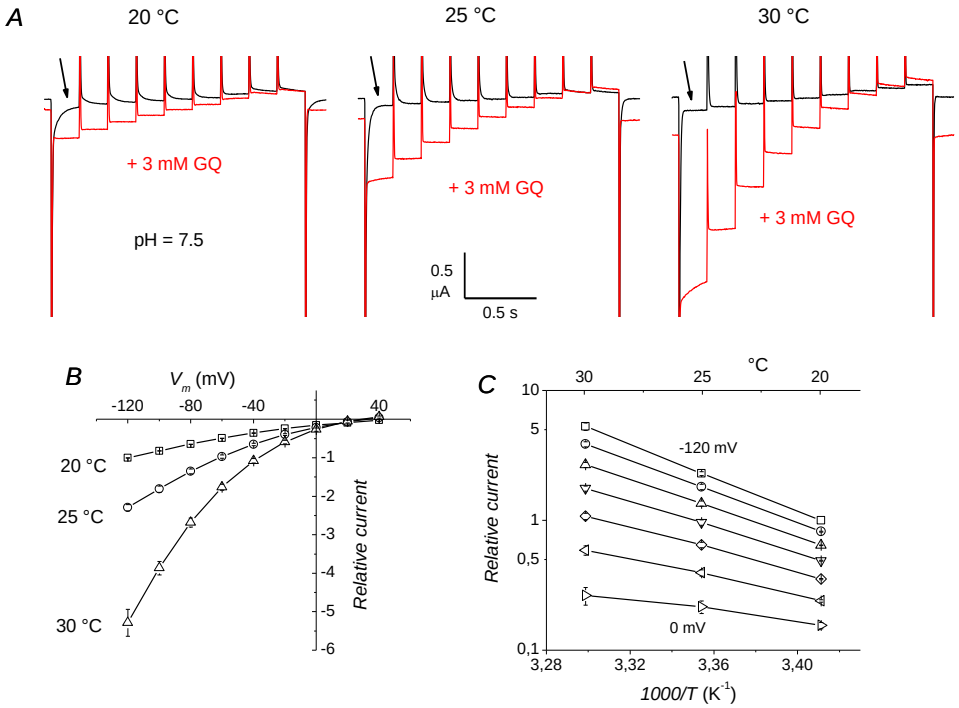

Fig. 3.5. Temperature effect on the transport current at pH 7.5. A: representative recordings of the current before (black) and during (red) application of 3 mM Gly-Gln (GQ) in the same oocyte at the three indicated temperatures. Same voltage protocol as in Fig. 3.4. Note the faster decline of the presteady-state currents compared to pH 6.5 (arrows). B: Voltage-dependence of the transport current (substrate present minus substrate absent) at the indicated temperatures. Values are mean ± SE from 8 oocytes (2 batches). Data have been normalized to the current value at -120 mV and 20 °C for each oocyte before averaging). C: Arrhenius plot of the current as a function of temperature at the different voltages.

Similar results were found at pH 7.5 (Fig. 3.5). The activation energies calculated from the data of Fig. 3.5C were 123.0 and 82.3 kJ/mol at -120 mV and -40 mV, respectively. The reliability of the apparent increase of E_{act} at -120 mV at this pH, compared to the value at pH 6.5, is however doubtful, given the lack of stability in the

transport current in these conditions (see Fig. 3.5A, rightmost panel, and (Renna *et al.*, 2011).

3.3.2 Temperature effects on rbPepT1 presteady-state currents

The effect of temperature on the presteady-state currents (pss) of PepT1 was already visible in the recordings of Figure 3.4A that show a progressively faster decline of these transient currents as the temperature is increased. As mentioned above, this kind of effect was already reported in other ion-coupled cotransporters (Binda et al., 2002) and reflects the acceleration in the rate constants of the intramembrane charge movement that underlies these currents. At pH 7.5 the acceleration of the decline rate induced by temperature adds up to that caused by the alkaline pH itself (Bossi *et al.*, 2011; Renna *et al.*, 2011). This combined effect makes it difficult to perform a reliable analysis of the presteady-state currents in these conditions, and for this reason we have limited this part of our study to pH 6.5.

Figure 3.6A shows sample recordings of the presteady-state currents in the same PepT1-expressing oocytes at four different temperatures. It can be seen that in addition to causing a faster decline, higher temperature produce a progressive shift of the transients towards more negative potentials. This kind of effect was already reported in two other transporters belonging to different families, i.e. SGLT1 (Hazama et al., 1997), and GAT1 (Binda et al., 2002). At the higher temperature tested (30 °C, Figure 3.6A), the combination of these two effects produces recordings that resemble those that can be

obtained in the Zebrafish isoform of PepT1 at 20 °C (Figure 3.6B and (Renna et al., 2011)).

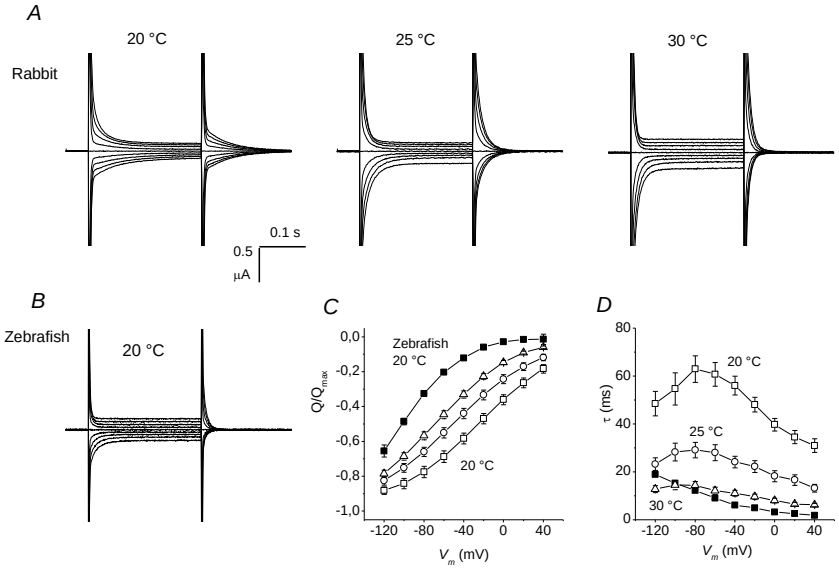

Figure 3.6. Effects of temperature on the presteady-state currents. A: representative recordings of the currents induced by voltage jumps from V_h = -40 mV (range-120 - +40 mV in 20 mV steps) in a rbPepT1-expressing oocyte at the indicated temperatures and pH = 6.5. B: recordings from an oocyte expressing the zebrafish isoform of PepT1 at 20 °C are shown for comparison. C: charge-voltage relationship obtained by integration of the transients after isolation of the presteady-state currents (open symbols: rbPepT1 at the three temperatures; solid squares. D: voltage dependence of the time constant of decline (same symbols as in C). Data from rbPepT1 are averages ± SE from eleven oocytes (two batches).

A more complete analysis of presteady-state currents at different temperatures is presented in Figure 3.6C and D. The voltage dependence of the intramembrane charge movement, obtained by integration of the isolated presteady-state currents, is plotted in Figure 3.6C for rbPepT1 (open symbols) as average curves after normalization to the maximal moveable charge (Q_{max}). The values of

the decline time constant are plotted in Figure 3.6D, quantitatively showing the acceleration produced by the higher temperatures. In both Q_{in}-V and τ-V graphs, the leftward shift induced by higher temperatures is evident, and this suggests that a further increase in temperature (considering that the rabbit physiological temperature is 38 – 39 °C) may bring both curves to approach those obtained in PepT1 isoforms from lower temperature-adapted animals, such as those for zebrafish, plotted as solid squares in Figs 3.6C and D.

The voltage dependence of the unidirectional rate constants of the charge movement can be derived from the experimentally determined values of Q_{in} and τ (Bossi *et al.*, 2011), using the relations:

$$inrate = \frac{1}{\tau}\frac{Q_{in}}{Q_{\max}}$$

$$outrate = \frac{1}{\tau}\left(1 - \frac{Q_{in}}{Q_{\max}}\right) \qquad \text{(see eq. 2.3)}$$

Plots of these rates, calculated in this way for each individual oocyte before averaging, are presented in Figure 3.7A for the three tested temperatures, and they show that the two rates are differently increased by temperature: that is the outward rate is affected more strongly than the inward rate, and this fact explains the shift towards negative potentials observed in the Q and τ values.

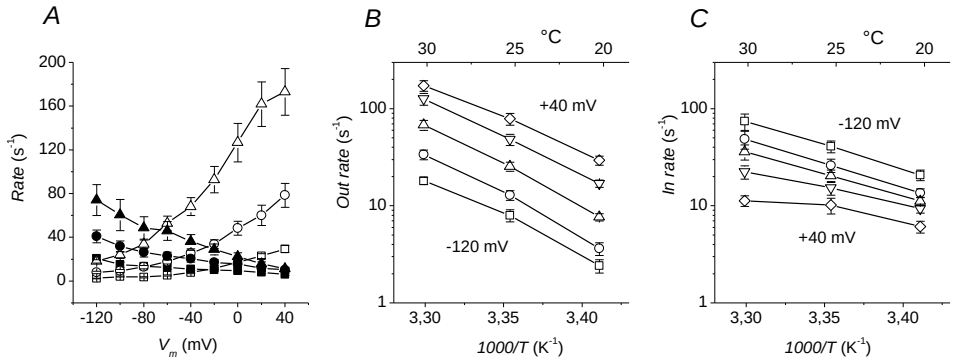

Figure 3.7. Temperature dependence of unidirectional rate constants. A: inward (solid symbols) and ouward (open symbols) rates obtained from the same oocytes of Fig. 3.6C and D. The effect of temperature is clearly stronger on the outward rate compared to the inward. B and C: Arrhenius plots for the outward and inward rate, respectively. All values are means ± SE

The Arrhenius plots showing the weaker temperature dependence of the inward rate are presented in Figures 3.7B and C.

The values of Eact were then calculated for each individual oocyte from a linear fit of the data such as in Fig. 3.7 and then averaged. The resulting values are plotted in Figure 3.8 as a function of voltage (open symbols). These graphs show that the activation energy for the outward charge movement is much larger than that involved in the inward charge movement. Furthermore, the filled symbols in Figure 3.8 represent the values of the activation energy derived from the Arrhenius plot shown in Figure 3.4C, that is, for the entire transport cycle. Interestingly, these values are quite close to

those calculated for the inward charge movement in the absence of organic substrate. The probability that these two sets of values are different is less than 20% at all voltages while, on the contrary, the difference between E_{act} for the inward charge movement and for the entire cycle is highly significant at all voltages ($P < 0.001$ level, T test in both cases)

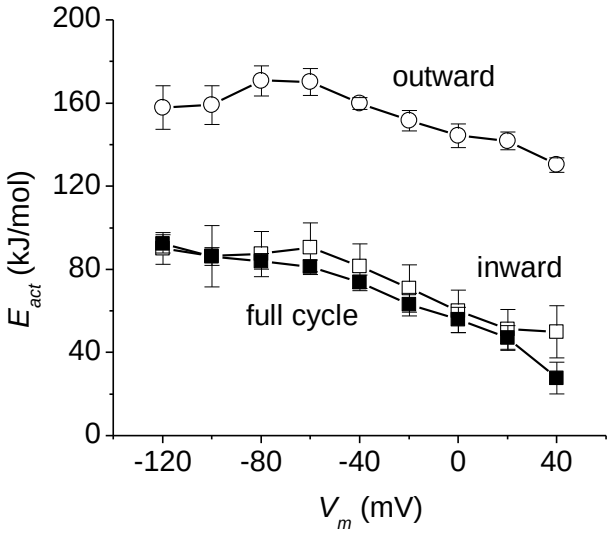

Figure 3.8. Voltage dependence of the activation energies. E_{act} for the inward and outward charge movement in the absence of substrate, calculated from the data of Fig. 3B and C are shown with the open symbols as functions of membrane voltage. Filled squares are the activation energy derived from Fig. 3.4C, concerning the complete transport cycle. All values are means ± SE. All values for the full cycle are significantly different from those of the outward rate ($P < 0.001$, Student T test), while they are not significantly different from those of the inward rate.

3.3.3 Affinity changes with temperature

The effects of temperature on the rates of charge movement suggest that the apparent substrate affinity might also be affected. We

have then performed dose-response experiments at two fixed temperatures (20 and 30 °C) in the same oocytes, in order to determine the maximal transport current (I_{max}) and the apparent affinity in terms of the substrate concentration eliciting half of the maximal current ($K_{0.5}$). The results, obtained using the same voltage protocol as in Fig.3.4 are illustrated in Fig. 3.9. The different shape of the I-V relationships at the two temperatures is shown in Fig. 3.9A and B, while the kinetic parameters, obtained after fitting a logistic equation to the data plotted as dose response curves, are shown in Fig.3.9C and D.

The maximal current increases almost four times at 30 °C relative to 20 °C, confirming that the 3 mM substrate concentration used in the experiments of Fig.3.4 is close to saturation. The values of $K_{0.5}$ are U-shaped, as already reported (Renna *et al.*, 2011;Sala-Rabanal *et al.*, 2006). Interestingly, a shift of this curve toward more negative potential is observed at the higher temperature. This shift produces a statistically significant increase in the value of $K_{0.5}$ (and therefore a decrease in apparent affinity) at 30 °C for membrane potential more positive than -60 mV, ($P < 0.01$, T test), confirming the expectations. To assess the overall gain, or loss, of efficiency of the transport activity at the two temperatures, the ratio $I_{max}/ K_{0.5}$ was calculated, and it is plotted in Fig. 3.9E. From these graphs a gain in efficiency is apparent at the higher temperature when the membrane potential is more negative than -20 mV.

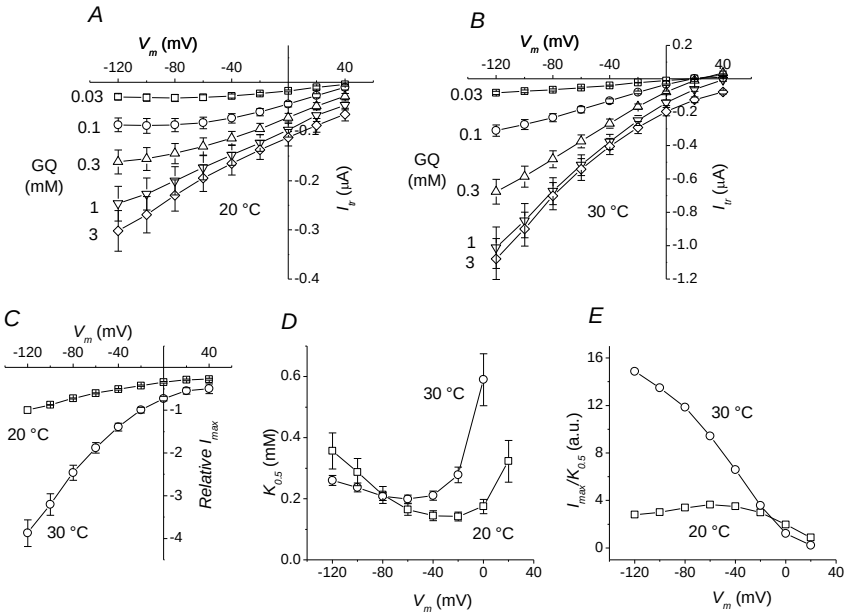

Figure 3.9. Effect of temperature on the kinetic parameters of transport. A and B: voltage dependence of the transport current elicited by the indicated substrate concentrations at 20 and 30 °C, respectively. Data are means ± SE from 10 oocytes (two batches). C: plots of I_{max} obtained by fitting a logistic equation to the dose-response curves from the same oocytes as in A and B, normalized to the current at -120 mV and 20 °C in each oocyte before averaging. D: plots of the substrate concentration eliciting half of I_{max} obtained from the same fitting. E: plot of the $I_{max}/K_{0.5}$ ratio from the data of panels C and D (arbitrary units). The $K_{0.5}$ values at the two temperatures are significantly different ($P < 0.01$) from each other for voltages ≥ -40 mV

3.4 REVERSE MODE OF OPERATION IN PEPT1

The question of reverse operation is a relevant issue in many cotransport systems, especially in the context of neurological disorders in which leakage of neurotransmitters into the extracellular space may have profound consequences. Although the physiological role of these transporters is reuptake, in several instances a release of neurotransmitter via the transporter has been reported. This reversed

mode of operation may be either the effect or the cause of abnormal or pathological conditions. In the case of the glutamate transporters, export of glutamate may lead to the elevated extracellular levels that cause excitotoxicity (Rossi *et al.*, 2000), while in the SLC6 family reversal of the operation of the dopamine transporter is caused by amphetamines (Khoshbouei *et al.*, 2003;Seidel *et al.*, 2005), and release of GABA through GAT1 has been hypothesized to concur in causing epileptic seizures (Richerson & Wu, 2003;Richerson & Wu, 2004).

To my knowledge, no indications of pathological conditions have been related to a reverse operation by PepT1, however this transporter is apparently capable of reverse transport especially when the external organic substrate concentration is low and the pH is alkaline (Kottra *et al.*, 2009;Kottra & Daniel, 2001;Verri *et al.*, 2003). Given the numerous functional and biophysical similarities among transporters belonging to different families, the study of the reverse transport in PepT1 was undertaken in order to compare its characteristics to those of the neurotransmitter transporters.

Mutational studies of Pept1 have helped to established vital amino acid residues in its operation. For example, His 57 ((Fei *et al.*, 1997) and tyrosine residues around His 57 (Pieri *et al.*, 2009) have all been shown to be important for the functioning of the transporter. In addition to these, arginine 282 and asp 341 have been reported to function as electrostatic gate in the transporter (Bossi *et al.*, 2011).

Previous reports from rabbit PepT1 (Meredith, 2004;Meredith, 2009;Pieri *et al.*, 2008) have suggested that two well-conserved

residues, arginine 282 and aspartate 341, may form a charge pair playing an important role in the transport function. The position of these two residues is shown in figure 3.10.

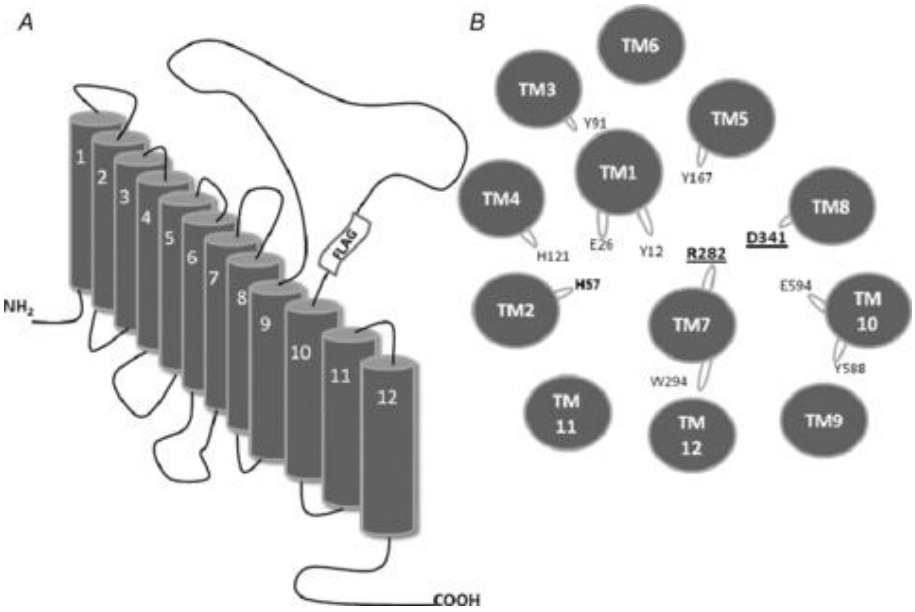

Figure 3.10. Cartoon of PepT1 topology and helical distribution

Representative traces from the various isoforms are shown in figure 3.11. All R282 mutants are able to generate pre-steady-state currents in the absence of substrate, as well as transport-associated currents with amplitudes comparable to the wild-type, while the currents observed in the D341R form were smaller, and neither transporter-related nor pre-steady-state currents could be observed in the double mutant R282D–D341R and in H57R (Bossi *et al.*, 2011). Also it can be observed that there are slowly developing outward currents visible in some of the records at the most positive pulses.

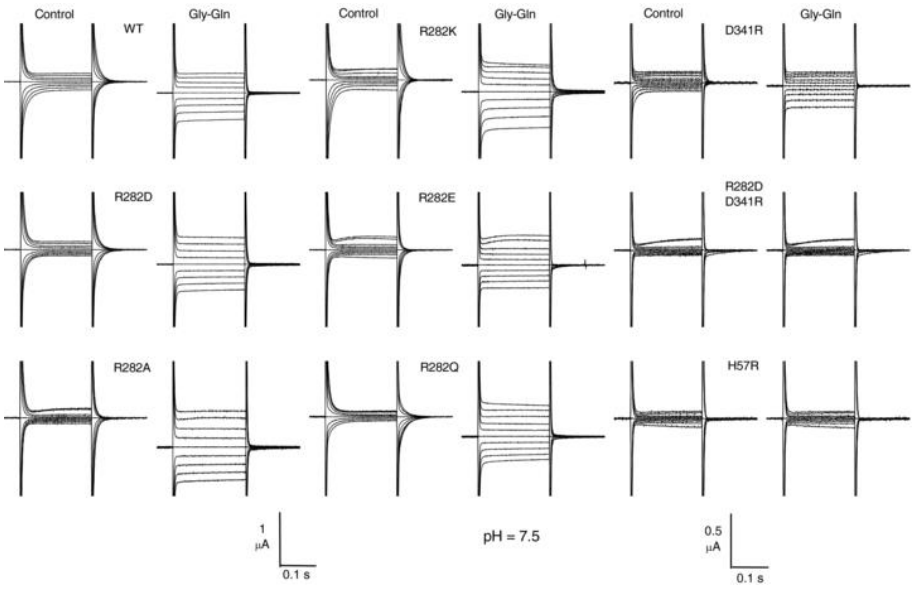

Figure 3.11. Current responses to voltage pulses from −140 to +20 mV (from V_h=−60 mV) in the absence and presence of substrate at pH 7.5 in the wild-type and indicated mutants of the rabbit PepT1

Given this background, the following studies have been carried out both in the wild type and different arginine mutants of the transporter.

3.4.1 Membrane expression of the FLAG protein

Immunolocalization experiments were performed to understand whether the various mutants were correctly inserted in the oocyte membrane. Representative images are shown in Fig.3.12 A. The negative controls (non-injected oocytes and oocytes expressing a wild-type transporter with no FLAG), gave no visible signal in the membrane of the oocytes. All the other isoforms were correctly localized in the membrane to a variable extent. These observations were confirmed by the single-oocyte chemiluminescence (SOC) experiments that were performed on larger numbers of oocytes from different batches (Fig.3.12 B). All functional mutants were present in

the membrane at levels similar or greater than the wild-type, in agreement with previous results (Kulkarni *et al.*, 2007). Our data also confirm the correct membrane localization of the non-functional mutant H57R (Uchiyama *et al.*, 2003). However, the double mutant R282D-D341R gave only very weak signals in both the immunolocalization and in the chemiluminescence experiments.

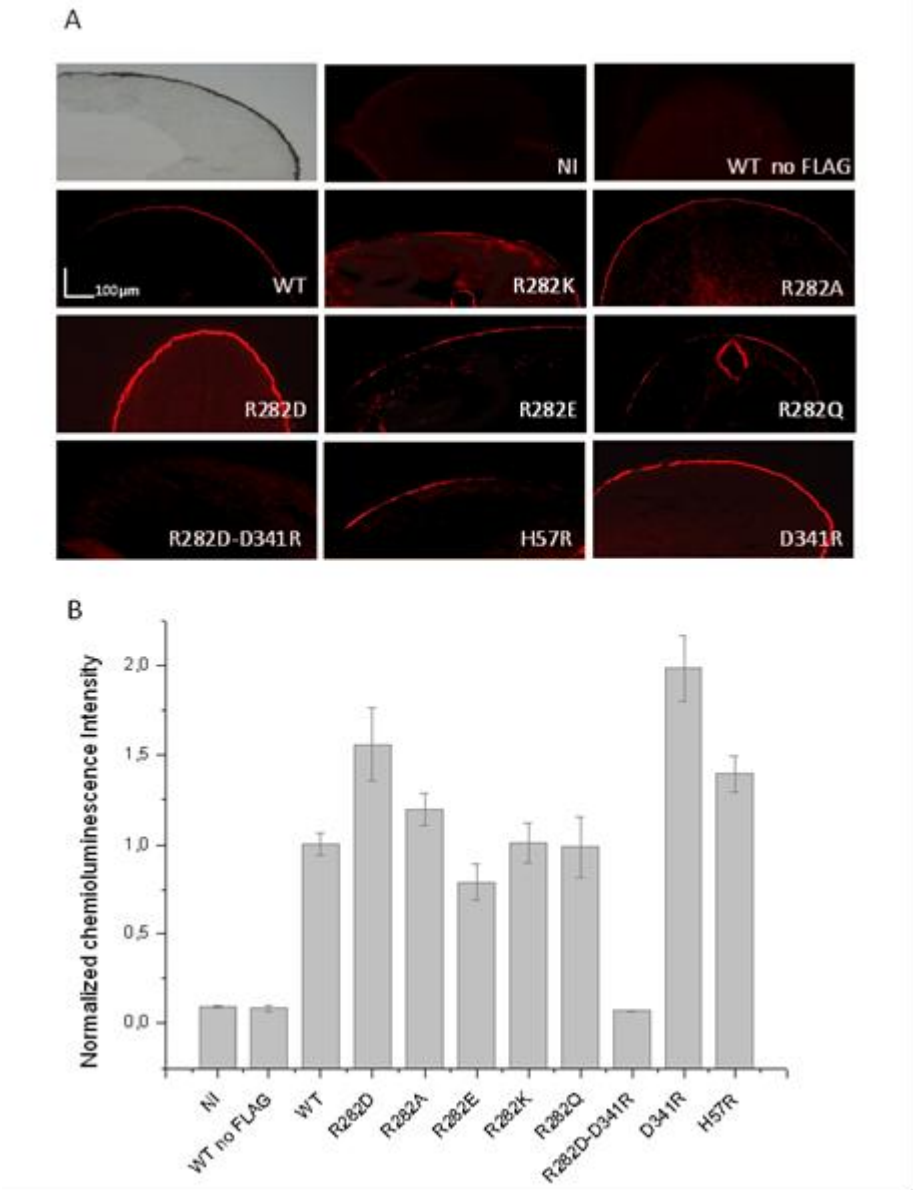

Figure 3.12. Surface expression of rbPept1wt and mutants. Immunohistochemistry (A) and chemiluminescence experiments (B) of oocytes expressing FLAG-rbPepT1 wt and the indicated mutants.

These results are generally well correlated to the electrophysiological observations: the lack of transporter-associated

currents seen in the R282D-D341R double mutant is paralleled by the weak luminescence signal in Fig.3.12 for this isoform, while the large currents displayed by the R282 mutants are in agreement with the strong signals of the localization and luminescence experiments. On the contrary the small presteady-state and transport currents recorded in the H57R and D341R forms are in contrast with the large membrane expression seen in the results reported in Fig.3.12. Based on these observations, the reduced functionality of this last mutant appears to be attributable to a defect in the molecular mechanism rather than to insufficient targeting to the membrane.

The presteady-state currents generated by the functional mutants maintained the sensitivity to external pH by showing a shift towards more negative potentials at more alkaline pH, as illustrated in Fig.3.13 for the R282D mutant. The isolated currents were analysed as explained in the Method, and the results of this analysis are plotted in the bottom row of Fig.3.13, showing the accelerating action of alkaline pH on the time constant and the shift towards more negative potentials induced by this pH on both τ/V and Q/V curves. Fitting a Boltzmann equation [eq.2.1] to the R282D data of Fig.3.13 gives $V_{0.5}$= -45 ± 0.9 mV at pH 7.5, and 7.8 ± 6 mV at pH 6.5 in this group of oocytes.

The estimated maximal moveable charge appears to remain substantially constant (41.4 ± 0.8 nC at pH 7.5 *vs* 37.6 ± 3.1 nC at pH 6.5), although these data are subject to significant errors especially at pH 7.5 because of lack of saturation at positive potentials. The comparison with the wild-type data (filled symbols in Fig.3.13) shows that at the same pH the decay time constants of the R282D mutant are

shorter and that both τ/V and Q/V curves of the mutant are shifted towards more positive potentials ($V_{0.5}$ = -59.2 ± 1.3 mV at pH 6.5 in this group). These effects were also seen, to various degrees, in all other arginine mutants.

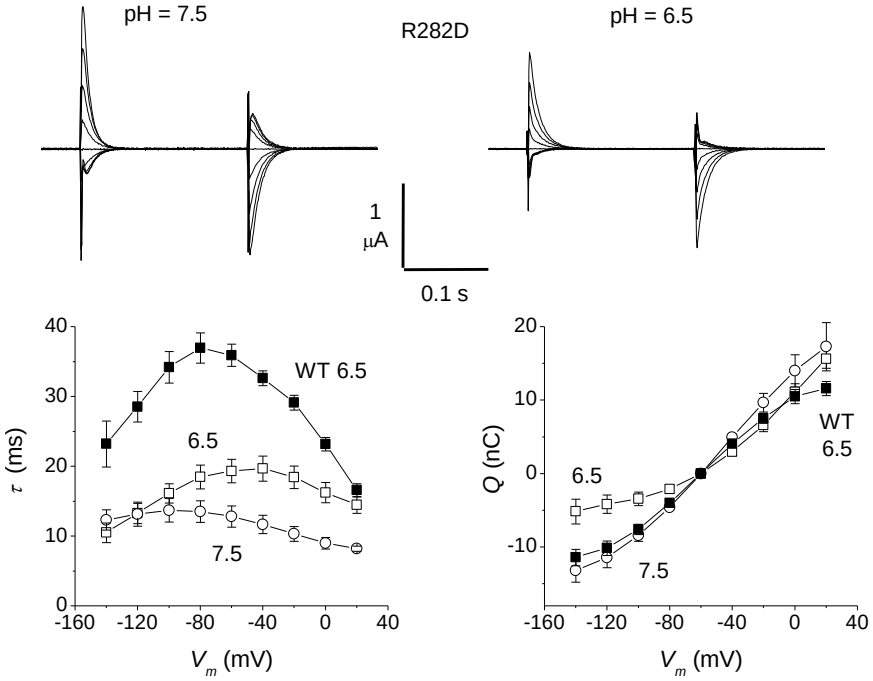

Figure3.13 Mutants in the charge-pair residues were pH-sensitive.Top row: traces of pre-steady-state currents isolated using the subtraction method in a representative oocyte expressing the rabbit R282D mutant at the two indicated pH values. Bottom row: values of the time constant of decay and of the amount of displaced charge at the two pH values.

3.4.2 Outward currents in PepT1

As mentioned above, outward transport currents have been observed in wild-type PepT1 when depolarizing pulses of relatively short duration (50–250 ms) are applied with the voltage-clamp technique from negative (−40, −60 mV) holding potentials (Kottra *et*

al., 2009;Kottra & Daniel, 2001;Verri *et al.*, 2003). In the wild type PepT1, these outward currents are most easily seen at alkaline pH and relatively low substrate concentrations, since increasing the concentration of either substrate or H^+ shifts the current-voltage relationships to more positive potentials, eventually bringing the reversal potential (E_{rev}) of the transport current out of the experimental range (Verri *et al.*, 2003).

Interestingly, some mutants in arginine 282, that were previously shown to act as electrostatic gates in the transport mechanism (Bossi *et al.*, 2011)are capable of conducting quite large outward currents, as shown in Figure 3.14.

The *I/V* relationships plotted in Figure 3.14b show that in the same conditions of pH and substrate concentration the value of E_{rev} becomes progressively more negative as the positive charge of arginine is first neutralized to alanine and then changed in sign with aspartate. Moreover, the R282D mutant (but not R282A) generated significantly larger currents than the wild type. On the contrary, reverting the sign of the negative aspartate 341 to a positive arginine produces a transporter that is still functional but shows reduced transport currents and no reversal in the explored voltage range. In the group of oocytes illustrated in Figure 3.14, the average currents at −140 mV were: 568 ± 58 nA for wild type, 998 ± 172 nA for R282D, 464 ± 94 nA for R282A, and 184 ± 35 for D341R (mean ± SE, n = 4–7).

Another evident feature in the traces of the transport currents generated by the R282D and R282A mutants is the slow decline

during the voltage pulse (arrows in Figure 3.14a), a behavior that may suggest either the existence of a deactivating process or a progressive reduction in the driving force.

Figure 3.14c shows estimates of the surface expression of the various isoforms, obtained with the SOC method. The level of membrane localization is in good correlation with the transport-associated current in the case of the wild-type transporter and of the R282D and R282A mutants, but not for D341R, which, in spite of being highly expressed on the oocyte membrane, generates much smaller currents compared to the other isoforms. These observations suggest that the reduced functionality of D341R may be attributable to a malfunctioning in the molecular mechanism rather than to defective targeting to the membrane.

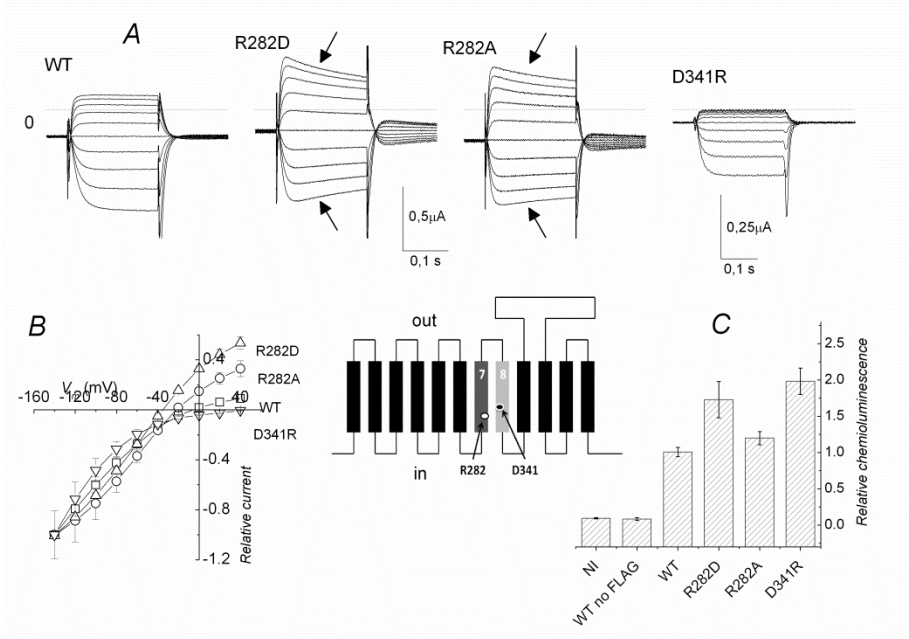

Figure 3.14 ***A*** *Representative transport currents recorded in the wild-type and indicated mutants in the presence of 1 mM Gly-Gln at pH 8.0. Voltage pulses from −140 to +40 mV were applied from* V_h *= −60 mV. The dotted lines indicate the zero-current level and the arrows the declining behavior of the currents. Note the amplified scale for the D341R mutant.* ***B*** *I/V relationships, averaged after normalization for each oocyte to the current at −140 mV (mean ± SE, n = 4–7 from two batches).* ***C*** *Surface expression, reported as results of the chemiluminescence experiments from oocytes expressing the wild-type and the indicated mutants of PepT1-FLAG. The chemiluminescence detected from 20 to 40 oocytes; from three different batches secondarily labeled with peroxidase-conjugated goat anti-mouse, IgG-HRP is shown. The data were normalized to the mean value of the wild-type FLAG-PepT1 of each batch.*

In both R282D and R282A mutants, the reversal potential of the transport current is shifted by changes in either the proton concentration or the substrate concentration (Figure 3.14). This result suggests that the translocation of the two species occurs in a coupled fashion.

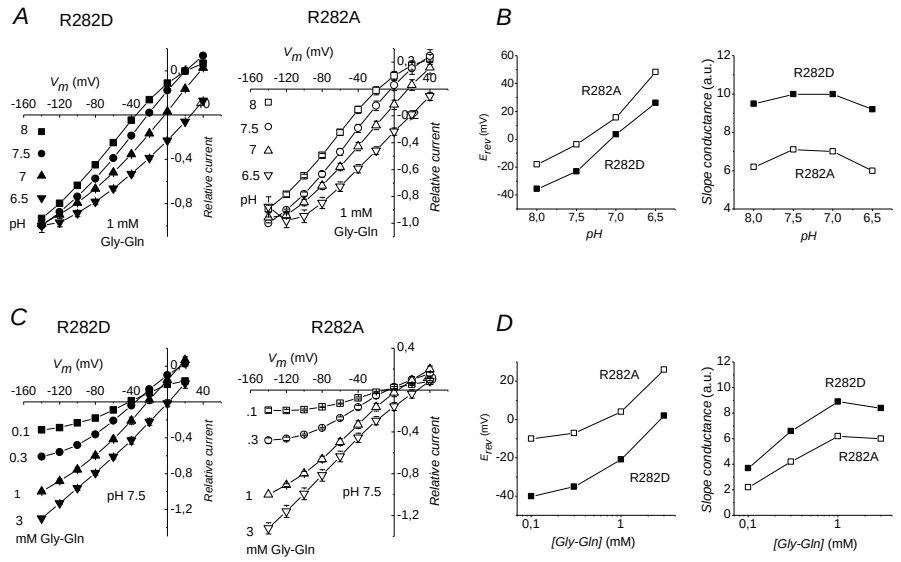

Fig. 3.15. I/V curves showing the effects of changing pH and substrate concentration on the R282D and R282A mutants. ***A*** *External alkalinization at fixed (1 mM) Gly-Gln concentration shifts the I/V curves towards more negative potentials. The change in* E_{rev} *with pH is shown in* ***B*** *for R282D (filled squares) and for R282A (open squares; these symbols are used throughout). No significant changes in the slope conductance at* E_{rev} *appear to be caused by alkalinization.* ***C*** *Positive shifts in the I/V curves produced by increasing the external Gly-Gln concentration at fixed pH (7.5) in the two mutants. The shifts in* E_{rev} *induced in this case are plotted in* ***D****, together with the slope conductance at* E_{rev}*; this parameter shows an increase at higher Gly-Gln concentrations. The current data were averaged after normalization for each oocyte to the current value at −140 mV and pH 7.5. Data points are mean ± SE (n = 4–5 from two batches). The slope conductance was calculated as the derivative of the relative I/V curve at* E_{rev}*. The value of* E_{rev} *for the R282A curve at pH 6.5 in* ***A*** *was linearly extrapolated.*

The shifts in E_{rev} caused by the pH and substrate changes in the mutants R282D and R282A are plotted in Fig. 3.15 b and d. The slopes of the E_{rev} versus pH curve are −42.3 and −43.7 mV/pH unit, respectively; although less than the 58 mV/pH unit predicted for a pure H^+ current on the basis of the Nernst equation, these values are

nevertheless consistent with a substantial contribution of H^+ to the current. Similarly, the semilog plots of E_{rev} versus [Gly-Gln] are not linear for both mutants (Fig. 3.15 d) with even lower slopes compared to the pH dependence.

We also estimated the slope conductance (g_{slope}) of the *I/V* curves at E_{rev}. This parameter is plotted in Fig. 3.15 as a function of pH and substrate concentration for both mutants. Interestingly, while g_{slope} increases with increasing concentrations of Gly-Gln (Fig. 3.15 d), it appears to be substantially independent from the proton concentration (Fig. 3.154b). This last result is contrary to the expectations for an electrodiffusive process, which would predict instead an increase in slope conductance when the concentration of the permeating species is raised (Hille, 2001).

3.4.3 Current reversal in the wild type and R282 mutants

The apparently anomalous effects mentioned above on the slope conductance around E_{rev}, prompted us to perform other experiments aimed at better understanding this phenomenon, both in the wild-type and in the R282D/A mutants. The necessity of further controls was also suggested by the declining behaviour seen in the current traces in Fig.3.14. Long-lasting voltage- and current-clamp experiments have been performed on both wild-type and R282D mutant to investigate this point. Fig.3.16 A shows voltage-clamp experiments in which the membrane voltage was stepped twice from -40 mV to +40 mV and back: the first step was given in the absence of substrate, and the second in presence of Gly-Gln 1 mM at pH 8. In these conditions, E_{rev} should be close to -30 mV in the R282D mutant.

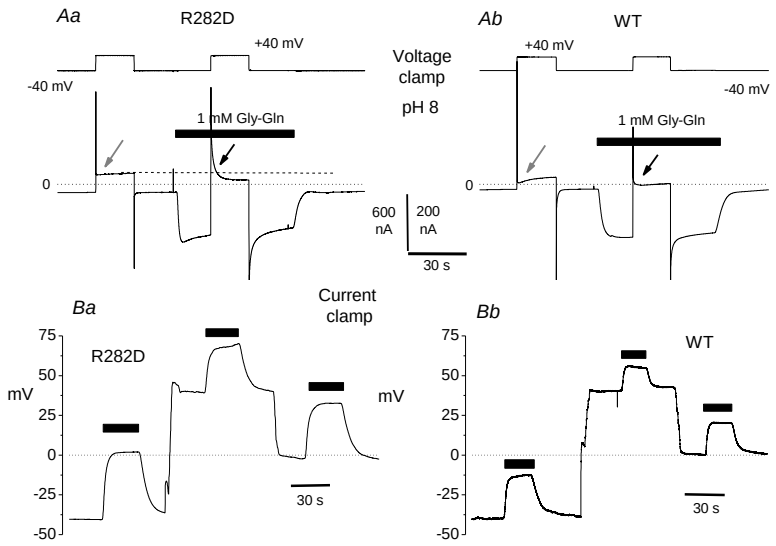

Figure 3.16 A: Long lasting records showing the slow deactivation process following step voltage changes in R282D and WT PepT1: during the first seconds after the jump at +40 mV the current in the presence of substrate is more positive than in its absence (gray arrow); however, at later times it becomes more negative; B: Current clamp recordings at pH 8 in R282D and WT PepT1: the addition of substrate induced depolarizations, implying that an inward current was generated by the transporter.

Fig.3.16 Aa shows that jumping to +40 mV when the transporter is activated by 1 mM Gly-Gln causes an instantaneous large outward current (black arrow) that declines with time constants in the order of fractions of seconds, and it is not seen in absence of the substrate (grey arrow). Initially the current is more positive than the value recorded at the same voltage in absence of substrate (dashed line), but at the end of the 20 s period at +40 mV it becomes less positive (that is, a negative current after subtraction). A qualitatively similar behaviour, although with smaller currents, was observed in the wild-type PepT1 (Fig.3.16 Ab).

Fig.3.16 B shows complementary experiments performed again on both wild-type and R282D with analogous results. The oocytes were kept in current-clamp conditions, i.e. an appropriate current was injected to keep the membrane voltage at a desired value before substrate application, but the membrane potential was left free to change as a consequence of transporter operation. The representative traces in Fig.3.16 Ba, from an oocyte expressing R282D, and in Fig.3.16 Bb, from an oocyte expressing wild-type PepT1, show that addition of 1 mM Gly-Gln at pH 8 (black bars) always induces a depolarization, irrespective of the starting value of the voltage (-40, 0 and +40 mV), indicating that using this experimental modality, the current generated by the transporter is in all cases in the inward direction.

3.4.4 The outward current is due to temporary accumulation of substrates

To discriminate whether the current decays seen in Figs 3.14 and 3.16 were due to changes in electrochemical gradient or to a transporter-intrinsic deactivation process, a series of experiments employing different strategies was performed. Fig.3.17 illustrates the results of a representative experiment using a protocol in which three fast (200 ms) voltage ramps ranging from +40 to -100 mV (or from -140 to +40 mV) were superimposed to a long lasting voltage step to +40 (or -140) mV in conditions inducing the decay of the transport current in both directions (pH 8, 1 mM Gly-Gln).

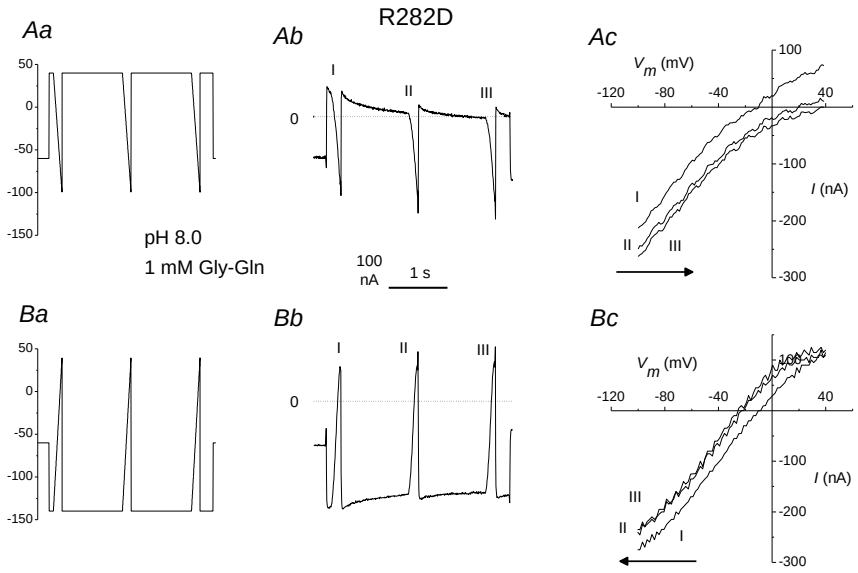

Figure 3.17. Step and ramps protocols to investigate the basis of the transport current decline. Ab and Bb show the subtracted (substrate minus control) transport currents: both records show the slowly declining currents, which are in the outward direction in Ab and in the inward direction in Bb. Ac and Bc: I/V relationships; in Ac the reversal potential moves toward more positive values with the second and third ramp, whereas in Bc the opposite behavior is observed. I/V curves remain substantially parallel to each other.

As shown in Fig.3.17. Ac and Bc, the *I/V* curves derived from the ramps shift along the voltage axis according to the application order and to the level of the long-lasting voltage pulse. The ramps superimposed to the depolarizing (+40 mV) pulse exhibit a progressive shift toward more positive potentials (Fig.3.17 Ac), while those applied during the pulse to -140 mV are moved with time toward more negative potentials (Fig.3.17 Bc). Interestingly, in both cases the curves remain parallel to each other, so that it may be

concluded that only the reversal potential is affected, not the conductance.

These observations represent a strong indication that the decline of the transport current during either the depolarizing or the hyperpolarizing pulses is due to substrate concentration changes in the vicinity of the transporters. In fact, as a consequence of the results of Fig. 3.15, that indicate a coupled proton-substrate translocation, E_{rev} may be written as a Nernst equation for the proton-substrate complex:

$$E_{rev} = \frac{RT}{F} \ln \frac{[TC]_{out}}{[TC]_{in}} \qquad \text{[eq.3.9]}$$

where TC stands for *transported complex*. Considering this equation, the results shown in Fig. 3.17 may be explained if the continuous inward flow during the hyperpolarizing pulse will increase $[TC]_{in}$ (and/or decrease $[TC]_{out}$) causing E_{rev} to change with time to more negative values, as observed in Fig.3.17 Bc. On the contrary, the initial outward current seen when stepping the potential from –60 to +40 mV (Fig.3.17 Ab) will decrease $[TC]_{in}$ (and/or increase $[TC]_{out}$) shifting E_{rev} to more positive potentials (Fig.3.17 Ac).

On the whole, the results shown in Fig.3.17 indicate that the outward current seen during short depolarizations is caused by a local accumulation of the transported complex at the intracellular side of the membrane and/or a local depletion of the complex at the extracellular side during the continuous inward transport occurring at the negative holding potential, confirming earlier suggestions (Kottra & Daniel, 2001).

In another series of experiments a prepulse lasting 2 s to +40 mV from V_h = -40 mV was applied to the membrane before moving

the potential to variable 1 s long test pulses (+40 to -140 mV). Fig.3.18 shows this kind of protocol applied to an oocyte expressing the R282D mutant at pH 7.5. Upon addition of 3 mM Gly-Gln a slowly declining outward current is seen during the prepulse, while an opposite behaviour (i.e. a slowly declining inward current) is observed at the most negative test pulse potentials (Fig.3.187 A middle traces). Subtraction of the currents in the absence from those in the presence of substrate gives the isolated transport currents (Fig.3.18) A rightmost traces), in which the declining behaviour at negative potentials during the test pulses is still visible. The average *I/V* relationship obtained from the currents values at the end of the test pulses is plotted in Fig.3.18 C (open squares). It can be seen that using this protocol no outward current can be observed up to +40 mV. In contrast, a clear current reversal around +10 mV is noticeable in the same conditions of pH and Gly-Gln concentration when using the short depolarizing pulses from V_h = -60 mV (filled squares in Fig.3.18 C).

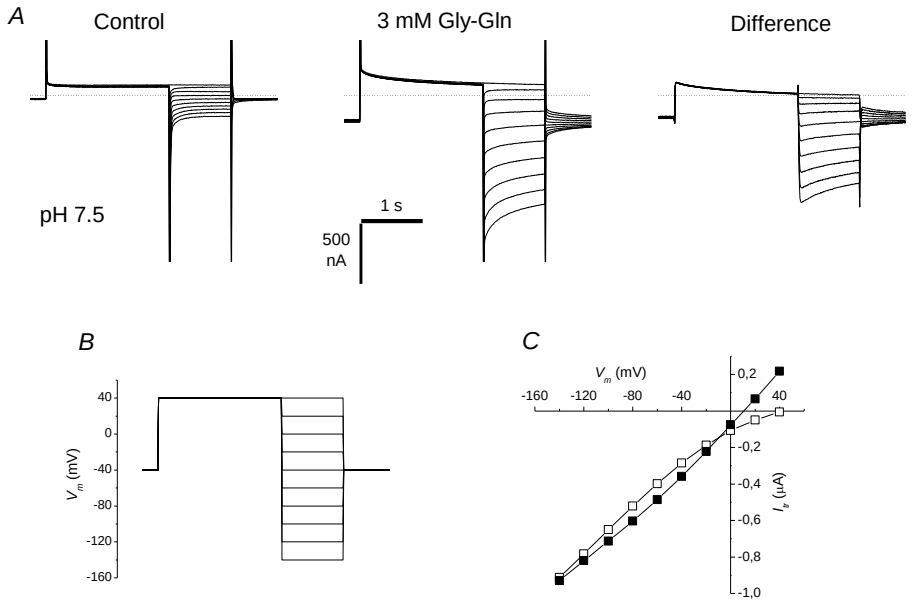

Figure 3.18. Currents elicited by the prepulse protocol shown in B, in the absence and in the presence of 3 mM GlyGln at pH 7.5 in an oocyte expressing the R282D isoform; C: Plot of the current at the end of the test pulse in Ac (open symbols); for comparison, the filled symbols are the data obtained using the short-duration pulse protocol (from Vh -60 mV) from another oocyte in the same conditions.

This experiment indicates that during the prepulse to +40 mV the accumulation/depletion effects are dissipated. To check the physiological relevance of this phenomenon, a similar approach was applied to oocytes expressing the wild-type form of PepT1. In this case a shorter (250 ms) prepulse to +40 mV was sufficient to abolish the temporary phase of outward current (Fig.3.19). The transport-associated currents, obtained as usual by subtracting the traces in the absence from those in the presence of substrate, were always inwardly directed, even in conditions of alkaline pH and low organic substrate concentrations (Fig.3.19 A rightmost traces). This correction, although

modest, allows an extension of the voltage range in which the values of apparent affinity ($1/K_{05}$) and maximal current (I_{max}) can be obtained from a Michaelis-Menten analysis.

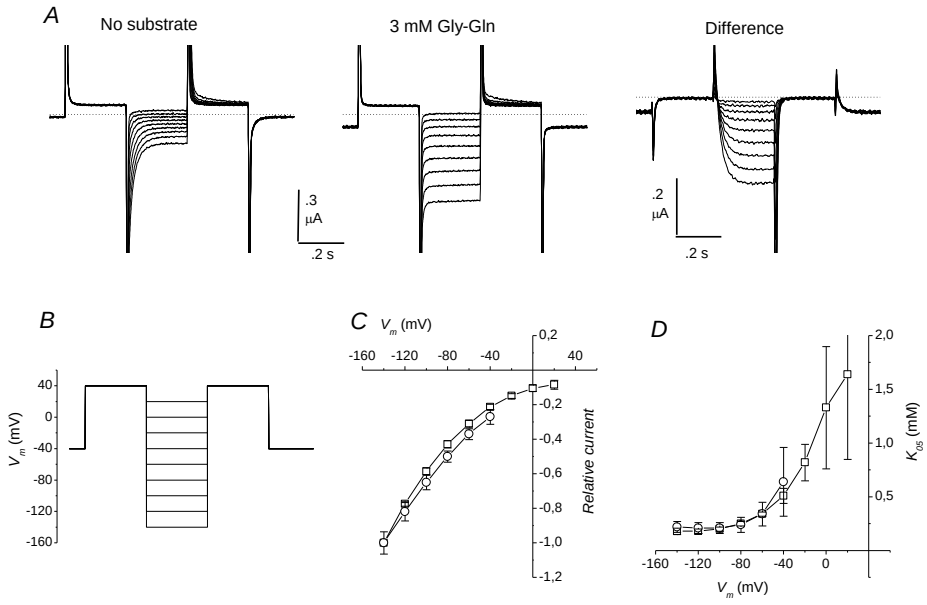

Fig.3.19. Transport currents with the prepulse protocol. In the wild-type PepT1 a 250 ms prepulse duration was sufficient to abolish any outward current elicited by the jump from the -60 mV holding potential to positive potentials. This is demonstrated by the fact that the subtracted currents (A, rightmost traces) are all in the inward direction; C, D: I_{max} and K_{05} obtained by Michaelis-Menten analysis on dose-current curves; open circles: same parameters calculated with the usual protocol.

The average values of K_{05} and I_{max} calculated from a group of oocytes tested with such protocol at pH 7.5 is shown in Fig.3.19 C and D (open squares), together with their counterpart obtained using the customary pulse protocol in which the test pulses were applied directly from V_h = -60 mV without prepulse (open circles). It can be seen that while the data from the classical protocol are limited to -40

mV, because at more positive potentials the current at low substrate concentration becomes outwardly directed, the prepulse protocol allows an extension of the analysis up to +20 mV, although for K_{05} the statistical error becomes very large also in this case.

3.4.5 Intra-cellular injection of substrates

In order to find further support for the results reported above, a series of experiments has been performed by injecting substrates in the cytoplasm of the oocyte. This procedure was already reported to produce significant outward transport currents in wild-type PepT1, when using hydrolysis-resistant dipeptides, or inhibiting intracellular peptidases (Kottra *et al.*, 2009). The results of our experiments on the wild-type and R282D, R282A and D341R isoforms are illustrated in Fig.3.20.

In the upper part of this figure, membrane voltage recordings in current-clamp condition are shown: first of all it can be noted that in all isoforms the resting membrane potential becomes significantly more negative after substrate injection (range -75 to -100 mV), compared to the initial -20 to -50 mV. This progressive hyperpolarization, already observed in the wild-type (Kottra *et al.*, 2009), develops in few minutes after injection and it is not observed in oocytes not expressing the transporters. The development of a strongly negative resting potential is clearly consistent with the activation of an outward current by the transporter as a consequence of the increased intracellular Gly-Sar concentration.

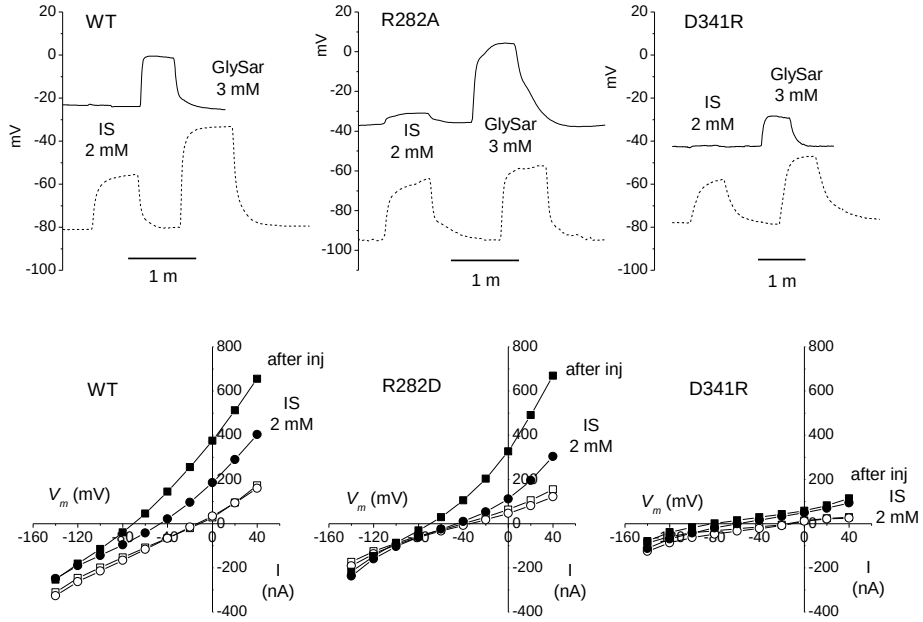

Figure3.20. Application of Irbesartan. Top row: current-clamp recordings showing the resting potential changes induced by application of Irbesartan (IS) and Gly-Sar. Bottom graphs: corresponding uncorrected I/V elationships before (open symbols) and after (filled symbols) the injection of Gly-Sar. Squares are data in the absence and circles in the presence of IS.

Additional evidence is provided by the application of the blocker Irbesartan (IS) (Knütter *et al.*, 2009): the traces in Fig.3.20 show that while external Gly-Sar 3 mM depolarizes the membrane when applied either before or after the intracellular injection, the application of Irbesartan (2 mM) is effective in producing a depolarization only after substrate injection. These last observations indicate that, while the depolarizations induced by external Gly-Sar are due to the development of an inward transport current, those induced by Irbesartan are due to the inhibition of an outward current. Interestingly, the hyperpolarization of the resting membrane potential

and the Irbesartan-induced depolarization are seen in all isoforms, including D341R, in spite of the much lower currents generated by this mutant. The *I/V* curves in Fig.3.20 confirm then the findings reported in the preceding figures, by showing the presence of a strong outward current following the intracellular injection of Gly-Sar, and a reduction of this current by Irbesartan.

3.4.6 Ion and substrate specificity

Previous results (Kulkarni *et al.*, 2007;Pieri *et al.*, 2008) (Meredith, 2004) have suggested that residues R282 and D341 form an ion bridge whose cyclic breaking and formation may gate the translocation process. Furthermore, it has been proposed (Meredith, 2009) that PepT1 may represent a transitional entity between transporters and channels. Then possible alterations in ion and substrate specificity in the R282D mutant have been investigated (the same results were obtained in R282A as well). The possible participation of other cations in the current elicited by the organic substrate was tested by replacing external Na^+ with K^+, Li^+ or tetramethylammonium ion (TMA^+). However these ionic substitutions did not significantly alter the shape of the *I/V* relationships in the presence of Gly-Gln at various concentrations and pH values, as shown in Fig.3.21 for pH 8 and Gly-Gln 1 mM. It can be seen that the reversal potential and the outwardly directed current are independent of the kind of cation representing the vast majority of external positive charges.

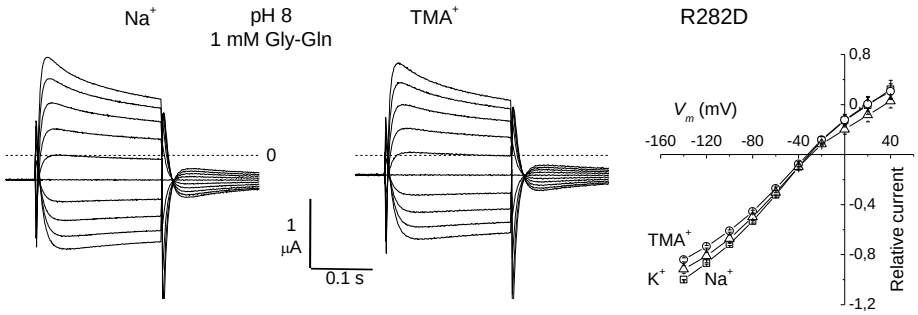

Figure.3.21. Replacement of Na^+ with TMA^+ or K^+ in the external solution did not alter significantly the amplitude or the reversal potential of the transport current elicited by the organic substrate.

This result, together with the observations of Fig.3.15 confirms therefore that the species carrying the electrical charge in both directions are indeed protons in complex with the organic substrate.

The substrate selectivity of R282D was also compared with that of the wild-type with special attention to the ability to generate reverse current. A first series of results is exemplified in Fig.3.22, where the capacity to transport di-, tri-, tetrapeptides, as well as histidine by the R282D mutant was tested. It is known (Herrera-Ruiz & Knipp, 2003; Daniel *et al.*, 2006) that PepT1 family members are able to transport several di- and tri-peptides, but not tetrapeptides.

Furthermore, among the SLC15A family of transporters, the PepT subfamily is differentiated from the PHT subfamily by its inability to transport histidine. The representative records of Fig.3.22 A show that, with respect to substrate selectivity, R282D behaves in a manner similar to the wild-type transporters. The same potency order was found in the other two tested mutants, R282A and D341R (not shown). Furthermore, as illustrated in Fig.3.22 B, tripeptides (LGG)

are also able to generate outward current when the short pulse protocol from V_h = -60 mV is used.

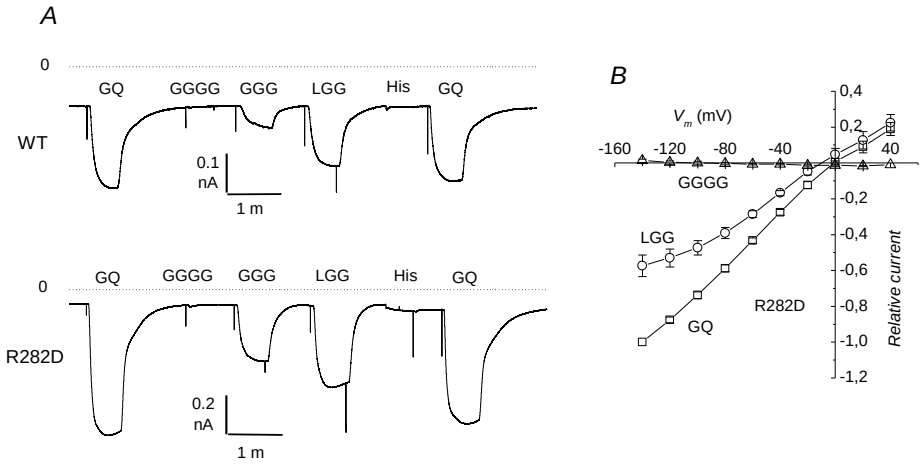

Figure 3.22 Transport current elicited by di-, tri-, tetrapeptides and histidine in the wild-type and in the R282D mutant (GQ: gly-gln; GGGG: tetra glycine; GGG: tri glycine; LGG: leu-gly-gly; His: histidine).

3.4.7 Charged dipeptides

In the context of the substrate selectivity analysis, it seemed particularly interesting to examine the behaviour of the mutants in the charge-pair residues when charged dipeptides were used in place of the neutral substrates employed in all previous experiments.

The relevance of introducing a negative or a positive amino acid in the substrate dipeptide, as well as its position was already studied in the wild-type PepT1 (Amasheh *et al.*, 1997; Kottra *et al.*, 2002). An important conclusion from these studies was that the binding pocket of PepT1 can accept only neutral amino acids at the carboxyl terminus, while at the amino terminus all kinds of charges can be accommodated.

Fig.3.23 compares the transport currents generated at the same pH (7.5) and substrate concentration (1 mM) when a positive or a negative residue is introduced in either position of the dipeptide. The transport currents were normalized to the current generated by the neutral dipeptide Gly-Gln at -140 mV in each oocyte before averaging. The previous observations on the wild-type are qualitatively confirmed in the mutants: the transport currents generated by Lys-Gly are larger compared to Gly-Gln in all isoforms, while those produced by Gly-Lys and by the two negatively charged dipeptides are smaller. However, the degree of reduction or increase is different in the two mutants: in the R282D the differences are enhanced Lys-Gly showing a much larger increase (150% vs 60% in the wild type), while the currents generated by Gly-Lys, Gly-Asp and Asp-Gly are reduced relatively more than in the wild type. In the D341R form, that produces in general smaller currents (see Fig.3.14), the Gly-Lys, Gly-Asp and Asp-Gly currents are less strongly reduced, and the Lys-Gly current increases similarly to the wild-type.

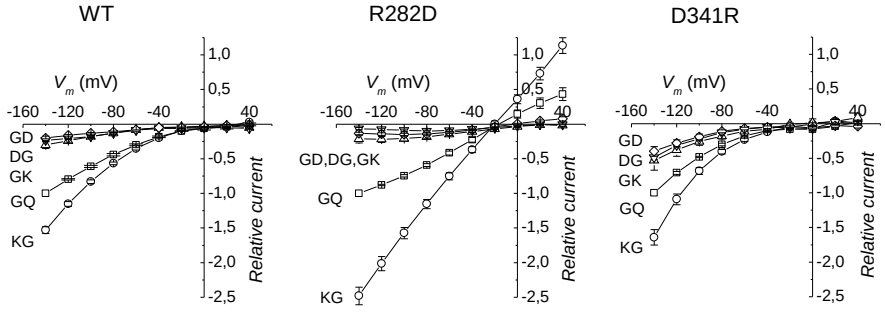

Figure 3.23 Current-voltage relationships of the transport currents elicited by differently charged dipeptides in comparison with Gly-Gln (all at 1 mM) in the indicated isoforms at pH 7.5.

Furthermore, Lys-Gly can produce large outward currents in R282D, while all substrates produce strongly inward-rectifying currents in D341R.

The results for the wild-type are in line with previous observations (Amasheh *et al.*, 1997; Kottra *et al.*, 2002), and qualitatively reflect the excess positive or negative charge of the different dipeptides at pH 7.5. The more than doubled slope of the *I/V* curves in the R282D mutant can be best explained with a nearly doubled charge/mole ratio and, in addition, with an increased turnover rate of the transporter.

On the contrary, the lack of alterations in the substrate selectivity order suggests that these mutations do not interfere with the binding pocket of the transporter. This prediction has been tested by evaluating the amount of presteady-state charge movement removed by interaction with the various dipeptides. It is known that in many transporters, including PepT1 (Sala-Rabanal *et al.*, 2006;Sangaletti *et al.*, 2009) the presteady-state currents in absence of substrate are mutually exclusive with the transport currents (i.e, they are progressively reduced with corresponding increases in transport current). Fig. 3.24 shows the residual charge movement in presence of 1 mM of different dipeptides (Gly-Gln, Lys-Gly and Gly-Asp) in representative oocytes expressing the wild-type and the mutants R282D and D341R.

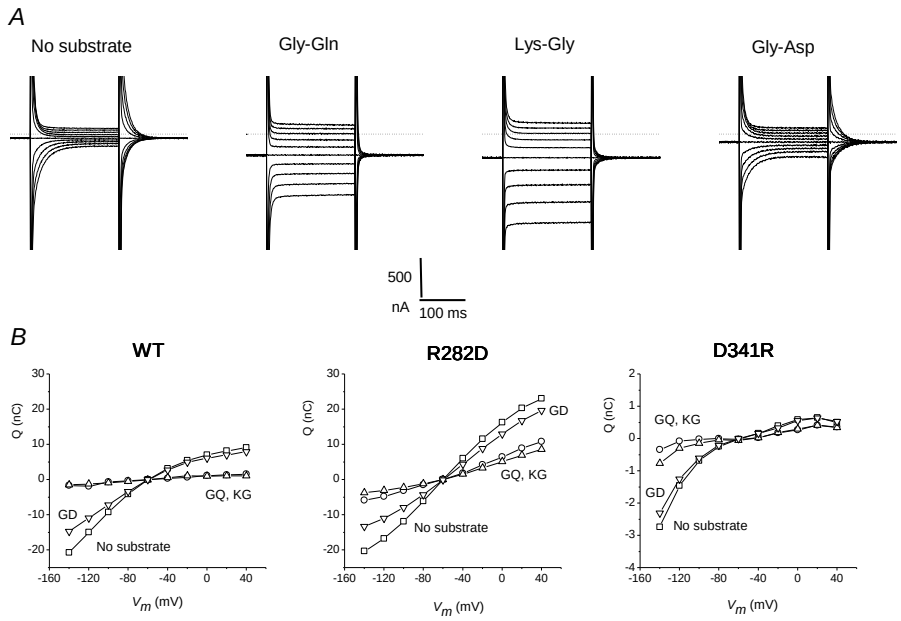

Figure 3.24 Residual charge movement for the wild-type and the R282D and D341R mutants in the presence of a neutral, a basic and an acidic dipeptide as indicated (all at concentration 1 mM and pH 7.5).

As shown in the traces of Fig. 3.23, 1 mM Gly-Gln and Lys-Gly remove almost completely the presteady-state currents in the wild type, while most of this kind of current remains in presence of the same amount of Gly-Asp (the same result was observed with Asp-Gly and Gly-Lys). These observations may be quantified comparing the *Q/V* curves obtained by integrating the presteady-state current isolated using a double exponential fitting of the traces in absence of substrate (considered to represent the total charge), to the integrals of the transient currents obtained by difference of the traces in absence and in presence of substrate (residual charge) (Fesce *et al.*, 2002a). These data are shown in the bottom graphs of Fig. 3.24. Clearly the residual charge in the presence of 1 mM Gly-Gln and Lys-Gly is close to zero

in the wild type, and for these substrates it remains a small fraction of the total charge in both mutants. In contrast, for Gly-Asp the residual charge is close to the total charge in all isoforms. Analogous results were obtained for the other, poorly functional dipeptides (not shown).

The amount of residual charge can be considered an estimate of the fraction of transporters not involved in the actual transport, i.e. transporters that do not interact with the substrate. In this view, the data of Fig. 3.24 indicate that for all isoforms Gly-Asp interacts poorly, while Gly-Gln and Lys-Gly show a comparable degree of interaction between each other, although in the mutants this level appears lower than in the wild type.

Taking together the results of Figs 3.23 and 3.24, it can be concluded that, since the level of interaction of Gly-Gln and Lys-Gly with the R282D mutant is similar, the more than twofold increase in transport current by Lys-Gly should be ascribed to the increased charge/mole ratio of the transported complex, and possibly to an increased turnover rate.

3.5 TRANSPORT EFFICIENCY OF DIFFERENT DIPEPTIDES ACROSS SPECIES

The need to optimize dietary nutrients in small animals has given rise to trials of different feed combinations in animal husbandry. This is perhaps strongest in aquaculture where optimized protein absorption is important for increased fish size, muscle mass and overall health. While commercial gain is a motivation, there is also a scientific angle to the feed combinations with respect to PepT1; as the use of different amino acid or peptides can shed more light on the

properties of the transporter, while at the same time giving an evidence-based feed formulation to aquaculturists.

The use of alternative protein sources in fish meal causes a reduction of fish growth and feed utilization efficiency and an increase of diseases. Plant protein sources are used to replace fish meal in feed formulations, but are inferior in their essential amino acid (EAA) composition. With increasing use of plant protein sources in fish feeds, EAA supplementation becomes necessary.

Available data show that common carp larvae (agastric fish) diets based on free amino acids and synthetic dipeptides are not appropriate (Zhang *et al.*, 2006); while trout (gastric fish) fed a formulated casein–gelatin diet supplemented with synthetic peptides show a growth rate similar to those fed a protein-based formulated diet or commercial feed (Terjesen *et al.*, 2006). Similar to trout, agastric silver bream (*Vimba vimba*) larvae and juveniles accepted, digested and absorbed dipeptide and casein-based diets containing 50% protein (Ostaszewska *et al.*, 2008). Their survival and growth rate was similar to fish fed casein–gelatin (protein) based diets. Also, histological examination of the digestive tract of silver bream fed dipeptides and casein-based diets containing 50% protein showed no nutritional deficiencies (Ostaszewska *et al.*, 2008).

The results of a recent study (Ostaszewska *et al.*, 2010) proved that rainbow trout (*Oncorhynchus mykiss*) fed a formulated Lysine–Glycine dipeptide supplemented diet — PP, free lysine and glycine supplemented diet — AA and commercial starter (Aller Futura — AF) showed a significantly higher growth compared to fish fed control diet with no lysine — CON. A statistically significant increase in relative

expression of PepT1 oligopeptide transporter was also observed in the intestine of fish fed with formulated diets as compared to the fish fed commercial starter AF.

Moreover, most of the studies in this area have been based on in vivo absorption models. This is understandable. However, given the many advantages of electrophysiology previously reviewed, and the fact that peptide absorption is predominantly carried out by PepT1 in a proton dependent process, it is possible to study the transport kinetics and interactions of many peptides with the transporter using an electrophysiological approach.

3.5.1 Species-specific Preferential transport of dipeptides

Species-specific differences were observed in the potency order among the various substrates (tested at 1 mM) (Fig 3.25), and in the voltage-dependence of the current amplitude (Fig 3.25). Particularly Lys-Met was the best substrate at all tested potentials in seabass PepT1, as well as in the rabbit transporter, while in the zebrafish isoform all tested dipeptides (except Gly-Lys) elicited similar currents independently of the charge position or amino acid composition. KK and KKK are already known not to elicit significantly high transport current with PepT1.

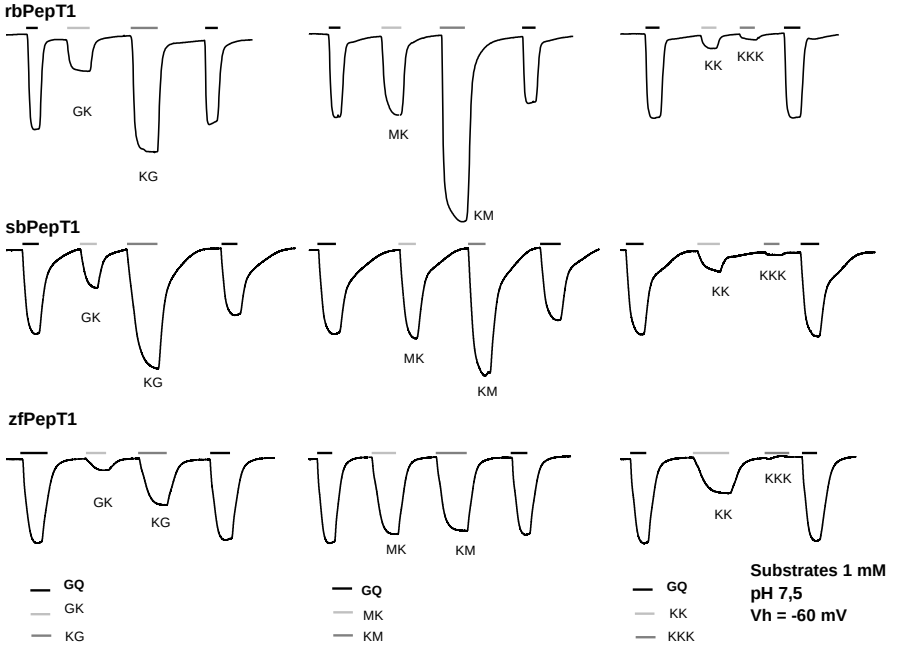

Figure 3.25. A record showing the transport current generated by each substrate (3mM) at pH 7.5. In rbPepT1 and zfPepT1, the dipeptide lysine-methionine gives the highest transport current which becomes less when the position of the lysine is changed in methionine-lysine (MK).The zfPepT1 does not show this preference.

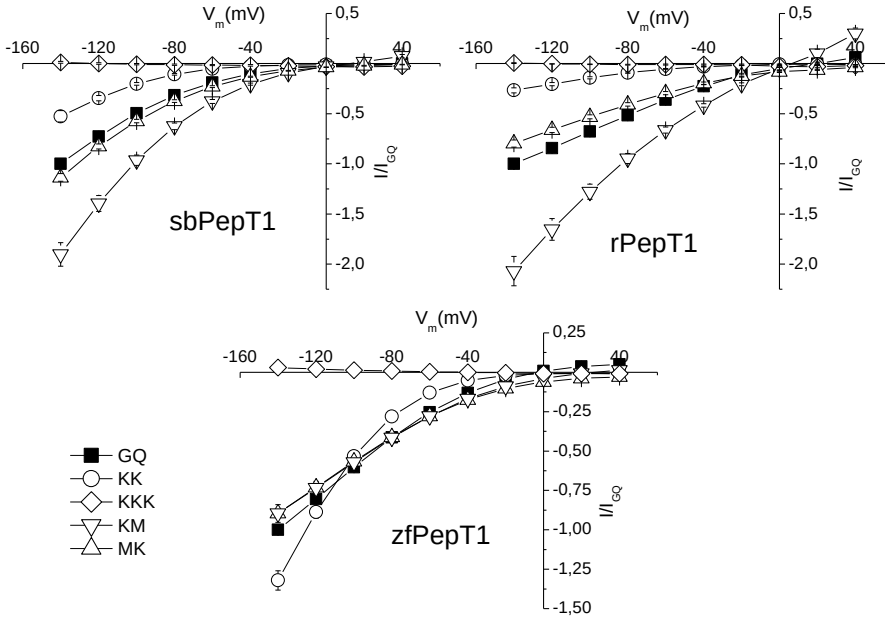

Figure 3.26. I/V curves showing transport current generated by the different dipeptides. From a holding potential of -60, current generated is recorded at different membrane voltages (-60 to +40) In sb and rb PepT1s, KM transport gives the highest current while KK and KKK are only modestly transported. However in zfpepT1, KK gives high transport current at more negative potentials.

3.5.2 Effects of extracellular pH

In all isoforms the substrate potency order was pH-independent in the range 6.5 -7.5 (Fig.3.27), and the tripeptide Lys-Lys-Lys did not give rise to any current. In rabbit and seabass PepT1s the dipeptide Lys-Lys was only modestly transported at all voltages, while in the zebrafish a strong current increase was observed at negative membrane potentials.

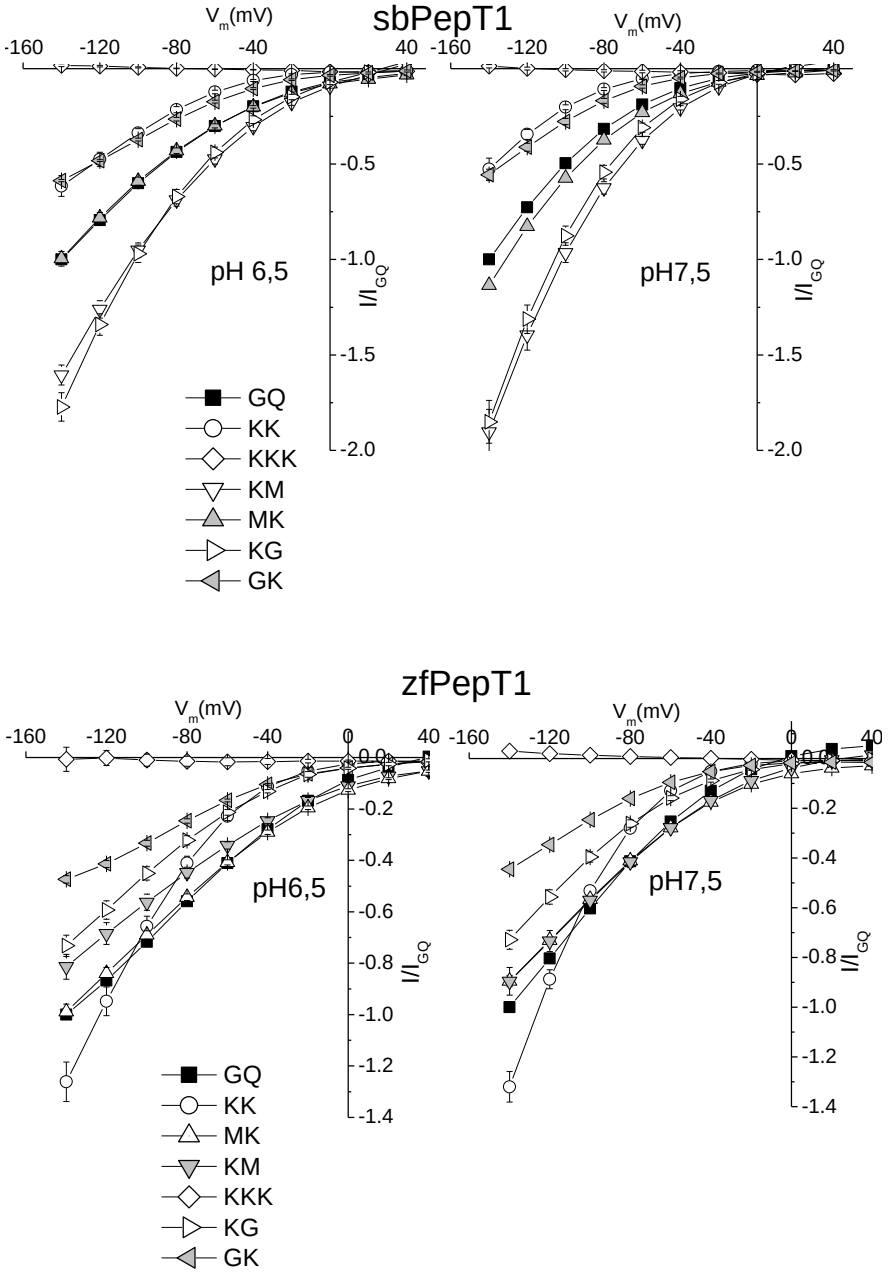

Figure 3.27. I/V curves showing transport current generated by the different dipeptides at two different pH values in the sb and zf PepT1s. In both isoforms, there is no significant effect of changing the pH on the transport current generated, however the high transport current of KK in zfPepT1 is still maintained at both pH values tested.

3.5.3 Transport efficiency

The dose response curves were determined at different voltages from -140 to -20 mV and the ratio of the relative Imax/$K_{0.5}$ was calculated. In the seabass and rabbit PepT1 these parameters show the importance of the position of lysine in the dipeptide (Figure 3.28a). These proteins have very low affinity for Lys-Lys and Gly-Lys that highly reduce the transport efficiency; the other dipeptides tested were quite similar in affinity (between 0.2-0.8 mM) with small changes with voltage, but the transport efficiency was significantly higher for Lys-Met and Lys-Gly. In zfPepT1 relatively high affinity and excellent transport efficiency were shown by Met-Lys and Lys-Met, while low efficiency was found for Gly-Lys (Figure 3.28b).

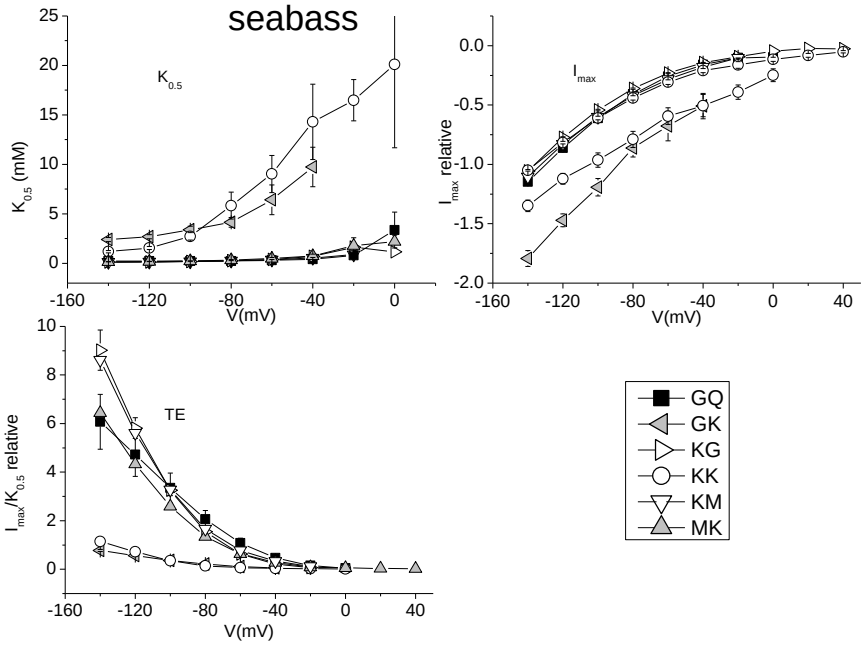

Figure 3.28a. Imax, affinity and transport efficiency (TE) plots in the sbPepT1. Here again, having lysine in the first position is more efficient for the transporter while the least transported substrate has very low efficiency of transport. Although GQ and GK have very high affinities, this does not translate into correspondingly high efficiencies of transport.

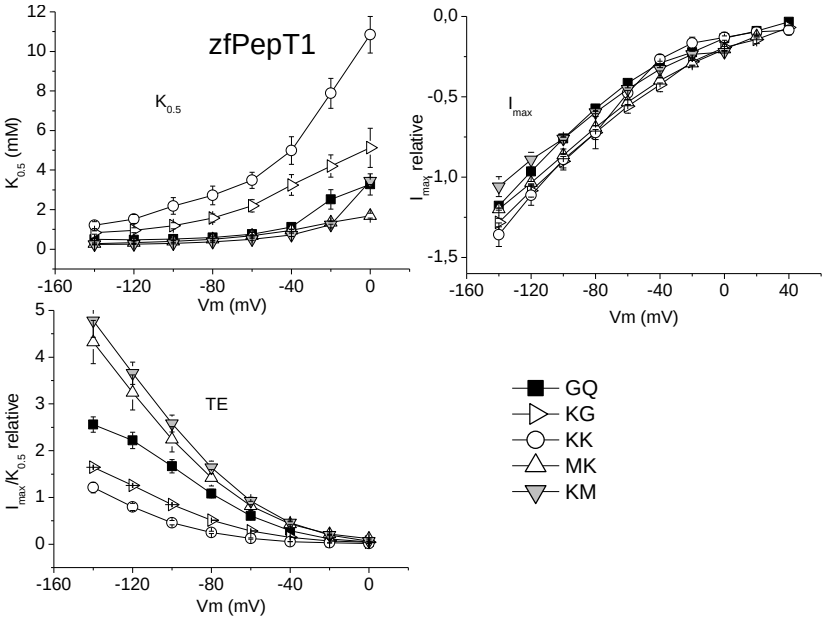

Figure 3.28b Imax, affinity and transport efficiency (TE) plots in the zebra fish. Compared to what was obtained in the rabbit and seabass isoforms, the tested dipeptides did not show wide variations in the maximum currents generated. KM and KG are transported with the highest efficiencies.

CHAPTER 4 DISCUSSION

4.1 Comparison of the presteady-state currents in the different species

An analysis of the presteady-state currents with respect to the voltage dependence of the decay time constant and the amount of displaced charge showed that they are positioned differently (at the same external pH) on the voltage axis. The rabbit curves are positively shifted compared to the zebrafish curves are negatively shifted; with the seabass curves located close to those of the zebrafish.

In addition, the decline in the presteady-state current following voltage jumps is faster in the zebrafish and seabass transporters than in the rabbit isoform. These results are in good agreement with the different isoelectric points of the three proteins: 7.47, 6.68, and 6.00 for rabbit, seabass, and zebrafish, respectively ((Daniel *et al.*, 2006) and our calculation). This suggests that rabbit PepT1 may be protonated more easily than the fish isoforms.

4.2 Temperature and PepT1

In contrast to the numerous advantages offered by the method of expressing heterologous proteins in *Xenopus laevis* oocytes, this approach has the disadvantage of working with oocytes which do not tolerate the temperature levels that are physiological for mammals. This limitation prevents a full knowledge of the properties of the protein under study in its ideal physiological condition. Commonly, oocyte studies are performed at room temperature (22 ± 2 °C) in our laboratory, and many others; irrespective of the thermoregulation

characteristics of the species.

4.2.1 Comparison with poikilotherm PepT1s and structural implications

In a recent work (Renna *et al.*, 2011), we compared the electrophysiological properties of three PepT1 isoforms from different species (rabbit, zebrafish and seabass). At room temperature, the two fish isoforms behaved similarly in terms of kinetic parameters of transport, while the rabbit isoform showed markedly slower kinetics. In addition, the parameters that characterize the presteady-state currents, i.e. the $Q_{in}V$ and τ/V curves were shifted to more negative potentials in both fish PepT1s compared to the rabbit isoform.

This result confirms that orthologous proteins from differently temperature-adapted species tested at the same temperature show variation in functionality, aimed at the compensation of the kinetic properties.

Clearly, the present kind of approach neglects possible differences in the lipid composition of the native membranes of each transporter isoform. These in turn may possess different fluidity properties that will influence the behaviour of the proteins. When expressed in the *Xenopus* oocyte membrane, the different transporters are studied in the same molecular environment, and consequently, the description of their properties in these conditions may not entirely reflect their behaviour in the real physiological situation..

Anyway, these results show that at higher temperature the properties of the rabbit PepT1 approach those of the fish species; suggesting that there will be no strong differences among the various

species when the transporters operate at their physiological conditions. Furthermore, this observation implies that structural differences should exist between the mammal and fish isoforms that would confer enhanced flexibility in the latter at lower temperature (Fields & Houseman, 2004).

4.2.2 Activation energies

The negative shift of the Q_{in}/V and τ/V curves observed in rbPepT1 at higher temperatures confirms analogous observations obtained for GAT1 and for SGLT1 (Binda *et al.*, 2002;Hazama *et al.*, 1997). This effect appears therefore to be of general relevance in the operation of cotransporters; since these three proteins belong to three different gene families, namely SLC15A1 (PepT1), SLC6A1 (GAT1) and SLC5A1 (SGLT1).

Derivation of the unidirectional rate constants for the intramembrane charge movement measured in the absence of organic substrate shows that the shift is caused by a stronger effect of temperature on the outward rate compared to the inward rate. Consequently, analysis of the Arrhenius plots of the unidirectional rates indicates that the transitions involving the inward and outward movement of electric charge in the membrane electrical field possess different activation energies, and particularly the *Eact* for the outward movement is two to three-folds larger than that for the inward movement. This result is consistent with the general observation that the apparent substrate affinity for reverse operation is for most transporters much lower than that for forward transport (Cammack *et al.*, 1994;Eskandari *et al.*, 2005;Kottra *et al.*, 2009;Lu & Hilgemann,

1999).

As shown in Fig. 3.8, the height of the energy barrier for the inward charge movement appears to increase at negative potentials. This result is puzzling because an opposite behaviour would be qualitatively expected (since the barrier will be decreased when the internal potential is made more negative), while for the outward transition the opposite effect could be presumed. Furthermore, the contribution of the electrical field across the cell membrane should be much smaller, as only 9.65 kJ/mole is needed for a 100 mV voltage change. This point will require further investigations.

Interestingly, the activation energy for the complete cycle, i.e. when the organic substrate is present, is the same as that for the inward charge movement in the absence of substrate (Fig. 3.8). This finding indicates that during the forward transport cycle, which is the physiological working condition, the main energy barrier to be overcome is the charge-moving initial step, while the other steps needed to complete the cycle will require only minor energy contributions.

The effects of temperature on the transport current are similar at the two tested pH (6.5 and 7.5). In both conditions the activation energy for the complete cycle is around 80 kJ/mole at the expected physiological membrane potentials (-40 - -60 mV). The high Q_{10} (> 5) observed at very negative potentials at pH 7.5 (Fig. 3.5C) is probably not very reliable, since at these potentials the transport current shows a significant decline during the voltage step.

4.2.3 Apparent substrate affinity

The results presented in Fig. 3.9, show a shift in the $K_{0.5}$-V relation when the temperature is increased. This shift goes in parallel with those observed for the Q_{in}-V and τ-V curves illustrated in Fig. 3.6 and gives support to the notion of an inverse causal correlation between the speed of the charge-moving transitions and the substrate affinity. Indeed such correlation has already been observed in PepT1 when the pH of the external solution is changed (Renna *et al.*, 2011), and more generally in other transporters; following conditions that affect the unidirectional rates of charge movement (Giovannardi *et al.*, 2003;Soragna *et al.*, 2005).

This causal link can be understood considering that in PepT1, as well as in several other transporters, the charge-moving transitions occurring before substrate binding, represent the limiting step of the turnover rate (Nussberger *et al.*, 1997;Renna *et al.*, 2011;Sala-Rabanal *et al.*, 2006)) . Consequently, the lifetime of the conformational state in which substrate binding can occur will be shortened when the charge equilibration rate is increased (e.g. in the present case, by a higher temperature).

Interestingly, a significant decrease in affinity at lower temperature was reported in the Drosophila serotonin transporter (Beckman & Quick, 2001), and results pointing in the same direction may also be found in an earlier paper on the noradrenaline transporter (De Oliveira *et al.*, 1989). It must be underlined however that temperature may also affect the flexibility/stability balance of the binding site structure, contributing to altering the substrate affinity (Fields, 2001;Fields & Houseman, 2004).

The lower affinity at higher temperature will in principle counterbalance the increased I_{max} in terms of overall transport efficacy. However, as shown in Fig. 3.9E, in the physiological range of membrane potentials the increase in I_{max} prevails over the affinity decrease, confirming a clear gain in efficiency at higher temperatures that could even be more significant at the body temperature of the animal.

In summary, the observed effects of temperature on the electrophysiological properties of the rabbit PepT1 show that they become qualitatively and quantitatively similar to their fish counterpart when both are examined at their physiological body temperature. Furthermore, the detailed analysis of the biophysical parameters reveals interesting correlations between the thermodynamics requirements of the different transitions in the transport cycle, as well as a significant decrease in the apparent substrate affinity at higher temperatures. Since this effect appears to be a direct result of the accelerated turnover rate, it is expected to be a common feature of ion-coupled cotransporters (Beckman & Quick, 2001), and it may be expected to occur for other transporters, with relevant consequences on their physiological functioning.

4.3 Reverse operation in PepT1

The PepT1 mutants investigated in the present work are correctly expressed in the oocyte membrane (Fig.3.12), and maintain the characteristics of true cotransporters, as it is shown by the fact that both protons and substrate concentrations affect the reversal potential of the transport current (Fig.3.15), and that the substrate selectivity is unaltered (figure 3.15). Although qualitatively in the correct direction,

the shifts in E_{rev} significantly deviate from the predictions of the Nernst equation. Further difficulties arise when examining the slope conductance of the transport current at the reversal potential: according to the theory of electrodiffusion (Hille, 2001), and intuitively as well, this parameter should increase when the concentration of the diffusing species is increased. As shown in Fig.3.15, this is verified for the dipeptide substrate Gly-Gln, but not for protons, for which no significant dependency of g_{slope} is found.

Having established that R282D and R282A can be considered as true cotransporters with some interestingly altered properties (conspicuous outward currents), the functional and structural determinants of reverse operation in these proteins have been investigated.

4.3.1 Determinants of reverse operation in PepT1

The experiments illustrated in Fig.3.16 show that the outward currents visible in Figs 3.14 and 3.15 are only temporary and may be consequent upon the active state of the transporters at negative holding potentials. These declining outward currents might be considered similar to the "tail" currents observed in voltage-activated ionic channels when stepping the voltage from a condition in which the channel is open, to other voltages where it will close (Hille, 2001;Hodgkin & Huxley, 1952). If this is the case, the *I/V* curves obtained from relatively short (<1 s) pulses may actually represent "instantaneous" *I/V* relationships of the current generated by the transporter at the level of activation of the holding potential.

The observation (Figs 3.13 and 3.17) that the transport current declines during strong voltage pulses not only in the depolarizing but also in the hyperpolarizing directions further suggests that this effect may arise from changes in the driving force, rather than from an intrinsic deactivation process of the transporter, because this last kind of process usually depends monotonically on voltage. The hypothesis of a reduction in driving force is demonstrated by the results of the experiments of Figs 3.17, 3.18 and 3.19, as well as from the long-lasting recordings of Fig.3.16. In fact, during a prolonged flux of the proton-substrate complex, a local accumulation and/or depletion of the complex may occur in the vicinity of the transporter, and this will decrease the concentration-dependent component of the electrochemical gradient causing a current decline.

The experiment of Fig.3.17 clearly demonstrates the occurrence of this phenomenon in both directions: in fact, during a long lasting hyperpolarization the reversal potential becomes progressively more negative in agreement with a decrease in the *out/in* ratio of the concentrations of the transported species [eq.3.9]. *Vice versa*, during a long lasting depolarization, the E_{rev} shift is toward more positive potentials; consistent with an increase in the *out/in* concentration ratio. However the *I/V* relationships measured at different times during the long pulses in either direction remain parallel to each other, excluding changes in the intrinsic rate of transport.

Although this effect is most evident in the two arginine 282 mutants, it was shown that the hypothesis of a transport-dependent local concentration change can also explain the findings regarding the

wild-type transporter (Kottra & Daniel, 2001). The experiments of Figs 3.18 and 3.19 show that using an appropriate protocol the accumulation/depletion effect can be eliminated, and this leads to more accurate determinations of the kinetic properties of transport (I_{max} and K_{05}), whose values can be obtained over an extended range of membrane potentials.

The ability to conduct current in the outward direction has already been demonstrated in the wild-type PepT1 (Kottra *et al.*, 2009). The results in the present work show that not only mutants in arginine 282 but also D341R exhibit the same capacity in the presence of high intracellular concentrations of a non-hydrolyzable substrate. This finding indicates that the different shapes of the *I/V* curves exhibited by the different isoforms (i.e. inward rectifying *vs* linear, see Figs 3.14 and 3.23), obtained using a classical pulse protocol from V_h = - 60 mV is not related to an intrinsic incapacity of the wild-type and D341R forms to transport in reverse mode, but depends on the different transport rates, producing different degrees of accumulation/depletion effects. Indeed the transformation from linear to inward rectifying can be obtained using appropriate protocols (see Fig.3.19).

4.3.2 Other substrates

Of the two residues forming a putative charge-pair in the PepT1 structure, R282 and D341 (Bossi *et al.*, 2011;Kulkarni *et al.*, 2007;Pieri *et al.*, 2008), only mutants in arginine 282 present the outward current phenotype (Fig.3.14). Our initial results using the neutral dipeptide Gly-Gln showed that the arginine mutants facilitate

the substrate flow both in terms of amplitude and direction, since the *I/V* relationships are approximately linear; while the symmetric mutation D341R has an opposite action, rendering more difficult the transport of substrates, and enhancing the inward rectification property already present in the wild-type.

The subsequent experiments in the presence of different cations (Li^+, K^+ and TMA^+), and using various organic substrates, showed that the mutations do not introduce qualitative alteration in ionic selectivity, nor in substrate specificity. Protons appear to remain the charge carriers, and the potency order of substrates of different size or bearing different charge is not changed compared to the wild-type. Furthermore, the reversal of the transport current can also be observed with tripeptides, suggesting that this property is not substrate-dependent, but is intrinsic in the mutated transporter.

The selectivity order of the charged dipeptides remains substantially unaltered in the mutants compared to the wild-type at pH 7.5. The two negatively charged dipeptides produce only small currents, reflecting the high percentage of the side chains bearing a negative charge at this pH. The two positive dipeptides highlight the relevance of the position of the charge: when the lysine is at the amino terminus the transporter is able to generate larger currents, while when it is located at the carboxyl terminus the currents are much reduced (Kottra *et al.*, 2002).

Quantitatively, the behaviour of the charge-reverting mutants R282D and D341R is opposite in many respects: while R282D shows increased current relative to the wild-type, the current generated by D341R is much reduced (see Fig.3.14). This observation is consistent

with the idea of these two residues being part of the gate controlling the flux of inward positive charges: neutralization of the positive arginine 282, or its replacement with a negative amino acid, may facilitate the approach of the positively charged transport complex, while the replacement of the negative aspartate 341 with a positive arginine may have the opposite effect.

This notion is also supported by the amplified increase (relative to Gly-Gln) in the current generated by Lys-Gly in the R282D mutant compared to wild-type and D341R. This effect is mirrored by the stronger reduction in the same mutant of the current generated by Asp-Gly, compared to the wild-type. Interestingly, this last substrate produces a higher fraction of the Gly-Gln current in the D341R mutant, compared to the wild-type.

4.4 Transport efficiencies of lysine-substrates

Many studies have examined the effects of single amino acids and dipeptides on the growth and performance of animals. For example, very recently, the group of Ostaszewska (Ostaszewska et al., 2012) examined the effects of a Lysine-Glycine-supplemented diet (LG) on the nutritional status and digestive tract histology of juvenile yellow perch (Perca flavescens). After 48 days of experimental feeding, fish fed LG diet showed the highest body mass, highest number of gastrin/cholecystokinin positive cells and the lowest number of CD3-positive cells; compared to fish on diet without supplementation (C), fish on a commercial starter diet (BO) and fish on a free lysine and glycine diet (FL).

According to the authors, the brush border of anterior intestine was the most PepT1 immunopositive in fish fed LG diet, and the

weakest in fish fed C diet. The largest hepatocytes were observed in fish fed BO, while the smallest in those fed FL diet, the difference being statistically significant. Relative hepatocyte cytoplasm volume occupied by lipids was higher in fish fed BO and FL compared to those fed C and LG. Number of proliferating cell nuclear antigen-positive hepatocyte nuclei did not significantly differ among experimental groups. The authors concluded that wheat-gluten-protein-based diets supplemented with dipeptide Lys-Gly (LG) were appropriate for yellow perch.

From our results, KK and KKK did not show high transport current with Pept1; perhaps underscoring the importance of charges as a factor in PepT1-substrate interactions (Terada et al., 2000). While lysine supplementation has been shown to be beneficial (Ostaszewska et al., 2010), the effect of the relative position of lysine in dipeptides used as feed supplements has not been shown. The fact that lysine-methionine (KM) and lysine-glycine (KG) showed higher transport activities than methionine-lysine (MK) and glycine-lysine (GK) respectively in rabbit and seabass isoforms of PepT1 points to the importance of the position of lysine in a dipeptide formation.

However it is not known whether this effect is limited to dipeptides where lysine is coupled to a neutral amino acid. Although these results show in general terms that rabbit and seabass PepT1s have higher affinities for a lysine-methionine dipeptide, it probably may not translate into a huge commercial advantage in rabbit breeding because both lysine and methionine, either as single amino acids or as a dipeptide, have been shown to increase hypercholesterolemia in rabbits (Giroux et al., 1999). This hypercholesterolemia effect could

however be reduced by arginine supplementation. The zebra fish isoform does not appear to discriminate between transport of lysine-methionine and methionine-lysine based on the position of the lysine, although it preferentially transports more KG than GK; quite like other isoforms tested. This lack of discrimination might reflect a specie difference.

PepT1 is a proton-coupled transporter, and as pointed out in Figure 3.1, its operation is affected by extracellular pH. The potency order of all the substrates tested is the same in all species regardless of the pH. Therefore the observed differences among the substrates might not be as a result of a change in pH. All the PepT1 isoforms exhibit low affinities for KK and KKK. In terms of transport efficiencies, in seabass and rabbit, KM and KG have the highest; with KK and GK having the lowest. The transport preference favours those substrates which improve transport efficiency over those that reduce it. A similar trend of preference is seen in zfPepT1 in which relatively high affinity and excellent transport efficiency were shown by Met-Lys and Lys-Met, while low efficiency was found for Gly-Lys.

CHAPTER 5 CONCLUSIONS

In this work, electrophysiological techniques have been used to study some functional aspects of the peptide transporter (PepT1), and a number of interesting contributions have been made to our knowledge of this transporter.

Rise in temperature 20 to 30 °C causes an increase in the maximal transport-associated current (I_{max}) with a Q_{10} close to 4 and also accelerates the rate of decline of the presteady-state currents observed in the absence of organic substrate. The voltage dependence of the intramembrane charge movement (Q_{in}) and of the time constant of decline (τ) are both shifted towards more negative potentials by higher temperatures.

The shift is due to a differential effect of temperature on the unidirectional rates of charge movement. The temperature effect is stronger on the outward rate of charge movement compared to the inward; indicating a lower activation energy for the latter process. Consistently, the activation energy for the complete cycle is similar to that of the inward rate of charge movement. Temperature also affects the apparent affinity for the substrate: the $K_{0.5} - V$ curve is shifted to more negative potentials by higher temperatures, resulting in a lower apparent affinity in the physiological range of potentials. The overall efficiency of transport, estimated as the $I_{max}/K_{0.5}$ ratio is also significantly increased at higher temperatures.

With respect to the rabbit pepT1, the observed effects of temperature on its electrophysiological properties show that the

transporter becomes qualitatively and quantitatively similar to its fish counterpart when both are examined at their physiological body temperature. In line with this, it is proposed that there would be specific amino acid residues that confer some form of thermal flexibility on the transporter. Furthermore, the detailed analysis of the biophysical parameters reveals interesting correlations between the thermodynamics requirements of the different transitions in the transport cycle, as well as a significant decrease in the apparent substrate affinity at higher temperatures. Since this last effect appears to be a direct result of the accelerated turnover rate, it is expected to be a common feature of ion-coupled cotransporters (Beckman & Quick, 2001), and it may be expected to occur for other transporters, with relevant consequences on their physiological functioning.

Mutants in the putative charge pair residues Arg282 and Asp341 of rabbit PepT1 have been shown to exhibit properties useful to better understand the possibility of reverse transport. In fact, wild-type and Arg282 mutants, while retaining the essential characteristics of proton-coupled cotransporters, exhibit outward currents in the presence of Gly-Gln. Long-lasting voltage- and current-clamp experiments have shown that these currents are only temporary, and reflect accumulation and/or depletion effects near the membrane.

The reversal potential of the outward currents is affected by both pH and substrate concentration, confirming coupled transport in the wild-type and in the mutants as well. Removal of arginine 282 appears to facilitate the flow of the transported complex in both directions, while replacement of aspartate 341 with a positive residue limits the transport rate and strengthens the inwardly-rectifying

characteristics of the wild-type transporter. This observation is consistent with the idea of these two residues being part of the gate controlling the flux of inward positive charges.

For the benefit of optimizing animal feed, different lysine-containing dipeptides have been tested. In all isoforms the substrate potency order was pH-independent in the range 6.5 -7.5, and the tripeptide Lys-Lys-Lys did not give rise to any current. In rabbit and seabass PepT1s, the dipeptide Lys-Lys was only modestly transported at all voltages, while in the zebrafish a strong current increase was observed at negative membrane potentials.

Transport efficiency data in the seabass and rabbit PepT1s show the importance of the position of lysine in the dipeptide; being higher when lysine in the first position. These proteins have very low affinity for dipeptides Lys-Lys and Gly-Lys which highly reduce the transport efficiency. Other dipeptides tested were quite similar in affinity (between 0.2-0.8 mM) with small changes with voltage, but the transport efficiency was significantly higher for Lys-Met and Lys-Gly. In zfPepT1 relatively high affinity and excellent transport efficiency were shown by Met-Lys and Lys-Met, while low efficiency was found for Gly-Lys. This result may be useful in the supplementation with essential amino acids.

In summary, the studies reported in this thesis have contributed to a better understanding of the mode of transport by PepT1. Since the transporter is of great interest in basic science, pharmacology and drug design, and animal husbandry, the detailed information generated from this work would complement what is already known to drug designers and animal nutritionists, and hopefully stimulate interest in

others to study the transporter more. My studies have generated some new hypotheses for further studies; and asides adding to the existing pool of literature on the subject matter, the studies have also raised observations which could form the basis of future research

Bibliography

Alpers, D. (2012). Digestion and absorption of carbohydrates and proteins. In *Physiology of the Gastrointestinal Tract*, ed. Jonhson, L., pp. 1469-1487. Raven, New York.

Amasheh, S., Wenzel, U., Boll, M., Dorn, D., Weber, W.-M., Clauss, W., & Daniel, H. (1997). Transport of Charged Dipeptides by the Intestinal H+/Peptide Symporter PepT1 Expressed in Xenopus laevis Oocytes. *J.Membr.Biol.* **155**, 247-256.

Armstrong, C. M. & Bezanilla, F. (1974). Charge movement associated with the opening and closing of the activation gates of the Na channels. *J.Gen.Physiol* **63**, 533-552.

Ashida, K., Katsura, T., Motohashi, H., Saito, H., & Inui, K. (2002). Thyroid hormone regulates the activity and expression of the peptide transporter PEPT1 in Caco-2 cells. *Am.J.Physiol Gastrointest.Liver Physiol* **282**, G617-G623.

Beckman, M. L. & Quick, M. W. (2001). Substrates and temperature differentiate ion flux from serotonin flux in a serotonin transporter. *Neuropharmacology* **40**, 526-535.

Binda, F., Bossi, E., Giovannardi, S., Forlani, G., & Peres, A. (2002). Temperature effects on the presteady-state and transport-associated currents of GABA cotransporter rGAT1. *FEBS Letters* **512**, 303-307.

Bolger, M. B., Haworth, I. S., Yeung, A. K., Ann, D., Von Grafenstein, H., Hamm-Alvarez, S., Okamoto, C. T., Kim, K.-J., Basu, S. K., Wu, S., & Lee, V. H. L. (1998). Structure, function and molecular modeling approaches to the study of the intestinal dipeptide transporter PepT1. *J.Pharmacol.Sci.* **87**, 1286-1291.

Boll, M., Markovich, D., Weber, W. M., Korte, H., Daniel, H., & Murer, H. (1994). Expression cloning of a cDNA from rabbit small intestine related to proton-coupled transport of peptides, beta-lactam antibiotics and ACE-inhibitors. *Pflugers Arch.* **429**, 146-149.

Bossi, E., Centinaio, E., Castagna, M., Giovannardi, S., Vincenti, S., Sacchi, V. F., & Peres, A. (1999b). Ion binding and permeation through the lepidopteran amino acid transporter KAAT1 expressed in Xenopus oocytes. *J.Physiol* **515 (Pt 3)**, 729-742.

Bossi, E., Fabbrini, M. S., & Ceriotti, A. (2007). Exogenous protein expression in Xenopus Laevis Oocyte, Basic procedure. In *In Vitro Transcription and Translation Protocols*, ed. Grandi, G., pp. 107-131. Humana Press, Totowa NJ.

Bossi, E., Renna, M. D., Sangaletti, R., D'Antoni, F., Cherubino, F., Kottra, G., & Peres, A. (2011). Residues R282 and D341 act as electrostatic gates in the proton-dependent oligopeptide transporter PepT1. *Journal of Physiology* **589**, 495-510.

Brandsch, M., Miyamoto, Y., Ganapathy, V., & Leibach, F. H. (1994). Expression and protein kinase C-dependent regulation of peptide/H+ co-transport system in the Caco-2 human colon carcinoma cell line. *Biochem.J.* **299**, 253-260.

Braun, A. P. (2009). Re-evaluating membrane transport processes: new insights and appreciation of protein behavior. *Channels (Austin.)* **3**, 143.

Burston, D. & Matthews, D. M. (1990). Kinetics of influx of peptides and amino acids into hamster jejunum in vitro: physiological and theoretical implications. *Clin.Sci.(Lond)* **79**, 267-272.

Cammack, J. N., Rakhilin, S. V., & Schwartz, E. A. (1994). A GABA transporter operates asymmetrically and with variable stoichiometry. *Neuron* **13**, 949-960.

Catterall, W. A. (1993). Structure and function of voltage-gated ion channels. *Trends Neurosci.* **16**, 500-506.

Chen, X.-Z., Steel, A., & Hediger, M. A. (2000). Functional roles of histidine and tyrosine residues in the H^+ -peptide transporter PepT1. *Biochemical and Biophysical Research Communications* **272**, 726-730.

Chung, Y. C., Shadchehr, A., Garrido, A., & MacGregor, I. L., Sleisenger, M.H. (1979). Protein digestion and absorption in human small intestine. Gastroenterology 76, 1415-1421..

Cole, K. S., Curtis, H. J. (1941). Membrane potential of the squid giant axon during current flow. *J.Gen.Physiol* **24**, 551-563.

Covitz, K. M., Amidon, G. L., & Sadee, W. (1998). Membrane topology of the human dipeptide transporter, hPEPT1, determined by epitope insertions. *Biochemistry* **37**, 15214-15221.

Dalmasso, G., Nguyen, H. T., Charrier-Hisamuddin, L., Yan, Y., Laroui, H., Demoulin, B., Sitaraman, S. V., & Merlin, D. (2010). PepT1 mediates transport of the proinflammatory bacterial tripeptide L-Ala-{gamma}-D-Glu-meso-DAP in intestinal epithelial cells. *Am.J.Physiol Gastrointest.Liver Physiol* **299**, G687-G696.

Daniel, H. (2004). Molecular and integrative physiology of intestinal peptide transport. *Annu.Rev.Physiol.* **66**, 361-384.

Daniel, H. & Kottra, G. (2003). The proton oligopeptide cotransporter family SLC15 in physiology and pharmacology. *Pflugers Archiv European Journal of Physiology* **447**, 610-618.

Daniel, H., Spanier, B., Kottra, G., & Weitz, D. (2006). From Bacteria to Man: Archaic Proton-Dependent Peptide Transporters at Work. *Physiology* **21**, 93-102.

De Oliveira, A. M., Shoemaker, H., Segonzac, A., & Langer, S. Z. (1989). Differences in the temperature dependence of drug interaction with the noradrenaline and serotonin transporters. *Neuropharmacology* **28**, 823-828.

Doring, F., Walter, J., Will, J., Focking, M., Boll, M., Amasheh, S., Clauss, W., & Daniel, H. (1998). Delta-aminolevulinic acid transport by intestinal and renal peptide transporters and its physiological and clinical implications. *J.Clin.Invest* **101**, 2761-2767.

Eskandari, S., Wright, E. M., & Loo, D. D. F. (2005). Kinetics of the reverse mode of the Na^+/glucose cotransporter. *J.Membr.Biol.* **204**, 23-32.

Ezra, A., Hoffman, A., Breuer, E., Alferiev, I. S., Monkkonen, J., Hanany-Rozen, N., Weiss, G., Stepensky, D., Gati, I., Cohen, H., Tormalehto, S., Amidon, G. L., & Golomb, G. (2000). A peptide

prodrug approach for improving bisphosphonate oral absorption. *Journal of Medicinal Chemistry* **43**, 3641-3652.

Fei, Y. J., Kanai, Y., Nussberger, S., Ganapathy, V., Leibach, F. H., Romero, M. F., Singh, S. K., Boron, W. F., & Hediger, M. A. (1994). Expression cloning of a mammalian proton-coupled oligopeptide transporter. *Nature* **368**, 563-566.

Fei, Y.-J., Liu, W., Prasad, P. D., Kekuda, R., Oblak, T. G., Ganapathy, V., & Leibach, F. H. (1997). Identification of the Histidyl Residue Obligatory for the Catalytic Activity of the Human H+/Peptide Cotransporters PEPT1 and PEPT2. *Biochemistry* **36**, 452-460.

Fesce, R., Giovannardi, S., Binda, F., Bossi, E., & Peres, A. (2002). The relation between charge movement and transport-associated currents in the GABA cotransporter rGAT1. *Journal of Physiology* **545**, 739-750.

Fields, P. A. (2001). Review: Protein function at thermal extremes: balancing stability and flexibility. *Comp Biochem.Physiol A Mol.Integr.Physiol* **129**, 417-431.

Fields, P. A. & Houseman, D. E. (2004). Decreases in activation energy and substrate affinity in cold-adapted A4-lactate dehydrogenase: evidence from the Antarctic notothenioid fish

Chaenocephalus aceratus. *Molecular Biology and Evolution* **21**, 2246-2255.

Forlani, G., Bossi, E., Perego, C., Giovannardi, S., & Peres, A. (2001). Three kinds of currents in the canine betaine-GABA transporter BGT-1 expressed in Xenopus laevis oocytes. *Biochim.Biophys.Acta* **1538**, 172-180.

Freeman, H. J. & Kim Y.S. (1978). Digestion and absorption of protein. *Annu.Rev.Aled.* **29**, 99-116.

Ganapathy, M. E., Brandsch, M., Prasad, P. D., Ganapathy, V., & Leibach, F. H. (1995). Differential recognition of beta -lactam antibiotics by intestinal and renal peptide transporters, PEPT 1 and PEPT 2. *J.Biol.Chem.* **270**, 25672-25677.

Gangopadhyay, A., Thamotharan, M., & Adibi, S. A. (2002). Regulation of oligopeptide transporter (Pept-1) in experimental diabetes. *Am.J.Physiol Gastrointest.Liver Physiol* **283**, G133-G138.

Gilbert, E. R., Wong, E. A., Vaughan, M., & Webb, K. E., Jr. (2007). Distribution and abundance of nutrient transporter mRNA in the intestinal tract of the black bear, Ursus americanus. *Comp Biochem.Physiol B Biochem.Mol.Biol.* **146**, 35-41.

Gilbert, E. R., Wong, E. A., & Webb, K. E. Jr. (2008). Peptide absorption and utilization: Implications for animal nutrition and health. *J.Anim.Sci.* **86**, 2135-2155.

Giovannardi, S., Fesce, R., Bossi, E., Binda, F., & Peres, A. (2003). Cl^- effects on the function of the GABA cotransporter rGAT1 preserve the mutual relation between transient and transport currents. *CMLS* **60**, 550-556.

Guan, D., Yoshioka, M., Eriksson, R. H., Heizer, W., & Kim, Y. S. (1988). Protein digestion in human and rat small intestine:Role of new neutral endopeptidases. *Am.J.Physiol.* **255**, G212-G220.

Hazama, A., Loo, D. D. F., & Wright, E. M. (1997). Presteady-state currents of the rabbit Na^+/glucose cotransporter (SGLT1). *J.Membr.Biol.* **155**, 175-186.

Hediger, M. A., Coady, M. J., Ikeda, T. S., & Wright, E. M. (1987). Expression cloning and cDNA sequencing of the Na+/glucose co-transporter. *Nature* **330**, 379-381.

Hediger, M. A., Romero, M. F., Peng, J. B., Rolfs, A., Takanaga, H., & Bruford, E. A. (2004). The ABCs of solute carriers: physiological, pathological and therapeutic implications of human membrane transport proteins. *Pflugers Archiv European Journal of Physiology* **447**, 465-468.

Herrera-Ruiz, D. & Knipp, G. T. (2003). Current Perspectives on Established and Putative Mammalian Oligopeptide Transporters. *J.Pharmacol.Sci.* **92**, 691-714.

Hilgemann, D. W. & Lu, C.-C. (1999). GAT1 (GABA:Na+:Cl-) cotransport function. Database reconstruction with an alternating access model. *Journal of General Physiology* **114**, 459-475.

Hille, B. (2001). *Ionic channels of excitable membranes*, 3 ed. Sinauer Ass., Sunderland, MA, USA.

Himukai, M., Kameyama, A., & Hoshi, T. (1983). Interaction of glycylglycine and Na+ at the mucosal border of guinea-pig small intestine. A non-mutual stimulation of transport. *Biochim.Biophys.Acta* **732**, 659-667.

Hodgkin, A. L. & Huxley, A. F. (1952). The components of membrane conductance in the giant axon of Loligo. *Journal of Physiology* **116**, 473-496.

Hodgkin, A. L., Huxley, A. F., & Katz, B. (1952). Measurement of current-voltage relations in the membrane of the giant axon of Loligo. *J.Physiol* **116**, 424-448.

Ihara, T., Tsujikawa, T., Fujiyama, Y., & Bamba, T. (2000). Regulation of PepT1 peptide transporter expression in the rat small intestine under malnourished conditions. *Digestion* **61**, 59-67.

Ikeda, T. S., Hwang, E. S., Coady, M. J., Hirayama, B. A., Hediger, M. A., & Wright, E. M. (1989). Characterization of a Na+/glucose cotransporter cloned from rabbit small intestine. *J.Membr.Biol.* **110**, 87-95.

Ingersoll, S. A., Ayyadurai, S., Charania, M. A., Laroui, H., Yan, Y., & Merlin, D. (2012). The role and pathophysiological relevance of membrane transporter PepT1 in intestinal inflammation and inflammatory bowel disease. *Am.J.Physiol Gastrointest.Liver Physiol* **302**, G484-G492.

Kelty, C. J., Brown, N. J., Reed, M. W., & Ackroyd, R. (2002). The use of 5-aminolaevulinic acid as a photosensitiser in photodynamic therapy and photodiagnosis. *Photochem.Photobiol.Sci.* **1**, 158-168.

Khoshbouei, H., Wang, H., Lechleiter, J. D., Javitch, J. A., & Galli, A. (2003). Amphetamine-induced Dopamine efflux. A voltage-sensitive and intracellular Na-dependent mechanism. *J.Biol.Chem*. **278**, 12070-12077.

Kim, Y. S., Kim, Y. W., & Sleisenger, M. H. (1974). Studies on the properties of peptide hydrolases in the brush-border and soluble

fractions of small intestinal mucosa of rat and man. *Biochim.Biophys.Acta* **370**, 283-296.

Knütter, I., Kottra, G., Fischer, W., Daniel, H., & Brandisch, M. (2009). High-Affinity Interaction of Sartans with H/Peptide Transporters. *Drug Metab.Dispos.* **37**, 143-149.

Kottra, G. & Daniel, H. (2001). Bidirectional electrogenic transport of peptides by the proton-coupled carrier PEPT1 in *Xenopus laevis* oocytes: its asymmetry and symmetry. *Journal of Physiology* **536**, 495-503.

Kottra, G., Frey, I., & Daniel, H. (2009). Inhibition of intracellular dipeptide hydrolysis uncovers large outward transport currents of the peptide transporter PEPT1 in Xenopus oocytes. *Pflugers Archiv European Journal of Physiology* **457**, 809-820.

Kottra, G., Stamfort, A., & Daniel, H. (2002). PEPT1 as a Paradigm for Membrane Carriers That Mediate Electrogenic Bidirectional Transport of Anionic, Cationic, and Neutral Substrates. *J.Biol.Chem.* **277**, 32683-32691.

Kulkarni, A. A., Davies, D. L., Links, J. S., Patel, L. N., Lee, V. H. L., & Haworth, I. S. (2007). A charge pair interaction between Arg282 in transmembrane segment 7 and Asp341 in transmembrane segment 8 of hPepT1. *Pharmaceut.Res.* **24**, 66-72.

Lester, H. A., Cao, Y., & Mager, S. (1996). Listening to neurotransmitter transporters. *Neuron* **17**, 807-810.

Loo, D. D., Hirayama, B. A., Gallardo, E. M., Lam, J. T., Turk, E., & Wright, E. M. (1998). Conformational changes couple Na+ and glucose transport. *Proc.Natl.Acad.Sci.U.S.A* **95**, 7789-7794.

Lu, C. C. & Hilgemann, D. W. (1999). GAT1 (GABA:Na+:Cl-) cotransport function. Kinetic studies in giant Xenopus oocyte membrane patches. *J.Gen.Physiol* **114**, 445-457.

Mace, O. J., Lister, N., Morgan, E., Shepherd, E., Affleck, J., Helliwell, P., Bronk, J. R., Kellett, G. L., Meredith, D., Boyd, R., Pieri, M., Bailey, P. D., Pettcrew, R., & Foley, D. (2009). An energy supply network of nutrient absorption coordinated by calcium and T1R taste receptors in rat small intestine. *Journal of Physiology* **587**, 195-210.

Mackenzie, B., Loo, D. D. F., Fei, Y.-J., Liu, W., Ganapathy, V., Leibach, F. H., & Wright, E. M. (1996). Mechanisms of the Human Intestinal H1-coupled Oligopeptide Transporter hPEPT1. *J.Biol.Chem*. **271**, 5430-5437.

Mager, S., Kleinberger-Doron, N., Keshet, G. I., Davidson, N., Kanner, B. I., & Lester, H. A. (1996). Ion binding and permeation at the GABA transporter GAT1. *J.Neurosci.* **16**, 5405-5414.

Mager, S., Naeve, J., Quick, M., Labarca, C., Davidson, N., & Lester, H. A. (1993). Steady states, charge movements, and rates for a cloned GABA transporter expressed in Xenopus oocytes. *Neuron* **10**, 177-188.

Matsumoto,H., Eriksson,R. H., & Kim,Y. S. (1989).Gastroenterology 96, A328.

Matthews, J. C., Wong, E. A., Bender, P. K., Bloomquist, J. R., & Webb, K. E., Jr. (1996). Demonstration and characterization of dipeptide transport system activity in sheep omasal epithelium by expression of mRNA in Xenopus laevis oocytes. *J.Anim Sci.* **74**, 1720-1727.

McAlear, S. D., Liu, X., Williams, J. B., McNicholas-Bevensee, C. M., & Bevensee, M. O. (2006). Electrogenic Na/HCO3 cotransporter (NBCe1) variants expressed in Xenopus oocytes: functional comparison and roles of the amino and carboxy termini. *Journal of General Physiology* **127**, 639-658.

Meredith, D. (2004). Site-directed Mutation of Arginine 282 to Glutamate Uncouples the Movement of Peptides and Protons by the Rabbit Proton-peptide Cotransporter PepT1. *J.Biol.Chem*. **279**, 15795-15798.

Meredith, D. (2009). The mammalian proton-coupled peptide cotransporter PepT1: sitting on the transporter-channel fence? *Philosophical Transactions of the Royal Society B* **364**, 203-207.

Mertl, M., Daniel, H., & Kottra, G. (2008). Substrate-induced changes in the density of peptide transporter PEPT1 expressed in Xenopus oocytes. *Am J Physiol Cell Physiol* **295**, 1332-1343.

Nalbant, P., Boehmer, C., Dehmelt, L., Wehner, F., & Werner, A. (1999). Functional characterization of a Na^+-phosphate cotransporter (NaP_i-II) from zebrafish and identification of related transcripts. *Journal of Physiology* **520**, 79-89.

Neumann, J. & Brandsch, M. (2003). Delta-aminolevulinic acid transport in cancer cells of the human extrahepatic biliary duct. *J.Pharmacol.Exp.Ther.* **305**, 219-224.

Newey, H. & Smyth, D. H. (1957). Intestinal absorption of dipeptides. *J.Physiol* **135**, 43-4P.

Newey, H. & Smyth, D. H. (1959). The intestinal absorption of some dipeptides. *J.Physiol* **145**, 48-56.

Newstead, S., Drew, D., Cameron, A. D., Postis, V. L., Xia, X., Fowler, P. W., Ingram, J. C., Carpenter, E. P., Sansom, M. S., McPherson, M. J., Baldwin, S. A., & Iwata, S. (2011). Crystal

structure of a prokaryotic homologue of the mammalian oligopeptide-proton symporters, PepT1 and PepT2. *EMBO J.* **30**, 417-426.

Nussberger, S., Steel, A., Trotti, D., Romero, M. F., Boron, W. F., & Hediger, M. A. (1997). Symmetry of H+ binding to the intra- and extracellular side of the H+-coupled oligopeptide cotransporter PepT1. *J.Biol.Chem.* **272**, 7777-7785.

Ostaszewska, T., Dabrowski, K., Hliwa, P., Gomolka, P., & Kwasek, K. (2008). Nutritional regulation of intestine morphology in larval/juvenile cyprinid fish, silver bream (Vimba vimba). *Aquaculture Res.* **39**, 1268-1278.

Ostaszewska, T., Kamaszewski, M., Grochowski, P., Dabrowski, K., Verri, T., Aksakal, E., Szatkowska, I., Nowak, Z., & Dobosz, S. (2010). The effect of peptide absorption on PepT1 gene expression and digestive system hormones in rainbow trout (Oncorhynchus mykiss). *Comp Biochem.Physiol A Mol.Integr.Physiol* **155**, 107-114.

Palacín, M., Estévez, R., Bertran, J., & Zorzano, A. (1998). Molecular biology of mammalian plasma membrane amino acid transporters. *Physiological Reviews* **78**, 1054.

Pan, X., Terada, T., Irie, M., Saito, H., & Inui, K. (2002). Diurnal rhythm of H+-peptide cotransporter in rat small intestine. *Am.J.Physiol Gastrointest.Liver Physiol* **283**, G57-G64.

Pan, Y. X., Wong, E. A., Bloomquist, J. R., & Webb, K. E., Jr. (1997). Poly(A)+ RNA from sheep omasal epithelium induces expression of a peptide transport protein(s) in Xenopus laevis oocytes. *J.Anim Sci.* **75**, 3323-3330.

Parent, L., Supplisson, S., Loo, D. D., & Wright, E. M. (1992). Electrogenic properties of the cloned Na+/glucose cotransporter: I. Voltage-clamp studies. *J.Membr.Biol.* **125**, 49-62.

Peres, A., Giovannardi, S., Bossi, E., & Fesce, R. (2004). Electrophysiological insights on the mechanism of ion-coupled cotransporters. *News in Physiological Sciences* **19**, 80-84.

Pieri, M., Gan, C., Bailey, P., & Meredith, D. (2009). The transmembrane tyrosines Y56, Y91 and Y167 play important roles in determining the affinity and transport rate of the rabbit proton-coupled peptide transporter PepT1. *Int.J.Biochem.Cell Biol.* **41**, 2204-2213.

Pieri, M., Hall, D., Price, R., Bailey, P., & Meredith, D. (2008). Site-directed mutagenesis of Arginine282 suggests how protons and peptides are co-transported by rabbit PepT1. *Int.J.Biochem.Cell Biol.* **40**, 721-730.

Rauh, R., Diakov, A., Tzschoppe, A., Korbmacher, J., Azad, A. K., Cuppens, H., Cassiman, J.-J., Dötsch, J., Sticht, H., & Korbmacher, C. (2010). A mutation of the epithelial sodium channel associated with

atypical cystic fibrosis increases channel open probability and reduces Na+ self inhibition. *Journal of Physiology* **588**, 1211-1225.

Renna, M. D., Sangaletti, R., Bossi, E., Cherubino, F., Kottra, G., & Peres, A. (2011). Unified modeling of the mammalian and fish proton-dependent oligopeptide transporter PepT1. *Channels* **5**, 89-99.

Richerson, G. B. & Wu, Y. (2003). Dynamic equilibrium of neurotransmitter transporters: not just for reuptake anymore. *Journal of Neurophysiology* **90**, 1363-1374.

Richerson, G. B. & Wu, Y. (2004). Role of the GABA transporter in epilepsy. In *Recent Advances in Epilepsy Research*, eds. Binder, D. K. & Scharfman, H. E., pp. 76-91. Kluwer Academic/Plenum.

Rinderknecht, H. (1986). Pancreatic secretory enzymes. In *The endocrine pancreas: Biology, pathobiology and diseases*, ed. Go, V. L. W. e. a., pp. 163-183. Raven, New York.

Rossi, D. J., Oshima, T., & Attwell, D. (2000). Glutamate release in severe brain ischaemia is mainly by reversed uptake. *Nature* **403**, 316-321.

Sala-Rabanal, M., Loo, D. D. F., Hirayama, B. A., Turk, E., & Wright, E. M. (2006). Molecular interactions between dipeptides, drugs and

the human intestinal H^+/oligopeptide cotransporter, hPEPT1. *Journal of Physiology* **574**, 149-166.

Sangaletti, R., Terova, G., Peres, A., Bossi, E., Corà, S., & Saroglia, M. (2009). Functional expression of the oligopeptide transporter PepT1 from the sea bass *Dicentrachus labrax*. *Pflugers Archiv European Journal of Physiology* **459**, 47-54.

Seidel, S., Singer, E. A., Just, H., Farhan, H., Scholze, P., Kudlacek, O., Holy, M., Koppatz, K., Krivanek, P., Freissmuth, M., & Sitte, H. H. (2005). Amphetamines take two to tango: an oligomer-based counter-transport model of neurotransmitter transport explores the amphetamine action. *Mol.Pharmacol.* **67**, 140-151.

Semenza, G. (1986). Anchoring and biosynthesis of stalked brush border membrane proteins: Glycosidase and peptidases of enterocytes and renal tubuli. *Annu.Rev.Cell.Biol.* **2**, 255-313.

Soragna, A., Bossi, E., Giovannardi, S., Pisani, R., & Peres, A. (2005). Relations between substrate affinities and charge equilibration rates in the GABA cotransporter rGAT1. *Journal of Physiology* **562**, 333-345.

Steel, A., Nussberger, S., Romero, M. F., Boron, W. F., Boyd, C. A., & Hediger, M. A. (1997). Stoichiometry and pH dependence of the rabbit proton-dependent oligopeptide transporter PepT1. *Journal of Physiology* **498**, 563-569.

Steiner, H. Y., Naider, F., & Becker, J. M. (1995). The PTR family: a new group of peptide transporters. *Mol.Microbiol.* **16**, 825-834.

Tamai, I., Nakanishi, T., Nakahara, H., Sai, Y., Ganapathy, V., Leibach, F. H., & Tsuji, A. (1998). Improvement of L-dopa absorption by dipeptidyl derivation, utilizing peptide transporter PepT1. *J.Pharm.Sci.* **87**, 1542-1546.

Terada, T., Saito, H., Mukai, M., & Inui, K. (1996). Identification of the histidine residues involved in substrate recognition by a rat H^+/peptide cotransporter, PEPT1. *FEBS Letters* **394**, 196-200.

Terada, T., Saito, H., Mukai, M., & Inui, K. (1997). Characterization of stably transfected kidney epithelial cell line expressing rat H+/peptide cotransporter PEPT1: localization of PEPT1 and transport of beta-lactam antibiotics. *J.Pharmacol.Exp.Ther.* **281**, 1415-1421.

Terada, T., Sawada, K., Saito, H., Hashimoto, Y., & Inui, K. (1999). Functional characteristics of basolateral peptide transporter in the human intestinal cell line Caco-2. *Am.J.Physiol* **276**, G1435-G1441.

Terjesen, B. F., Lee, K. J., Zhang, Y., Failla, M., & Dabrowski, K. (2006). Optimization of dipeptide protein mixtures in experimental diet formulations for rainbow trout alevins. *Aquaculture* **254**, 517-552.

Thwaites, D. T. & Anderson, C. M. (2011). The SLC36 family of proton-coupled amino acid transporters and their potential role in drug transport. *Br.J.Pharmacol.* **164**, 1802-1816.

Thwaites, D. T. & Anderson, C. M. H. (2007). H+-coupled nutrient, micronutrient and drug transporters in the mammalian small intestine. *Experimental Physiology* **92**, 603-619.

Thwaites, D. T., Kennedy, D. J., Raldua, D., Anderson, C. M. H., Mendoza, M. E., Bladen, C. L., & Simmons, N. L. (2002). H^+/dipeptide absorption across the human intestinal epithelium is controlled indirectly via a functional Na^+/H^+ excahnger. *Gastroenterology* **122**, 1322-1333.

Uchiyama, T., Kulkarni, A. A., Davies, D. L., & Lee, V. H. L. (2003). Biophysical evidence for His57 as a proton-binding site in the mammalian intestinal transporter hPepT1. *Pharmaceut.Res.* **20**, 1911-1916.

Van, D. (1989a). Mechanisms of digestion and absorption of food. In *Gastrointestinal disease, Pathophysiology, Diagnosis Management*, eds. Sleisenger, M. & Fordtran, J., pp. 1062-1088. Saunders, Philadelphia.

Van, D. (1989b). Mechanisms of digestion and absorption of food. In *Gastrointestinal Disease, Pathophysiology, Diagnosis, Management*,

eds. Sleisenger, M. & Fordtran, I., pp. 1062-1088. Saunders, Philadelphia.

Verri, T., Kottra, G., Romano, A., Tiso, N., Peric, M., Maffia, M., Boll, M., Argenton, F., Daniel, H., & Storelli, C. (2003). Molecular and functional characterization of the zebrafish (*Danio rerio*) PEPT1-type peptide transporter. *FEBS Letters* **549**, 115-122.

Wadiche, J. I. & Kavanaugh, M. P. (1998). Macroscopic and microscopic properties of a cloned glutamate transporter/chloride channel. *J.Neurosci.* **18**, 7650-7661.

Watanabe, K., Sawano, T., Terada, K., Endo, T., Sakata, M., & Sato, J. (2002). Studies on intestinal absorption of sulpiride (1): carrier-mediated uptake of sulpiride in the human intestinal cell line Caco-2. *Biol.Pharm.Bull.* **25**, 885-890.

Weitz, D., Harder, D., Casagrande, F., Fotiadis, D., Obrdlik, P., Kelety, B., & Daniel, H. (2007). Functional and structural characterization of a prokaryotic peptide transporter with features similar to mammalian PEPT1. *J.Biol.Chem*. **282**, 2832-2839.

Wenzel, U., Kuntz, S., Diestel, S., & Daniel, H. (2002). PEPT1-Mediated Cefixime Uptake into Human Intestinal Epithelial Cells Is Increased by Ca2 Channel Blockers. *Antimicrobial Agents and Chemotherapy* **46**, 1375-1380.

Xu, L., Haworth, I. S., Kulkarni, A. A., Bolger, M. B., & Davies, D. L. (2009). Mutagenesis and cysteine scanning of transmembrane domain 10 of the human dipeptide transporter. *Pharm.Res.* **26**, 2358-2366.

Yeung, A. K., Basu, S. K., Wu, S. K., Chu, C., Okamoto, C. T., Hamm-Alvarez, S. F., Von Grafenstein, H., Shen, W. C., Kim, J. K., Bolger, M. B., Haworth, I. S., Ann, D. K., & Lee, V. H. L. (1998). Molecular identification of a role for tyrosine 167 in the function of the human intestinal proton-coupled dipeptide transporter (hPepT1). *Biochemical and Biophysical Research Communications* **250**, 103-107.

Yoshioka, M., Eriksson, Y. H., & Kim, Y. S. (1988). Digestion and assimilation of proline-containing peptides by rat small intestinal brush border membrane carboxypeptidases: Role of the combined action of angiotensin-converting enzyme and carboxypeptidase P. *J.Clin.Invest.* **81**, 1090-1095.

Zerangue, N., Schwappach, B., Jan, Y. N., & Jan, L. Y. (1999). A new ER trafficking signal regulates the subunit stoichiometry of plasma membrane K(ATP) channels. *Neuron* **22**, 537-548.

Zeuthen, T. & MacAulay, N. (2012). Cotransport of water by Na+-K+-2Cl- cotransporters expressed in Xenopus oocytes: NKCC1 versus NKCC2. *Journal of Physiology* **590**, 1139-1154.

Zhang, Y., Dabrowski, K., Hliwa, P., & Gomulka, P. (2006). Indispensable amino acid concentrations decrease in tissues of stomachless fish, common carp in response to free amino acid- or peptide-based diets. *Amino.Acids* **31**, 165-172.

Zhu, T., Chen, X. Z., Steel, A., Hediger, M. A., & Smith, D. E. (2000). Differential recognition of ACE inhibitors in Xenopus laevis oocytes expressing rat PEPT1 and PEPT2. *Pharm.Res.* **17**, 526-532.

Ziegler, T. R., Fernandez-Estivariz, C., Gu, L. H., Bazargan, N., Umeakunne, K., Wallace, T. M., Diaz, E. E., Rosado, K. E., Pascal, R. R., Galloway, J. R., Wilcox, J. N., & Leader, L. M. (2002). Distribution of the H+/peptide transporter PepT1 in human intestine: up-regulated expression in the colonic mucosa of patients with short-bowel syndrome. *Am.J.Clin.Nutr.* **75**, 922-930.

Zucchelli, M., Torkvist, L., Bresso, F., Halfvarson, J., Hellquist, A., Anedda, F., Assadi, G., Lindgren, G. B., Svanfeldt, M., Janson, M., Noble, C. L., Pettersson, S., Lappalainen, M., Paavola-Sakki, P., Halme, L., Farkkila, M., Turunen, U., Satsangi, J., Kontula, K., Lofberg, R., Kere, J., & D'Amato, M. (2009). PepT1 oligopeptide transporter (SLC15A1) gene polymorphism in inflammatory bowel disease. *Inflamm.Bowel.Dis.* **15**, 1562-1569.